Fluid Inclusions in Fibrous Diamonds

Yaakov Weiss, Janina Czas, Oded Navon

Institute of Earth Sciences
The Hebrew University
Jerusalem, 9190401
Israel
yakov.weiss@mail.huji.ac.il

*Now at Earth and Planets Lab, Carnegie Institution for Science jczas@carnegiescience.edu

INTRODUCTION

Most diamonds are metasomatic minerals, which means they grew from fluids or melts that moved through solid mantle rocks and chemically interacted with them. The involvement of fluids was recognized in the early days of diamond research (e.g., Sobolev 1960; Kennedy and Nordie 1968; Meyer and Boyd 1972; Harte et al. 1980) and was mostly attributed to kimberlite melts (either the erupting kimberlite, or a deeper proto-kimberlite composition). Based on Rb–Sr and Sm–Nd systematics of garnet inclusions in diamonds, Richardson et al. (1984) suggested that it involves "introduction and entrapment of asthenosphere-derived alkali, LREE and CO_2 enriched interstitial melt, which remained liquid until the time of diamond crystallization". However, only sporadic reports on the occurrence of alkali-rich mineral inclusions or fluid- or melt-inclusions in diamonds were reported at that time. In later years, evidence for such fluids and the metasomatic origin of diamonds accumulated, including, the association of diamonds with other metasomatic minerals and with alteration zones in xenoliths (e.g., Schulze et al. 1996; Anand et al. 2004; Zedgenizov et al. 2018); trace element abundance patterns of garnet and clinopyroxene inclusions in diamonds that point to interaction with, or growth from melts that are extremely enriched in incompatible trace elements (Shimizu and Richardson 1987; Stachel and Harris 1997; Stachel et al. 2004 and references therein) and observations of fluids or melts in microinclusions in diamonds, which are the subject of this review.

Before proceeding to the observations of fluids in diamonds, it is necessary to define the terms 'fluid' and 'melt'. The definition of 'fluid' in dictionaries is commonly "capable of flowing" (Merriam-Webster Dictionary), or "a substance that flows" (Cambridge and Oxford Learner's dictionaries). Physics textbooks use a similar definition "a substance (or a phase) that flows under the application of a shearing stress". This definition includes both liquids and gases, as well as supercritical fluids (Landau and Lifshitz 1987). In inclusion studies, a similar broad definition was suggested by Roedder (1984) and Bodnar (2003). The latter explained that some researchers relate to the state of the inclusion at room temperature and exclude glassy inclusions. However, he suggests including all inclusions that were fluid at the time of entrapment. This definition covers both high- and low-density fluids (Bodnar 2003). High-density fluids (HDFs) include silicate, sulfide, metallic, carbonatitic or saline supersolidus melts and dense supercritical fluids that are above the second critical endpoint (the termination of the solidus in a *P–T* space; Wyllie and Ryabchikov 2000; Kessel et al. 2005). At lithospheric pressures and temperatures, low-density fluids would have densities of ~1000 kg/m³. The most common are C–O–H-bearing supercritical fluids like H_2O, CO_2, CH_4, H_2, and their mixtures, together with the solute they carry (which can reach up to a few tens of percent). The values for the high-density ones are ~2000 kg/m³ or more, but past the second critical endpoint, the transition between low-and high-density fluids is continuous.

This review concentrates on HDFs that are encapsulated in diamonds. It begins with the historical perspective of the research of fluids in diamonds. We then review the shape and texture of fibrous diamonds which commonly carry HDFs, including the description of the three main forms of such diamonds: 'fully fibrous' where the whole diamond consists of fibers (~10 μm in diameter) and grows to develop cuboid {100} faces; 'cloudy' where a cuboid fibrous core is surrounded by a non-fibrous, octahedral zone; and 'coated' where a clear core is surrounded by fibrous overgrowth. This section also includes a short review of the chemistry of the diamonds themselves, focusing on nitrogen speciation as well as carbon and nitrogen isotope composition. The next section describes the various analytical techniques employed to explore the nature of the trapped fluids. Here the attitude is historic, and in the case of analytical techniques that are not common, or that do not provide compositional information (e.g., X-ray diffraction or transmission electron microscopy), we also present a review of the results. The following section focuses on the geochemistry of the HDFs trapped in fibrous diamonds and their four compositional types: **silicic**, which are rich in SiO_2, K_2O, Al_2O_3 and water, and form a continuous array with **low-Mg carbonatitic** compositions, rich in CaO, FeO, MgO and CO_2; **High-Mg carbonatitic** HDFs are distinguished by their very high MgO (>15 wt%) and high CaO, FeO, K_2O and CO_2; **saline** HDFs have high K, Na and Cl values, and contain varying proportions of FeO, BaO, CO_2 and water. This section ends by reviewing the direct and indirect evidence for the occurrence of such HDFs and other fluids in non-fibrous diamonds.

The discussion begins with a section on the temporal and geographical distribution of HDFs and a possible connection between HDF type and lithospheric lithology. The following section deals with estimations of pressure and temperature of diamond growth and HDF entrapment, and the current hypotheses on the origin of the four compositional types. We then review the role of HDFs in the formation of diamonds, where the collection of observations to date suggest they are the media from which the majority of lithospheric diamonds grew. The final sections highlight that all HDF types are excellent metasomatic agents, which impact the chemical composition of the continental lithosphere and possibly other mantle environments, emphasize the close relation between high-Mg carbonatitic HDF type and kimberlites, and discuss the possible role of HDFs in alkaline basaltic magmatism.

FLUIDS IN DIAMONDS—EARLY OBSERVATIONS

The earliest mention of fluids in diamonds was, most probably, by Bauer in his book "*Edelsteinkunde*" (1896, translated into *Precious Stones*, 1904). He described observations of liquid and gas-bearing microscopic inclusions within diamonds (as quoted by Melton et al. 1972 and Fesq et al. 1975).

Early studies of the three types of microinclusion-bearing diamonds were conducted by Shah and Lang (1963), Kamiya and Lang (1965) and Moore and Lang (1972), who applied X-ray topography to study their internal structure: a) cloudy diamonds with an internal cloud of microinclusions, b) coated diamonds in which a clear octahedral core is surrounded by fibrous growth, and c) cuboid diamonds that consist mostly of fibrous growth, sometimes with a small core (Fig. 1). Orlov (1977) summarized optical studies of diamonds and designated the cuboid diamonds as Variety III and the coated diamonds as Variety IV.

Angress and Smith (1965) used infrared spectroscopy to investigate the coat of a coated diamond but reported mainly on the nitrogen concentration. In a subsequent study, Chrenko et al. (1967) detected characteristic bands of molecular water (~3400 and ~1640 cm^{-1}), carbonate (1430 and 880 cm^{-1}) and nitrate (1360 and 835 cm^{-1}) in the IR spectra of the opaque coat of a diamond, but not in its transparent core (the presence of nitrate was not confirmed by later studies).

Melton and Giardini (1974, 1975) reported the composition of gases released by crushing diamonds under vacuum. Gas signals of transparent or light-yellow diamonds were similar to the system blank levels ($0.2–2 \times 10^{-5}$ cm^3 STP, for an empty crushing chamber at 0 °C and 1 bar). However, the crushing of cubic and translucent diamonds at 200 °C yielded gas volumes that were an order of magnitude larger. The main gases released were H_2O and CO_2. Gas released by graphitization of diamonds contained mostly CO with minor H_2 and the quantities were $>10^{-2}$ cm^3 STP (Kaiser and Bond 1959; Melton and Giardini 1976), but the H_2 may be attributed to a reaction of water during graphitization (Fesq et al. 1975).

Early attempts to determine the nature of the material trapped in the microinclusions by X-ray diffraction and X-ray fluorescence were not conclusive (Lonsdale and Milledge 1965; Seal 1966, 1970; Harris 1968). Prinz et al. (1975) found "fluffy, filamentous material" in two diamonds from the Democratic Republic of the Congo (DRC), but did not describe the diamonds. The composition obtained by electron probe microanalysis (EPMA) of this material was SiO_2 67 wt%; TiO_2 2.5 wt%; Al_2O_3 14–17 wt%; FeO 2–3 wt%; MgO 1 wt%; Na_2O 0.2–2.5 wt% and K_2O 8.5–10 wt%. As mentioned below, this composition agrees roughly with that of later studies of microinclusion-bearing fibrous diamonds.

Fesq et al. (1975) used instrumental neutron activation analysis (INAA) to investigate the nature of impurities in diamonds. They examined groups of diamonds (~10–20 crystals in each sample) with mineral inclusions as well as diamonds with no visible inclusions. They concluded that in addition to mineral inclusions, the diamonds also carried picritic (high-Mg basaltic) melt associated with an H_2O+CO_2 rich component or phase that carried incompatible trace elements. The presence of a sulfide-rich phase was inferred from the correlation between Fe, Ni, Cu and Co. These impurities were found in diamonds with and without visible inclusions.

INAA of coated diamonds was attempted by Kodochigov and co-workers (according to Orlov 1977) and Glazunov et al. (1967). Bibby (1979) used INAA to determine the trace-element composition of a coated diamond. He found low levels in the core, but the coat carried up to 50 ppm Fe and a few ppm of Na, K, Ba and Ce. Based on the good intercorrelation of K, Na, Ba, and the REE and their poor correlation with Sc, Cr, and Mn, he suggested the presence of carbonate microinclusions.

FIBROUS DIAMONDS

Morphology and texture

Fibrous diamonds are imperfect single crystals, consisting of parallel microscopic fibers that are slightly misaligned from the diamond crystallographic axes. They have one set of crystal faces and they produce a single X-ray diffraction pattern (Orlov et al. 1980; Smith et al. 2011). However, they are distinct from the non-fibrous monocrystalline diamonds (i.e., octahedral, cubic and macles) that grew layer by layer with a higher degree of perfection. Although fibrous diamonds are monocrystalline, in view of these differences and the absence of a better distinction, in the present paper we will use the term 'non-fibrous monocrystalline' (NFMC) when addressing other monocrystalline varieties as opposed to fibrous ones throughout the paper.

Optical microscopy is a straightforward method for identifying fibrous growth. Microinclusions trapped in the fibrous zones result in a translucent or opaque appearance of the diamond. Under high magnification, the tiny microinclusions (<1 μm) can be observed (but not their internal structure; Fig. 1d). Crossed nicols reveal high birefringence by the diamond due to stresses that may be the result of the fibrous growth or the presence of microinclusions.

Fibrous growth leads to the development of cuboid faces (Lang 1974a), thus 'fully fibrous' diamonds have a cubic shape (Fig. 1a). If octahedral, layer by layer growth develops
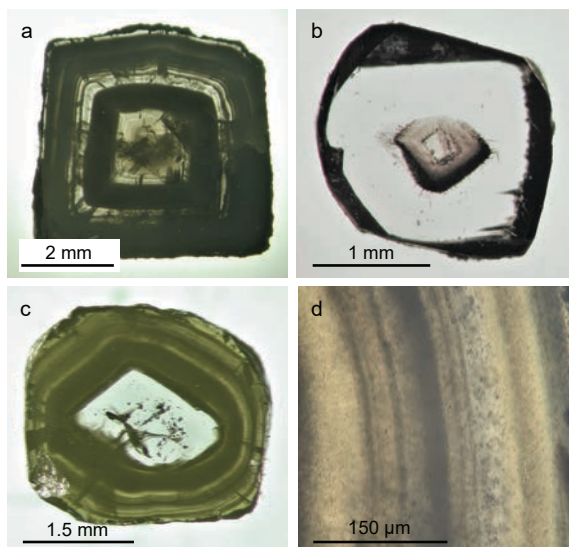
Figure 1. Photomicrographs of polished slabs of microinclusion-bearing fibrous diamonds. (**a**) 'fully fibrous' cuboid diamond from Canada (exact mine is unknown). The concentric layers define variation in microinclusion-density from center to edge. In this specific diamond (and in most fibrous diamonds) the composition of the microinclusions is homogeneous and does not show chemical radial variation, indicating it formed in pulses, but during a single growth event. (**b**) 'cloudy' diamond from Finsch, South Africa (Weiss and Goldstein 2018); with a cuboid internal zone of fibrous growth that is full of microinclusions, overgrown by a clear octahedral outer zone. (**c**) 'coated' diamond from Kankan, Guinea (Weiss et al. 2009); consists of an octahedral non-fibrous monocrystalline (NFMC) core and a fibrous coat. In this diamond, the concentric layers in the coat are characterized by different microinclusion compositions (i.e., a zoned diamond). (**d**) high magnification image of the fibrous coat in (c), showing thousands of microinclusions (black dots). See section '*Morphology and Texture' and 'Homogeneity and zoning in individual diamonds*' for additional details.

on a fibrous diamond, a 'cloudy' diamond forms with a cuboid, fibrous, inclusion-rich, translucent or opaque inner zone and an outer transparent NFMC zone (Fig. 1b). External fibrous overgrowth on an existing NFMC diamond produces a 'coated diamond' where the triangular, octahedral {111} faces conserve their original size, while the cubic {100} faces expand with the growing thickness of the coat (Fig. 1c).

X-ray topography can be used to reveal the details of the fibrous texture (e.g., Lang 1974a,b; Yelisseyev et al. 2004; Zedgenizov et al. 2006; Rondeau et al. 2007; Skuzovatov et al. 2011). The fiber diameter varies from 10 μm down to the resolution of the technique (<1 μm). The fibers grow with an average orientation parallel to the <111> direction, but individual fibers may be misoriented by up to 0.5° (Lang 1974b). Branching allows the fibers to fill the full volume of the growing diamond and leads to the formation of cuboid surfaces (parallel to {100}; Moore and Lang 1972; Orlov et al. 1982; Rondeau et al. 2007). The microinclusions (<1 μm) are scattered between the fibers (Moore and Lang 1972).

The fibrous zones have weak cathodoluminescence (CL), but it is still useful to emphasize different stages of growth. Most studies record the total intensity of the luminescence, which is sufficient to produce a map of the diamond growth layers (similar to the growth rings of a tree). An example is Fig. 1c of Klein-BenDavid et al. (2004) that reveals a transparent core and 5 concentric growth layers. In coated diamonds, the NFMC core is usually brighter than the fibrous coat, whereas, in cloudy diamonds, the fibrous inner zone is darker than the NFMC outer one (e.g., Fig. 3 of Zedgenizov et al. 2006, but see Rondeau et al. 2007 for a counterexample).

In summary, fibrous diamonds or growth zones are defined by the presence of fine fibers, as revealed by X-ray topography. They commonly carry microinclusions in variable numbers, but may also be clear of inclusions. Branching of the fibers leads to space-filling and the development of cuboid external faces.

Nitrogen concentration and aggregation

Nitrogen is the main element that substitutes for carbon in the diamond lattice (see Green et al. 2022). Its concentration can reach levels of a few thousand ppm. Fibrous diamonds typically carry a high concentration of N (~60% with more than 500 ppm and 20% with more than 1000 ppm) that resides mostly in A-centers (two nitrogen atoms replacing two carbon atoms, see Green et al. 2022), but some fibrous diamonds show the yellow tint caused by C-centers (a single nitrogen atom substituting for a single carbon atom) and others carry both A- and B-centers (4 nitrogen atoms around a vacancy) and platelets (interstitial planes carrying carbon and nitrogen atoms; Speich et al. 2018). The concentration is determined from the IR spectrum of the diamond based on the unique absorption of each of the three centers (e.g., the CAXBD97. xls spreadsheet produced by Dr. David Fisher, Diamap of Howell et al. 2012 or Quiddit by Speich and Kohn 2020). When analyzing the spectrum of microinclusion-rich diamonds, care must be taken for the overlap between nitrogen absorption at 900–1400 cm^{-1} and the major peaks of the silicates and phosphates. Most fibrous diamonds carry only A-centers and allow an easy escape from the problem. However, when B- or C-centers are present or suspected, one cannot simply use the standard fits and more elaborate treatment of the baseline and the deconvolution of the various peaks is needed (e.g., Kopylova et al. 2010; Weiss et al. 2018).

Taylor et al. (1990, 1996) compiled experimental data on the systematics of nitrogen aggregation (Evans and Qi 1982; Clark and Davey 1984) with ages and thermometric data of natural diamonds, and quantified the aggregation kinetics. They showed that it is controlled by the residence temperature and the initial amount of nitrogen (assumed to be equal to the total nitrogen measured). Most fibrous diamonds, with only A-centers, had to reside in the mantle long enough to allow the merging of C-centers into A-centers, but not too long to avoid conversion of the A- into B-centers (Fig. 2). For example, according to Taylor's calibrations, a diamond that carries 1000 ppm nitrogen with 10% in C-centers could not have spent more than 10 Myr at 950 °C or 0.1 Myr at 1050 °C. Formation of a few percent of B-centers calls for longer times, ~100 Myr at 1150 °C and billions of years at ~1000 °C (Fig. 2). Figure 2 demonstrates that the estimation of absolute times is very imprecise (as the time axis is logarithmic), but the aggregation data allow for the separation of distinct growth events. In Fig. 2, an individual diamond would appear as a diagonal line representing the interdependence of time and temperature for a given nitrogen concentration and B/(A+B) ratio. A population of diamonds formed in a single event would appear as a group of closely spaced parallel lines (e.g., Kempe et al. 2021a).

Carbon and nitrogen isotopes

NFMC diamonds cover a wide range of carbon isotope composition (δ^{13}C) with a distinct peak at −5‰ (relative to the PDB standard). Diamonds carrying eclogitic mineral inclusions peak at −5±1.2‰ (at half maximum), but about one-third of them have lower isotopic compositions (−10 to −42‰) and a few have more positive δ^{13}C values (0 to +3‰; Cartigny et al. 2014). Those with peridotitic inclusions have a somewhat wider peak of δ^{13}C at −4.5 ± 1.5‰ (Cartigny et al. 2014), but very few diamonds fall outside this range (most of the light grey area in Fig. 3c consists of eclogitic diamonds). Fibrous diamonds have more negative δ^{13}C values with a mode at −6.5 ± 1.2‰ (Fig. 3a,c). Early studies of fibrous diamonds found a narrow range between −6 and −8‰ (Galimov 1984; Javoy et al. 1984; Boyd et al. 1987; Cartigny et al. 2001), but later studies (Klein-BenDavid et al. 2004, 2007; Shiryaev et al. 2005; Zedgenizov et al. 2006, 2009, 2011, 2016, 2017; Skuzovatov et al. 2016; Timmerman et al. 2018a; Gubanov et al. 2019) widened the range, mainly towards heavier values (Fig. 3a).
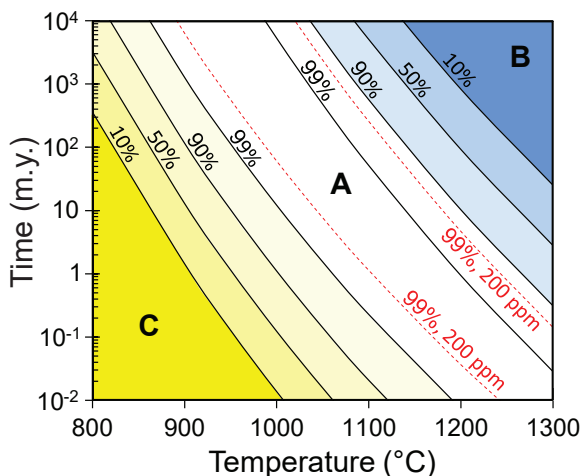
Figure 2. Mantle residence time–temperature (*t*–*T*) relations implied by the total nitrogen concentration and level of aggregation in diamonds. The **yellow region** at the lower left side shows the aggregation of nitrogen from C-centers (single nitrogen atom) to A-centers (paired nitrogen atoms), and the blue region in the upper right side indicates the combination of A-centers to form B-centers (aggregates of four nitrogen atoms surrounding a vacancy), as a function of *t*–*T*. The **black solid lines** are calculated for a total nitrogen concentration of 1000 atomic ppm and differ by the level of aggregation expressed as the percentage of nitrogen in A-centers. Diamonds with lower concentrations take longer or need higher temperatures to aggregate, as shown by the shift between the 99% lines for 1000 (**black**) and 200 atomic ppm (**red**). The concentration and aggregation state of the nitrogen in a specific diamond allow the calculation of *t* as a function of *T*. The resulting diagonal line for that diamond is similar and parallel to the lines that appear on the diagram. Most fibrous diamonds show only A-centers in their FTIR spectra and plot in the **white central region** (> 99% A-centers with a small, unresolved fraction of either C- or B-centers). Note that they are not necessarily young and can reside at low lithospheric temperatures for a considerable time. The method is very sensitive to residence temperature but provides only rough constraints on time. The parameters used for the calculations are an activation energy of $E_a = 6.0$ eV and a rate constant of $\ln(A) = 18.81$ (Taylor et al. 1996) for the C to A transition and $E_a = 7.0$ eV ($E_a/R = 81160$) and $\ln(A) = 12.59$ for the A to B transition (Taylor et al. 1996; Leahy and Taylor 1997). These are our preferred values for fibrous diamonds. Other estimations are slightly different and variations between octahedral and cubic growth zones were also reported for the A to B reaction (Taylor et al. 1990, 1996; Zedgenizov et al. 2017). We prefer the values for octahedral diamonds because the diamond fibers grow in the <111> octahedral direction.

Although more data is needed, the figure also shows that there is no correlation between the type of HDF and a specific range of carbon isotope compositions of its host fibrous diamonds.

The range of nitrogen isotope compositions ($\delta^{15}N$) of fibrous diamonds is also narrow (−8 to −2‰, relative to air standard) compared with the full range of NFMC diamonds (−24 to +12‰; see Figs. 7 and 8 of Cartigny et al. 2014). Only a handful of fibrous diamonds were analyzed for both the isotopic composition of their nitrogen and the composition of their HDF microinclusions (Fig. 3b), not enough to search for regularities and correlations.

Most fibrous diamonds exhibit uniform carbon isotope compositions, or small variations (<2‰), but some are zoned. Some present a continuous evolution during growth and appear to evolve in different directions (e.g., the arrows in Fig. 3c). A few others exhibit sharp changes that are accompanied by a change in the chemistry of the trapped HDF (Klein-BenDavid et al. 2004; Shiryaev et al. 2005; Zedgenizov et al. 2011). As discussed in *'Homogeneity and zoning'* below, this coupled variation is a strong indication that the diamond carbon is supplied by the HDF.
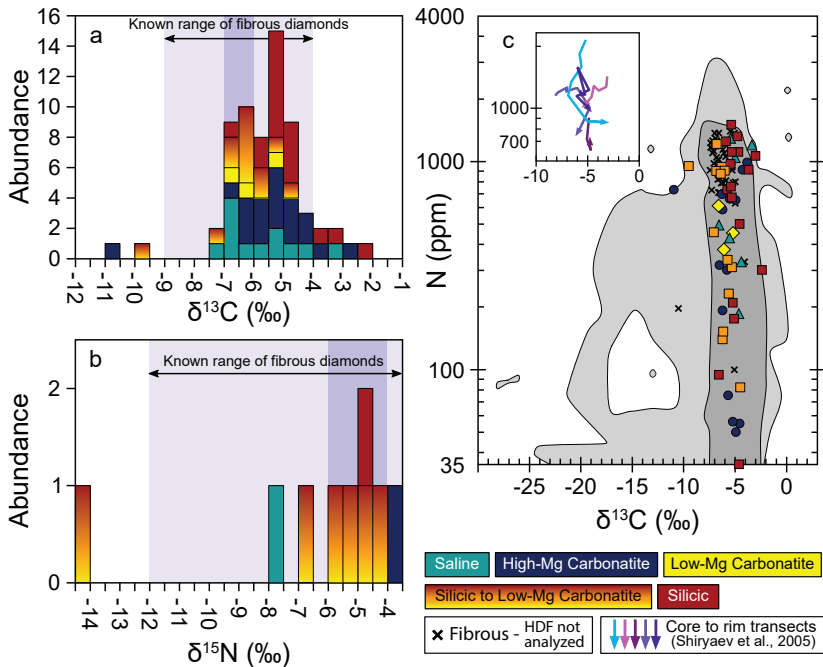
Figure 3. Stable isotope compositions of HDF-bearing fibrous diamonds. (**a**) and (**b**) histograms of carbon and nitrogen isotope composition of fibrous diamonds with known HDF type. The previously reported $\delta^{13}C$ and $\delta^{15}N$ ranges for fibrous diamonds (Cartigny et al. 2014) are shown in **light purple**. They include diamonds where the HDF composition was not analyzed. The main modes of the data are highlighted in **dark purple**. (**c**) $\delta^{13}C$ versus N content of fibrous diamonds. The **light grey outline** indicates the known range of all diamond compositions (Cartigny et al. 2014), with **dark grey** indicating the highest density of the dataset. The arrows in the inset indicate the core to rim evolution in isotopically zoned diamonds analyzed by Shiryaev et al. (2005). The Xs mark the isotopic composition and nitrogen content of diamonds that were not analyzed for their HDF composition.

THE ANALYSIS OF FLUID INCLUSIONS IN FIBROUS DIAMONDS: HISTORICAL PERSPECTIVE AND METHODS

The microinclusions and the mineralogy of their secondary assemblage

Optical microscopy of the microinclusions. High magnification optical microscopy allows observations of the individual microinclusions but is insufficient to resolve their internal structure (Fig. 1d). In some cases, it is possible to see the microinclusions arranged in linear arrays (e.g., Fig. 1 of Navon et al. 1988), but in most cases, their distribution appears to be random, except for radial variation in the number-density of the microinclusions (Fig. 1d). The number-density varies widely, from no microinclusions at all (commonly close to the rim) to more than 10^8 inclusions/mm^3 in densely populated bands, corresponding to distances of ~2 μm between neighboring microinclusions (Klein-BenDavid et al. 2006). Light reflected from polished surfaces also reveals the microinclusion-bearing zones. The microinclusions appear as tiny holes that are the origin of fine polishing grooves that extend from each hole.

Except for very rare cases, the fluid inclusions trapped in fibrous diamonds are smaller than 1 μm in size and are designated as microinclusions throughout the paper (where it is clear that we refer to microinclusions we sometimes use 'inclusions' for short). Most mineral inclusions in NFMC diamonds are larger than 1 μm and are referred to as mineral inclusions.

However, some fibrous diamonds carry mineral inclusions that are smaller than 1 μm. We refer to these as micro-mineral inclusions. Larger mineral inclusions are extremely rare in the fibrous zones, while micro-mineral inclusions are not common in NFMC diamonds.

Transmission electron microscopy (TEM) and high-resolution scanning electron microscopy (SEM). The first glimpse into the microinclusions was achieved using TEM (Lang and Walmsley 1983). In these early days, a 0.5 mm thick diamond wafer was sawn and thinned first by conventional polishing (down to ~50 μm) and then by ion beam down to electron transparency. More recent works by Wirth and coworkers used a focused ion beam (FIB) of gallium ions to cut ultra-thin foils (15 × 10 × 0.1–0.2 μm) that can be mounted directly for examination (Wirth 2004). Lang and Walmsley (1983) found numerous, mostly empty holes, 100–1000 nm in diameter, but in a few cases some material remained, and they succeeded to identify one of the phases as apatite. Energy dispersive spectroscopy (EDS) revealed clear peaks of P and Ca and convergent beam electron diffraction (CBED) revealed hexagonal symmetry with $a = 9.55$ Å. Using similar methods, Walmsley and Lang (1992a,b) found biotite (with excess silica) and ferroan dolomite in other fibrous diamonds. Guthrie et al. (1991), Klein-BenDavid et al. (2006) and Logvinova et al. (2008a, 2011, 2015, 2018, 2019a) provided more comprehensive descriptions of the microinclusions, studying both open and intact inclusions. Bright-field images reveal microinclusions, a few tens to a few hundred nanometers in size, that were sliced open during the preparation of the 10 nm thick foils. Microinclusions in the fibrous diamonds are dominantly multiphase assemblages that consist of a few mineral phases and a hole that held a low-density fluid before the inclusion was opened (Fig. 4). In some cases, amorphous material is also present. The mineral assemblage is secondary and grew from the trapped HDF during cooling, leaving a residual, low-density hydrous phase.

TEM allows the use of various techniques to identify the phases and determine their composition and structure. As CBED leads, in many cases, to fast destruction of the phase under the focused beam, high-resolution electron microscopy (HREM) is used for lattice fringe images
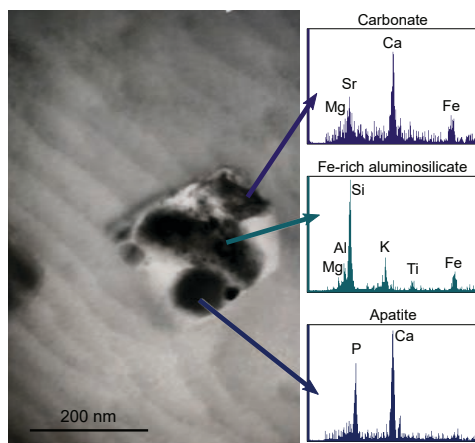

Figure 4. Transmission electron microscope (TEM) image of a microinclusion in a fibrous diamond from the DRC (courtesy of George Guthrie, Los Alamos National Laboratory). The microinclusion shows a fairly well-defined shape imposed by the diamond preferred growth habit. The inclusion contains a multi-phase assemblage of daughter minerals (**dark phases**) and a hydrous low-density fluid (**light areas**). In this specific inclusion, energy-dispersive spectra (EDS) revealed carbonates, silicates and phosphates. The solid phases take most of the volume, but water and its solute occupy ~20% of the area. The diamond trapped a uniform HDF, and the secondary assemblage crystallized upon cooling during or after the eruption. For additional details see section '*Transmission electron microscopy (TEM) and high-resolution scanning electron microscopy (SEM)*'.

of the various phases, and a Fast Fourier Transform algorithm is used to compute diffraction patterns from these images. Cell symmetry and parameters derived from the patterns are compared with libraries and literature data and allow identification of the phases. EDS spectra can be obtained from very small volumes and yield the composition of phases, down to a few nanometer scales (Fig. 4), but care should be taken as the beam can pass through two, and even more, phases that overlie each other. Electron energy loss spectroscopy (EELS) is used to detect the presence of various elements and to distinguish the chemical environment of various elements, e.g., to tell carbon in carbonates from the diamond carbon. Further details on the FIB and TEM-related techniques are provided in Wirth (2004, 2009) and Jacob et al. (2014).

The inclusions and their internal structure can also be imaged using high-resolution scanning electron microscopy (SEM) and the various crystals can be analyzed. However, the need to coat the surface disturbs either the imaging (carbon coating) or the analyses (gold coating).

Microinclusions with **high-Mg carbonatitic** compositions carry dolomite and phlogopite as the major phases with magnesite, Ba- and Sr-bearing carbonates, apatite, sylvite, rutile, ferropericlase, magnetite, clinohumite and sulfide, and a fluid phase that was lost during sample preparation (Klein-BenDavid et al. 2006; Logvinova et al. 2011, 2019a). Pyroxene was found in a single microinclusion (Klein-BenDavid et al. 2006), but it may have been trapped as a solid mineral together with the fluid (as described by Izraeli et al. 2001). Inclusions carrying **saline** HDFs crystallized KCl, ferroan dolomite, Ca–Sr–Ba-carbonate, mica, and apatite and single occurrences of halite and Ba–P phosphate (Klein-BenDavid et al. 2006; Logvinova et al. 2011). In inclusions with **low-Mg carbonatitic** HDFs the secondary assemblage consists of dolomite and Ca-carbonate (sometimes with Ba and Sr), sheet-silicates, apatite, KCl, ilmenite, magnetite, ferropericlase and sulfides. The sheet silicates were identified as biotite (Walmsley and Lang 1992b) or phlogopite (Logvinova et al. 2008a) and the sulfides include pyrrhotite, Ni-sulfide and K–Fe-sulfide (Logvinova et al. 2008a). When compositions are more **silicic**, quartz crystallizes and the sheet silicates are phengite and in some cases paragonite (Guthrie et al. 1991; Kvasnytsya and Wirth 2009; Logvinova et al. 2019a). Both are rich in silica and alumina. Klein-BenDavid et al. (2006) obtained compositions that fit high-silica mica with up to 7.6 Si atoms per formula unit (22 oxygen atoms). The above phases are joined by Ca±Sr±Ba-carbonate, a single occurrence of sulfide and some unidentified Al-Si rich phases (Logvinova et al. 2019a).

Fourier-transform infrared spectroscopy (FTIR). Infra-red spectroscopy was the analytical technique that first detected the presence of water and carbonates in the microinclusions (Chrenko et al. 1967). Navon et al. (1988) used FTIR spectroscopy to detect water, carbonate, apatite, a sheet silicate and an additional silicate phase (which was later identified as quartz, Navon 1991) in coated and cuboid diamonds from the DRC. They also estimated the carbonate and water concentrations based on absorption coefficients they measured or adapted from the literature. Fig. 5 presents a typical spectrum of a diamond carrying silicic to low-Mg carbonatitic HDF.

In 1991 Navon recognized that the observed absorption peaks at 782–786 and 809–813 cm^{-1} were caused by secondary quartz in microinclusions. These peaks were shifted from their 1 bar position (779 and 798 cm^{-1}) because of elevated internal pressures of (1.5–2.1 GPa) in the inclusions. He used this pressure at room temperature to show that the diamonds originated from the shallow part of the diamond stability field in the lithospheric mantle. A somewhat lower and uniform pressure of 1.5 ± 0.1 GPa was reported by Schrauder and Navon (1994) for diamonds from Botswana. Kagi et al. (2000) used near-IR to provide another indication for high internal pressure within the microinclusions. In addition to liquid water absorption at 5180 cm^{-1}, they identified a shoulder at 5000 cm^{-1}, which they attribute to ice-VI at 1.9 GPa, similar to the pressure indicated by the shift of the quartz absorption.
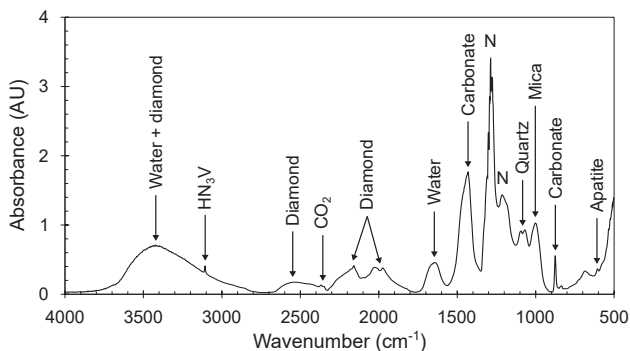
Figure 5. FTIR spectrum of a fibrous diamond from Diavik, Canada. The intrinsic diamond absorbance is at 1800–2700 cm^{-1}. The two absorption bands of nitrogen (N) are typical of aggregation in A-centers; no B- or C-centers are detected in this spectrum. A small peak at 3107 cm^{-1} is due to C–H vibration in VN$_3$H centers in the diamond matrix. Absorbance due to phases in the microinclusions is also observed. The peak at ~1650 cm^{-1} and the broad band at ~3440 cm^{-1} are caused by bending and stretching modes, respectively, of liquid water. Hydrogen bonding leads to lower frequencies, down to 2800 cm^{-1} (Weiss et al. 2013a). Carbonates (calcite, dolomite and magnesite) absorb at ~1430–1450 cm^{-1} and can be distinguished by their absorption peak at ~880–870 cm^{-1}. Quartz, apatite and mica in the microinclusions absorb at ~1100, 1066 and 1004 cm^{-1}, respectively. The presence of apatite is also indicated by the small peak at 605 cm^{-1}.

Zedgenizov et al. (2004) pointed out that Udachnaya diamonds are richer in the carbonatitic component relative to diamonds from DRC and Botswana. They also noted that water absorption in the Udachnaya diamonds extends to lower wavenumbers and, as a result the intensity ratio of the stretching and bending modes of water I_{3420}/I_{1650} is lower than that of the African diamonds. Weiss et al. (2010) calibrated the absorption of calcite, dolomite, magnesite, apatite, quartz and phlogopite, and combined them with that of water (Thompson. 1965; Venyaminov and Prendergast 1997) to measure the concentration of the various secondary phases in the diamonds. The IR data agree well with modal calculations based on EPMA data (see '*H$_2$O and CO$_2$ in the HDFs: Connecting EPMA and FTIR*' below). Weiss et al. (2013a) found that the width of the water stretching mode and the position of the bending mode vary between HDF types and used it to identify the nature of the trapped HDF (saline, high-Mg carbonatitic, or silicic to low-Mg carbonatitic; see '*Major element compositions*' below) based on its IR spectrum. This explains the observed differences in I_{3420}/I_{1650} mentioned above between Siberian and African diamonds (Zedgenizov et al. 2004).

Together all these studies turn FTIR analyses into a powerful tool that yields important information on the type of the trapped HDF, the identity and abundance of most of the major phases: carbonates, silicates, phosphates, and water (but not halides), and in the case of silicic HDFs, even an estimation of the internal pressure within the inclusions. Additional absorption bands at 2340 and 669 cm^{-1} appear in many spectra but in most cases, they are caused by atmospheric CO$_2$ in the spectrometer. A similar case can be made for the absorption at 2700–3000 cm^{-1} that may be the result of surface hydrocarbons, but it is also possible that these bands are contributed by CO$_2$ and/or organic compounds in the inclusions (Kopylova et al. 2010).

Micro-Raman spectroscopy. Raman spectroscopy was used by Zedgenizov et al. (2004) and allowed the identification of carbonates, silica glass and apatite in a few microinclusions in fibrous diamonds from Udachnaya which were large enough for analysis. They also found an olivine inclusion and graphite. The analyses did not capture the multiphase nature of the inclusions (aside from the detection of apatite and carbonate in a single inclusion). Most of the inclusions are too small and do not yield useful spectra (Kopylova et al. 2010).

X-ray diffraction (XRD). Another method used to identify the secondary assemblage in the microinclusions is X-ray diffraction. Harris (1968) pioneered the application of this technique to diamond studies and it is now used extensively to characterize mineral inclusions in diamonds and to determine their internal pressure. However, its application to fibrous diamonds was always problematic and did not yield useful results. Kopylova et al. (2010) reported lines corresponding to micas and clay minerals, but noted that the technique failed to identify carbonates or apatite, two main phases in the microinclusions. Smith et al. (2011) conducted the most comprehensive XRD study of fibrous diamonds. They also concluded that the technique fails to identify some important phases. Nevertheless, they were able to confirm the presence of sylvite, halite and Ba–Cl hydrate; dolomite, ikaite ($CaCO_3 \cdot 6H_2O$), Na–Mg carbonate, two types of Ba–Mg carbonates and an unidentified phase with a 2.63 Å band. The powder-like patterns confirmed the random orientation of the secondary phases within the microinclusions.

Major elements analysis

Secondary ion mass-spectrometry (SIMS). This technique was the first to yield a complete chemical analysis of the major elements in the microinclusions (Navon et al. 1988). They used the O^- beam of the Cameca IMS-3F at Caltech to drill into fibrous diamonds and read the intensities of the secondary positive ions formed by the diamond carbon and the various major elements in the microinclusions. Ion yields were calibrated via EPMA analysis of the volume that was later drilled by SIMS, and by analysis of mixed graphite and glass pellets. The yields were high and the background, measured on gem-quality diamonds, was very low. However, the analysis of a volume with a few hundred microinclusions, some of them larger than others, produced large fluctuations in the intensity of the various ions. As the ions were counted sequentially, this was problematic and very long counting times were needed to reach a stable average counting rate (Navon 1989).

Navon et al. (1988) compared the SIMS results to those of EDS analyses of individual, subsurface microinclusions and instrumental neutron activation analysis (INAA) and reported good agreement between element ratios determined by the three methods. However, the complex sample preparation and the long duration of the SIMS analysis needed to obtain precise counting statistics, compared with the ease and accuracy of EPMA-EDS analysis of the major elements in individual microinclusions (see next section) led to the prevalence of the latter in following studies.

Electron-probe microanalysis (EPMA). Electron-probe microanalysis of individual, subsurface microinclusions is the main technique used to analyze the major element composition of the trapped HDFs (e.g., Schrauder and Navon 1994; Izraeli et al. 2001; Tomlinson et al. 2006; Zedgenizov et al. 2009). Navon (1989) showed that it is more accurate than broad beam analysis of many inclusions. The inclusions are identified by comparing back-scattered electron (BSE) and secondary-electron (SE) images of the same area. In the BSE images, the microinclusions appear as bright fuzzy dots due to their high electron density relative to the diamond. However, they can be mistaken for dust particles. This is solved by examination of the SE image, which presents surface topography. The dust is clear and sharp, but the subsurface microinclusions are not visible. An electron beam with a typical current of 10–15 nA is accelerated to 15 KeV and focused to a ~0.5 μm diameter or less at the center of the inclusion. The X-rays generated from the microinclusion and the surrounding carbon matrix are analyzed by an energy dispersive spectrometer (EDS) and wavelength dispersive spectrometers (WDS). Using a standard correction procedure and mineral standards for each of the elements of interest, the number of counts for each element is translated into element concentrations.

Monte Carlo simulations of electron scattering indicate a penetration depth of ~2 μm into the diamond and a similar range of scattering to the sides (at 15 kV). As a result, most X-rays are emitted by the diamond carbon atoms and only a few percent of the calculated analysis

are due to elements in the microinclusions. The correction procedure calculates the sum of chlorine and the major oxides and assumes that the difference to 100% (commonly >95%) is all carbon. Finally, to get the composition of the HDF itself, the total of chlorine and oxides is normalized to 100%, plus accounting for excess calculated oxygen due to the presence of Cl (see '*Introduction*' in the supplementary compilation of HDF data, Weiss et al. 2022). In reality, the concentration of the oxides in the HDF is lower, as water and CO_2 (in carbonates) must be included as well. However, because they are measured by FTIR in a different volume, we must first normalize each EPMA analysis in order to combine them and calculate the average composition for the diamond (or a zone in the diamond). Only then, the average EPMA composition and the FTIR dataset can be merged to provide the full major element composition including the volatiles (see next section).

The very low background produced by the carbon matrix allows observations of very small peaks, but the low concentrations of the various elements still lead to large relative errors in the composition of individual inclusions. Jablon and Navon (2016, their Fig. A3) estimated the precision and concluded that the error for major elements of the inclusion is a few percent (*relative*), but it increases to tens of percent for the minor elements. However, except for a few zoned diamonds, the composition of the HDFs in any one diamond is uniform. Thus, the standard error on the average composition of the HDF in each diamond is reduced by a factor of $\sqrt{n-1}$, relative to the standard deviation of the individual analyses. Commonly, 30–50 inclusions along a few profiles are analyzed for each diamond. Plotting the profiles allows verification of homogeneity. Most diamonds are homogeneous, and the standard errors are smaller by factors of 5–7 relative to the standard deviation of the individual analyses. When calculating the average composition, it is important to remove analyses of microinclusions that trapped discrete minerals or mixtures of mineral+fluid (Izraeli et al. 2001; Tomlinson et al. 2006; Weiss et al. 2018; Weiss and Goldstein 2018). As the diamonds are cleaned with HF, fluorine concentration is monitored, and F-rich analyses, which are indicative of exposed inclusions, are also removed.

Other methods. Information on the concentration of some major elements can be obtained using INAA and LA-ICP-MS, along with data on many trace elements. The two techniques are discussed in section '*Trace element analyses*' below.

H_2O and CO_2 in the HDFs: Connecting EPMA and FTIR

To fully characterize the HDF major element composition, it is necessary to integrate both EPMA and FTIR data. Izraeli et al. (2001) provided a rough estimate of carbonate ions as the sum of the molar proportions of Mg+Fe+Ca and calculated the water content using the relative proportions of carbonates and water determined from the IR data. Klein-BenDavid et al. (2007) accounted, in a simplified manner, for cations taken by chlorides, silicates and phosphates and Weiss et al. (2010) provided a better framework. Below, we present their method and examine one more case.

We begin with translating the EPMA data into modal proportions, using the various minerals of the secondary assemblage as a guide. Silicates, phosphates and halides are determined, and the excess cations are assumed to be compensated by carbonate ions. First, the molar proportion of halides and apatite is calculated based on the Cl and P_2O_5 concentrations determined by EPMA. If Cl<K+Na, the excess Na is added to the carbonate. If Cl>K+Na, the excess Cl bonds with Ca. The case of the silicates is more complex. IR and TEM data indicate that the silicate phase is mostly phlogopite-biotite solid solution, $K(Mg,Fe)_3AlSi_3O_{10}(OH)_2$, but that silica-rich mica is found in the silicic HDF microinclusions (Klein-BenDavid et al. 2006). In most cases, the Si/Al ratio of HDFs is larger than 3 (Table 1), and both micas are necessary.

In pure phlogopite-biotite, Fe+Mg=Si=3Al and K/2=Si/6. We assume that Ti^{4+} resides in the phlogopite, and obtain:

$$\text{Carbonate} = (Mg + Fe + Ca + Ba + (Na + K)/2) - Cl/2 - 5P/3 - Si - Si/6 + 2Ti \qquad (1)$$

If $Al < Si/3$, we assume that the mica is: $K(Mg,Fe)_{3-x}Al_{1-x}Si_{3+x}O_{10}(OH)_2$, which leads to:

$Mg_{(mica)} + Fe_{(mica)} = (5Si + 9Al)/8$, and $K_{(mica)}/2 = (Al+Si)/8$ in the mica.

The carbonate is then (Weiss et al. 2010):

$$\text{Carbonate} = (Mg + Fe + Ca + Ba + (Na + K)/2) - Cl/2 - 5P/3 - (6Si + 10Al)/8 + 2Ti \qquad (2)$$

In the case of silicic HDFs, where $Fe + Mg < 3Al < Si$, we assume that all the iron and magnesium, as well as the Al, Ti and Si are in the silicate phases (mica and quartz) and possibly in titanates, and estimate the K bound in the silicates as $K_{(silicates)} = Al$. In this case, the carbonate is (Weiss et al. 2010):

$$\text{Carbonate} = Ca + Ba + (Na + K - Cl - Al)/2 - 5P/3 \qquad (3)$$

If $Al > Si/3$, the excess Al should enter the octahedral sites (muscovite solid solution) and with $Mg_{(mica)} + Fe_{(mica)} = 3(Si - Al)/2$ and $K_{(mica)}/2 = Si/6$, the proper equation is:

$$\text{Carbonate} = (Mg + Fe + Ca + Ba + (Na + K)/2) - Cl/2 - 5P/3 - (10Si - 9Al)/6 + 2Ti \qquad (4)$$

Once the weight fraction of the CO_2 component is determined from the molar proportion of carbonates, the water is estimated based on the $CO_2/(CO_2 + H_2O)$ ratio determined from the FTIR absorption bands of water and carbonates. The main obstacle here is that there is no available absorption coefficient for the residual hydrous fluid in the microinclusions, and even for pure water, the two values in the literature differ by ~25%. Venyaminov and Prendergast (1997) determined $\varepsilon_{water} = 109$ (AU/cm)/(mole/liter), compared with the old value of 86 (AU/cm)/(mole/liter) of Thompson (1965). We use the newer value. Using the older, the water proportion will be higher by 15–20%. Now it is possible to determine the composition of the HDF as wt% of all oxides + Cl + CO_2 + H_2O (Table 2); in molal proportions (moles per 1 kg or 55.5 moles of water, Table 3) or as wt% of the major components: silicates (+titanates), carbonates, halides, phosphates and water (Table 4).

As can be seen in Fig. 6, this procedure works well. The comparison is close for high-Mg carbonatitic HDFs, which have relatively simple secondary mineral assemblage—mostly dolomite, calcite or magnesite, and less (K,Na)Cl (not active in IR), phlogopite, apatite and a hydrous fluid with dissolved halides and carbonates. The fit is reasonable in the case of the low-Mg carbonatitic compositions, but poor for the silicic HDFs. The likely reasons are that the mica is no longer phlogopite, but rather, a Si-rich mica (Klein-BenDavid et al. 2006; Logvinova et al. 2019a) with different absorption coefficient, the presence of an unidentified Al-Si-rich phase (Logvinova et al. 2019) or silicic glass (Zedgenizov et al. 2004). Still, it shows that FTIR spectroscopy alone can be used for identifying the type of HDF present and to provide a semiquantitative estimate of the mineralogy and hence the chemistry of all the major constituents of an HDF.

Trace element analysis

Instrumental neutron activation analyses (INAA). This technique involves irradiation of the sample with neutrons in a nuclear reactor. Nuclear reactions transform (activate) the elements in the sample into short-lived isotopes that emit γ-rays upon their decay. The γ-rays are counted to determine the concentrations of the new isotopes and consequently, the abundance of their parents in the diamond.

Table 1. Average composition* of the four endmembers on H_2O- and CO_2-free basis (wt%).

	Silicic	Low-Mg carbonatitic	High-Mg carbonatitic	Saline
*n**	37	11	32	24
SiO_2	56.5	13.2	9.0	4.2
TiO_2	2.9	2.7	1.2	0.8
Al_2O_3	9.1	3.8	2.8	0.8
FeO	6.0	23.6	13.9	8.0
MgO	3.9	11.7	23.7	3.7
CaO	4.7	20.7	22.8	6.5
BaO	0.5	0.4	2.0	8.4
Na_2O	1.9	6.1	6.3	11.8
K_2O	12.4	13.0	12.9	30.0
P_2O_5	1.5	3.0	2.8	0.6
Cl	0.9	2.3	3.4	32.6
Total	100.2*	100.5	100.8	107.4

Note: *n* - Number of HDF compositions averaged in calculating the composition of each type (ignoring isolated extreme analyses). Totals are higher than 100 wt% because of excess oxygen due to the presence of chlorine.

Table 2. Average composition of the four endmembers, including H_2O and CO_2 (wt%).

	Silicic	Low-Mg carbonatitic	High-Mg carbonatitic	Saline
SiO_2	48.6	8.3	5.5	2.8
TiO_2	2.5	1.7	0.7	0.5
Al_2O_3	7.8	2.4	1.7	0.6
FeO	5.1	14.9	8.4	5.5
MgO	3.3	7.4	14.4	2.5
CaO	4.0	13.1	13.8	4.4
BaO	0.4	0.3	1.2	5.7
Na_2O	1.6	3.9	3.8	8.1
K_2O	10.7	8.2	7.8	20.4
P_2O_5	1.3	1.9	1.7	0.4
Cl	0.8	1.4	2.1	22.1
CO_2	4.2	26.1	31.7	10.7
H_2O	9.8	10.7	7.6	21.3
Total	100.2	100.3	100.5	105.0

Bibby (1979) reported the first INAA study of a coated diamond, but did not have all the major elements needed to obtain the composition of the HDFs. Fragments of coated and fully fibrous diamonds from DRC and Botswana were also analyzed by Palme and Spettel (unpublished, reported in Navon 1989). Schrauder et al. (1996) used INAA to determine a large number of elements in a suite of diamonds from Botswana. Diamonds were fragmented

and hand-picked before cleaning in acids in order to expose and avoid cracks. They were then irradiated, cleaned once more, counted 5, ~10 and ~40 days after the irradiation, and analyzed for the concentrations of Na, K, Fe and 28 trace elements in the diamonds. Na/K and Fe/K ratios obtained via INAA compared well with EPMA measurements (Schrauder and Navon 1994) and allowed re-normalization and determination of the trace element concentrations of the HDFs themselves. Br, I and U (along with a few major elements) were also measured following their transformation to noble gases via neutron activation and noble gas mass spectrometry (see '*Noble gas and halogen analysis*' below).

Table 3. Average composition of the four endmembers (molal units).

	Silicic	Low-Mg carbonatitic	High-Mg carbonatitic	Saline
Si	82.7	13.0	12.0	2.2
Ti	3.2	2.0	1.2	0.3
Al	15.7	4.4	4.4	0.5
Fe	7.3	19.4	15.4	3.6
Mg	8.4	17.1	46.9	2.9
Ca	7.3	21.9	32.4	3.7
Ba	0.3	0.2	1.0	1.7
Na	5.3	11.7	16.2	12.2
K	23.2	16.3	21.9	20.3
P	1.8	2.5	3.1	0.3
Cl	2.3	3.8	7.7	29.3
CO_2	9.8	55.5	94.5	11.4
H_2O	55.5*	55.5	55.5	55.5
Total	100.2	100.3	100.5	105.0

Note: *55.5 moles of water weigh one kilogram and hence, the concentrations of all other components is in molal units (moles/1 kg water).

Table 4. Melt components* in the average composition of the endmembers (wt%).

	Silicic	Low-Mg carbonatitic	High-Mg carbonatitic	Saline
Silicates	75	22	14	7
Carbonates	11	60	71	27
Phosphates	3	4	4	1
Halides	2	3	4	43
Water	10	11	8	21
Total	100	100	100	100

Note: *See section 'H_2O and CO_2 in the HDFs: Connecting EPMA and FTIR' for the calculations of the various components.

Proton induced X-ray emission (PIXE). Rege et al. (2005) presented results obtained by Griffin et al. (1993) using PIXE (also known as proton probe, Ryan et al. 1990). Two diamonds previously studied by Schrauder et al. (1996) were re-analyzed and the duplicate analysis of Ca, Ti, Cr, Fe, Ni, Cu, Zn, Sr, Zr and Ba were used to calibrate a standard for LA-ICP-MS.
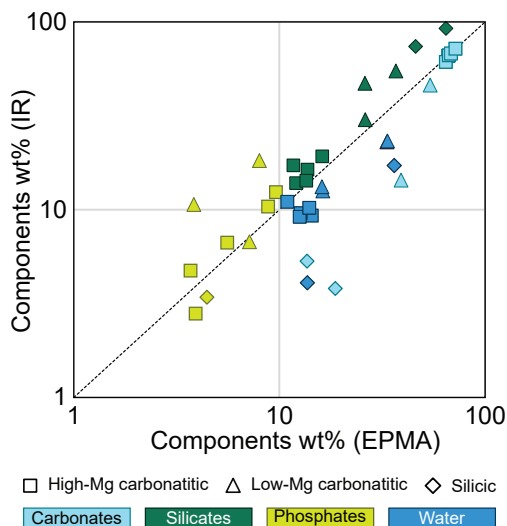
Figure 6. Daughter phase concentrations (wt%) in microinclusions as determined by FTIR and calculated based on EPMA analyses for carbonatitic and silicic HDFs. **Colors** denote the phases and the **symbols** stand for the HDF type. Selected analyses for 10 fibrous diamonds are from Weiss et al. (2009) and Klein-BenDavid et al. (2009). The proportions determined using FTIR are based on the absorbance (AU/cm) at the main peak of each phase and its conversion factor (ppm·cm/AU; Weiss et al. 2010). Oxide concentrations of HDFs as determined by EPMA are translated to modal proportions according to the scheme outlined in section '*H_2O and CO_2 in the HDFs: Connecting EPMA and FTIR*'.

Early mass-spectrometry—combustion and crushing. Early analyses of trace elements in diamonds used emission spectroscopy to analyze impurities in the ash left after burning the diamond, but no specific analysis of fibrous diamond was reported (see Bibby 1982 for review). Akagi and Masuda (1988) burnt cuboid fibrous diamonds in a platinum foil within a quartz tube under oxygen flow. They collected the residue from the Pt foil and the gas-trap and analyzed the solution using isotope dilution mass spectrometry. Akagi (1999) crushed the diamonds, leached soluble elements first in water and then with hydrochloric acid, and determined the concentration of Rb, Sr, Ba, REE and [87]Sr/[86]Sr ratios.

Laser-ablation inductively coupled plasma mass-spectrometry (LA-ICP-MS). The development of LA-ICP-MS allows for a much faster and easier measurement of some major and many trace elements in fibrous diamonds. The laser beam is focused into a 20–100 μm spot on the diamond surface ablating the diamond and its microinclusions. Part of the ablated material accumulates around the ablation pit, but most of it is carried into the plasma torch, ionized and analyzed using a quadrupole mass-spectrometer.

The technique was first applied to NFMC diamonds by Watling et al. (1995), who defined their investigation as preliminary. It took 8 more years for Resano et al. (2003) to try again, using an improved laser and mass spectrometer set-up, but here too, the purpose was looking for chemical fingerprint of diamond provenance for identification of conflict diamonds, and no fibrous diamonds were analyzed. Wang et al. (2003) also reported concentrations of 28 elements determined using LA-ICP-MS, but provided no details.

To date, most LA-ICP-MS analyses of fibrous diamonds have been carried out at the GEMOC lab at Macquarie University, Australia. The method was developed by Rege et al. (2005) and utilizes a 266 nm Nd:YAG laser focused into a custom-made ablation cell. Helium is used as the carrier gas and is mixed with argon before its introduction into the plasma

torch of an Agilent 7500 ICP-MS. They introduced a cellulose standard that is doped with ~1000 ppm of a variety of elements. Carbon is also measured on the sample and the standard, allowing the translation of count-rate ratios into the concentration of the various elements in the diamond. A comparison of the concentrations determined by LA-ICP-MS with those determined by INAA (Schrauder et al. 1996) and by PIXE (Griffin et al. 1993) indicated good accuracy with most elements falling close to the 1:1 line (Rege et al. 2005). Rege et al. (2010), Araújo et al. (2009), Zedgenizov et al. (2007, 2009, 2011, 2018), Weiss et al. (2009, 2011, 2013b, 2018) and Weiss and Goldstein (2018) all used the Macquarie system and procedures for determining trace element concentration in the diamonds and their HDFs.

Tomlinson et al. (2005) used an ArF excimer laser at 193 nm, a GeoLes illumination system and an Elan 6100 ICP-MS to analyze 5 coated diamonds from DRC. They used a NIST 612 glass standard, but no carbon standard and thus could report only element ratios. In a later paper, Tomlinson et al. (2009) assumed that matrix effects are not too important and used the NIST 612 to derive concentration in the diamond. They used the carbonate content as measured by FTIR and EPMA in the diamond and the HDF, respectively, to get the trace element content of the HDF. Dalpé et al. (2010) used a CRM-S2150 doped oil standard.

As diamonds have a simple matrix, consisting mostly of carbon and minor nitrogen, the number of significant interferences is limited to ion pairs of C, N, O and Ar (see Supplementary Table 2 in Rege et al. 2010). These interferences affect many of the major elements, up to ^{58}Fe = ^{40}Ar^{18}O. However, the high abundance of the major elements of the HDFs still allows for reasonable precision in their determination. Weiss et al. (2008) compared element/Fe ratios for the major elements determined by LA-ICP-MS with those measured using EPMA and found good agreement between the two methods. They followed Schrauder et al. (1996) in using potassium that was measured by both EPMA and LA-ICP-MS to translate the concentrations in the diamond to concentrations in the HDF.

We note that, in principle, a carbon standard is not needed. A preliminary study in our lab at the Hebrew University found similar counting-rate ratios for various element pairs comparing analyses of the pure NIST 610 with analyses of pressed pellets made of graphite powder to which 20% of ground NIST 610 were added (Elazar and Weiss 2021). The similarity suggests that it is sufficient to measure the NIST standard. That means that if the major elements are determined by EPMA, and potassium, and/or other elements, are measured by both techniques, the element/K concentration-ratios determined using the NIST standard can be converted to the trace element concentrations in the HDF.

For example, for the case of La:

$$\text{La}_{\text{ppm}}^{\text{HDF}} = \frac{\text{La}_{\text{cps}}^{\text{d}}}{\text{K}_{\text{cps}}^{\text{d}}} \frac{\text{K}_{\text{cps}}^{\text{st}}}{\text{K}_{\text{ppm}}^{\text{st}}} \frac{\text{La}_{\text{ppm}}^{\text{st}}}{\text{La}_{\text{cps}}^{\text{st}}} \left[\text{K}_2\text{O}\right]_{\text{wt\%}}^{\text{HDF}} \frac{10^4 \cdot 78.2}{94.2}$$

where d = diamond,
st = standard,
ppm = parts per million,
cps = count per second,
$\left[\text{K}_2\text{O}\right]_{\text{wt\%}}^{\text{HDF}}$ = the concentration of K$_2$O in the HDF as obtained by normalizing the concentrations of all major oxides and Cl measured by EPMA to 100 wt% (or, alternatively, allowing for water and carbonate as well) and the factor at the end translates $\left[\text{K}_2\text{O}\right]_{\text{wt\%}}^{\text{HDF}}$ into $\left[\text{K}\right]_{\text{ppm}}^{\text{HDF}}$.

Noting the similar concentration of K$_2$O in silicic and carbonatitic HDFs, we suggest that in the lack of major element data, the trace element concentrations in the HDFs can be estimated using K$_2$O abundance of 9 wt% for silicic and carbonatitic HDFs and 20 wt% for saline compositions (Table 2). The nature of the fluid can be determined using IR spectroscopy.

Although this is an approximation, the added inaccuracy will only lead to a minor uniform vertical shift of all elements on the trace element abundance diagram.

Off-line laser ablation of fibrous diamonds. In an effort to lower the limit of quantification and to open the way for trace element analysis of NFMC diamonds and Sr–Nd–Pb isotopic analysis of fibrous diamonds, Pearson and co-workers developed the off-line approach (McNeill et al. 2009; Klein-BenDavid et al. 2010, 2014). Following cleaning in ultra-pure HF and HNO_3 and weighing, the diamond was placed in a sealed PTFE beaker with an optical window and ablated using a UP-213 New wave laser system. The sample was moved under the laser so that a large area (a few hundred μm in size) was ablated. The ablated material was collected in HCl that was dried and taken in HNO_3 before splitting into two aliquots: 10% for trace element and 90% for isotopic analysis. The carefully pre-cleaned beakers and windows as well as the use of ultrapure acids in an ultraclean lab led to blanks at the picogram levels and allowed trace element and isotopic analyses of ~500 μg of ablated diamond.

The technique yielded very accurate results for fibrous diamonds, confirming the on-line analyses (see Fig. 2 and 4 of Klein-BenDavid et al. 2014). It was used successfully in trace element analyses of a few NFMC gemmy diamonds, where concentrations were very low, but the patterns resembled those of fibrous diamonds (Melton et al. 2012; Krebs et al. 2019), and for radiogenic isotopic analysis of fibrous diamonds (following section). Recently, a new custom-made off-line ablation system equipped with a Spectra-Physics Talon 532-20 laser was installed in Yaakov Weiss' lab in Jerusalem.

Radiogenic isotope analysis

Radiogenic isotopes are an important tool in dating geologic events and as tracers of melt and fluid sources. Their use as tracers is based on the preservation of isotopic ratios of heavy elements during melting, fractionation, and separation of immiscible liquids. Akagi and Masuda (1988) were the first to determine the Sr isotopic composition of HDFs after burning a diamond in a platinum crucible under flowing oxygen. They dissolved the residue in HCl and used half of the material for the analysis of Sr isotopes, using standard wet chemical methods. The other half was used for analyzing the trace element concentrations. Klein-BenDavid et al. (2010, 2014) replaced the burning of the diamond by laser ablation and the quartz tubes by Teflon beakers fitted with an optical window. The details of the ablation and dissolution procedures were described above, in the off-line laser ablation of fibrous diamonds (*'Trace element analysis'* section). Separation chemistry and isotopic analysis of the derived solution were performed using standard techniques. To date, only 42 fibrous diamonds from Canada, Botswana, DRC, Guinea, and Siberia were analyzed for their Sr isotopic compositions and a handful of those for their Nd and Pb isotopic compositions (Klein-BenDavid et al. 2010, 2014; Smith et al. 2012; Weiss et al. 2015).

Noble gas and halogen analysis

Fibrous diamonds were first analyzed for their Ar content and isotopic composition using noble gas mass spectrometry by Zashu et al. (1986), without noticing their unique character and the presence of microinclusions. They determined the K, ^{36}Ar, and ^{40}Ar content of a group of diamonds from DRC and obtained linear correlations between K and ^{40}Ar concentrations and between $^{40}K/^{36}Ar$ and $^{40}Ar/^{36}Ar$ ratios. Interpreting the slope of the correlation between the two ratios as age (an isochron diagram) they obtained 6±0.3 Ga, older than the age of the Earth. It took three more studies to reach the correct explanation - the correlations reflect the presence of microinclusions full of HDFs that contain not only K_2O and other oxides, but also excess argon that came with the fluid and is not the result of potassium decay in the diamond. The very old age reflects the stronger enrichment of the original trapped fluid in Ar relative to K. Measurement of Cl, after its activation into ^{38}Ar, revealed an even tighter $^{40}Ar/^{36}Ar$–$Cl/^{36}Ar$ correlation, demonstrating that the Ar–K correlation has nothing to do with the diamond age (Turner et al. 1990).

Following studies yielded data on the concentrations and the isotopic composition of He, Ne, Ar, Kr and Xe in fibrous diamonds from DRC, South Africa, Botswana, Guinea, Yakutia and Canada (Ozima and Zashu 1991; Burgess et al. 1998, 2009; Wada and Matsuda 1998; Weiss et al. 2017, 2021 Broadley et al. 2018; Timmerman et al. 2018b, 2019; Johnson et al. 2000). Noble gas analyses of fibrous diamonds were performed by diamond graphitization and gas released at $T > 1800$ °C (commonly at ~2000 °C) using a low blank, high-temperature resistance furnace (e.g., Wada and Matsuda 1998), a laser heating system (Broadley et al. 2018), or by crushing the diamond in a high-vacuum crushing vessel (e.g., Burgess et al. 1998). While the heating techniques extract all the gas from the diamond, including microinclusions and diamond lattice, the crushing technique preferentially extracts the gases trapped in the microinclusions (Burgess et al. 1998; Sumino et al. 2011). This issue is important because nuclear production of noble gases can add ^{3}He, ^{4}He and ^{21}Ne in diamonds (Basu et al. 2013 and references therein), almost entirely to the diamond lattice and not in the microinclusions (which constitute only ~0.1% of the diamond by mass, Navon et al. 1988). Crushing the diamonds rather than burning them, reveals the signature of the microinclusions, and allows the distinction, for example, between the He compositions of the trapped HDFs (mantle source) and He confined to the diamond lattice (from secondary sources; Burgess et al. 1998).

Burgess et al. (1998), Weiss et al. (2017, 2021), Timmerman et al. (2018b, 2019) and Broadley et al. (2018) reported results on He, Ne, Ar, Kr, and Xe concentrations and isotopic composition obtained by crushing fibrous diamonds, rather than graphitizing them. If the extraction efficiency by crushing is not high enough, only part of the gas trapped in the microinclusions is released. This may affect the absolute gas concentrations but should not influence their isotopic ratios. Timmerman et al. (2019) graphitized the crushed diamond material and estimated that only 4–20% of the gas in the microinclusions is released by crushing. However, these measurements yielded a significant variation in ^{3}He/^{4}He ratios, of up to 10 Ra values, between crushing and heating techniques (where Ra is the atmospheric ratio of 1.39×10^{-6}). In contrast, Broadley et al. (2018) reported ^{4}He concentrations during crushing that are higher by 2–3 orders of magnitude compared with final heating results, and similar ^{3}He/^{4}He ratios for the two modes of extraction. Thus, gas extraction efficiency by crushing may be much higher (as a result of different crushing methods and initial sample size), and the measured concentrations and isotopic ratios represent the trapped HDF compositions.

Following the activation of diamonds by neutrons, they provide information on additional elements, whose isotopes react to form synthetic noble gas isotopes that can be measured as well. The best-known example is the 'Ar–Ar dating' method where ^{39}K reacts to ^{39}Ar. Turner et al. (1990), Wada and Matsuda (1998) and Burgess and co-workers (Burgess et al. 1998, 2002, 2004, 2009; Johnson et al. 2000) have used neutron activation to determine K (via ^{39}Ar), Cl (^{38}Ar), Ca (^{37}Ar), Br (^{80}Kr), I (^{128}Xe) and U (^{134}Xe) concentrations and study noble gases and halogens in fibrous diamonds from Africa, Siberia and Canada.

THE COMPOSITION OF HIGH-DENSITY FLUIDS

The discovery of the various types of high-density fluids

More than 20 years of research lead to the discovery of the four types of HDFs. Navon et al. (1988) first published compositions that span a range between carbonatitic and silicic HDFs. Thirteen years later Izraeli et al. (2001) described a new saline HDF. Last, Klein-BenDavid et al. (2009) distinguished between low-Mg carbonatitic endmember that forms a continuous array towards the silicic one, and high-Mg carbonatitic HDFs that were defined as a new, fourth type. Many other studies confirmed the global distribution of all four compositional types (Figs. 7 and 8, Tables 1–4), but no new major element composition has been discovered since. Trace element analyses revealed two repeating patterns of enrichment in incompatible

elements (Weiss et al. 2008b; Rege et al. 2010): highly fractionated patterns with negative anomalies of alkalis, HFSE and in most cases Sr, and less fractionated, smoother patterns. These two types of patterns have been identified in all four types of HDFs (Fig. 9). Radiogenic isotope ratios correlate with the trace elements indicating a relationship between metasomatic enrichment of the source rocks and HDFs signatures (Klein-BenDavid et al. 2014).

Homogeneity and zoning in individual diamonds

Many fibrous diamonds exhibit radial variation in the number density of microinclusions (Fig. 1). However, out of ~300 fibrous diamonds analyzed for the major element composition of their microinclusion, only a handful are chemically zoned and show significant radial (core-to-rim) variation of HDF composition. Even in these diamonds, there is no consistent chemical evolution of fluid composition (e.g., from silicic to carbonatitic) or systematic isotopic trend in the diamond carbon (Klein-BenDavid et al. 2004; Shiryaev et al. 2005; Weiss et al. 2009; Zedgenizov et al. 2011; see arrows in the inset in Fig. 3c). Thus >95% of known HDF-bearing fibrous diamonds recorded growth from a homogeneous medium. Oxide concentration in individual microinclusions varied randomly with no clear core-to-rim evolution and by less than 20% relative. Hence, a single, major element composition achieved by averaging a few tens of HDF inclusions is representative of the diamond to better than ±15% (Weiss et al. 2008a), reflecting analytical errors and a limited real variation between the individual microinclusions.

LA-ICP-MS analyses determine the average trace element composition of thousands of microinclusions in the ablated volume of the diamond. Multiple ablation analyses of different parts of a single diamond agree to better than 15% (Tomlinson et al. 2009; Weiss et al. 2009, 2013b, 2018; Rege et al. 2010; Klein-BenDavid et al. 2014), thus showing that HDFs in an individual diamond are also homogenous for trace elements.

We note that the available isotopic data on HDFs in fibrous diamonds provide contrasting evidence. In some cases, repeated analyses of the same diamond reveal homogeneity (Weiss unpublished data), in other cases significant variation is documented (Klein-BenDavid et al. 2010). To clarify this issue of uniform vs. variable HDF isotopic compositions in a single diamond, additional data are necessary.

Most zoned diamonds reflect two or more distinct growth events, for example, two Kankan (Guinea) fibrous diamonds exhibit inner zones with silicic HDFs and outer ones with low-Mg carbonatitic compositions (Weiss et al. 2009). Similar variations from silicic to carbonatite HDFs were reported by Shiryaev et al. (2005) and the reversed direction by Zedgenizov et al. (2011). Weiss et al. (2014) reported two distinct microinclusion-rich layers in a clear octahedral NFMC diamond from Finsch (South Africa); the inner one carries a low-Mg carbonatitic HDF and the outer one a saline composition. The contrasting radial change of the composition and the sharp boundaries that are also reflected by CL imaging suggest that zoning is the result of growth from different HDFs, rather than *in situ* evolution of a single composition.

Such zoning allows constraining whether the HDFs carry the carbon from which their host diamond grows. Klein-BenDavid et al. (2004) reported saline and high-Mg carbonatitic HDFs in the inner and outer zones, respectively, of a diamond from Diavik (Canada). The carbon isotope compositions of the two zones show a clear difference: −8.1 to −8.9‰ in the inner vs. −11.4 to −12.8‰ in the outer. Shiryaev et al. (2005) reported similar relationships in a cuboid fibrous diamonds from Brazil. The inner part was silicic, while the outer part carried low-Mg carbonatitic HDFs and the carbon isotopic composition changed sharply at the boundary. The simultaneous changes of CL, major element compositions of the HDF and the carbon isotope compositions of the host diamonds thus indicate that the carbon and nitrogen for diamond growth are carried and supplied by the HDFs.
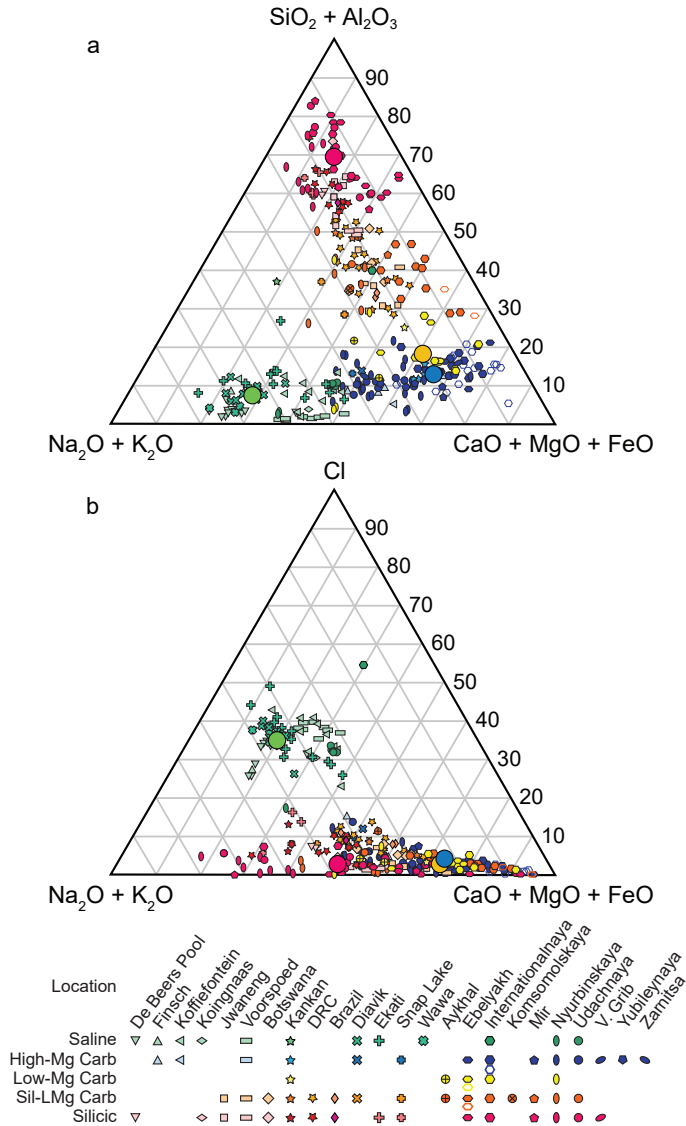
Figure 7. Ternary diagrams of (**a**) $SiO_2+Al_2O_3$–Na_2O+K_2O–$CaO+MgO+FeO$ and (**b**) Cl–Na_2O+K_2O–$CaO+MgO+FeO$ showing the global range of HDF composition in fibrous diamonds (in wt%). HDF types are coded by color: **greens** for saline, **reds** for silicic, **orange** shading for silicic to low-Mg carbonatitic, **yellows** for low-Mg carbonatitic, and **blues** for high-Mg carbonatitic HDFs. The different mine localities are indicated by shape. Each data point represents an average of >10 microinclusions analyzed in an individual diamond. The compositions of the four HDF types from Table 1 are shown as large **semitransparent circles with black rims**. HDFs with MgO >40 and CaO >35 wt% are presented by open symbols (see also Fig 8a,b); all are from Siberia (Internationalnaya, Ebelyakh), and likely represent a mixture between HDF and micro-mineral inclusions (carbonates/silicates that were not identified in the original studies). See the supplementary compilation of HDF data (Weiss et al. 2022) for classification of the HDF compositional types based on oxide wt% parameters, and for the full database and references.
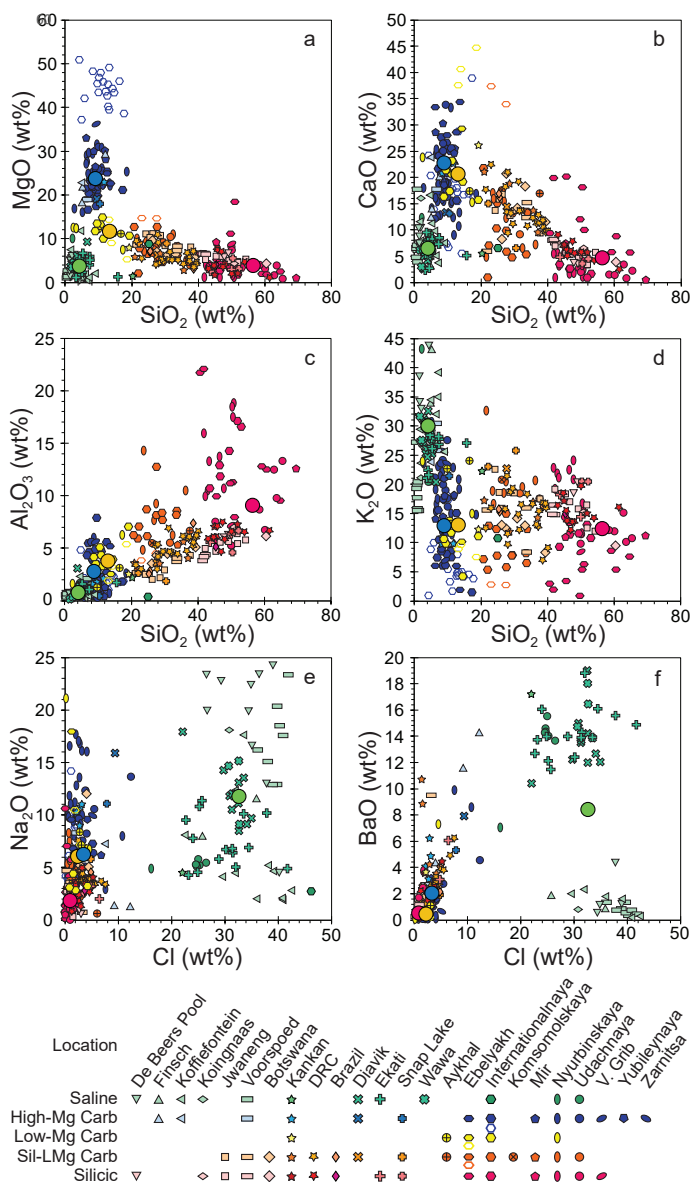
Figure 8. Major oxide variation diagrams of HDF compositions in fibrous diamonds (in wt%, normalized on water- and CO_2-free basis). The compositions of the four HDF types (Table 1) are shown as large **semi-transparent circles with black rims**. (**a**) MgO vs. SiO_2 best expresses the four compositional HDF types: high-Mg carbonatitic HDFs with very high MgO, low silica and alumina, silicic to low-Mg carbonatitic composition with varying amount of carbonates and saline HDFs that carry mostly K, Na, Cl and water and are depleted in carbonates and silicates. **Open symbols** represent HDFs from Siberia with MgO >40 and CaO > 35 wt% (See Fig. 7 for explanation). (**b–d**) CaO, Al_2O, and K_2O vs. SiO_2; note the high-Al trend and low K_2O values of some HDFs from Siberia compared to similar HDF compositions from all other localities. (**e, f**) Na_2O and BaO vs. Cl show large variations in Na_2O of saline HDFs, and the distinction between high-Ba saline compositions of Canadian (and Siberian) and low-Ba ones of South African HDFs. Full data and references are provided as a supplementary compilation of HDF data (Weiss et al. 2022).
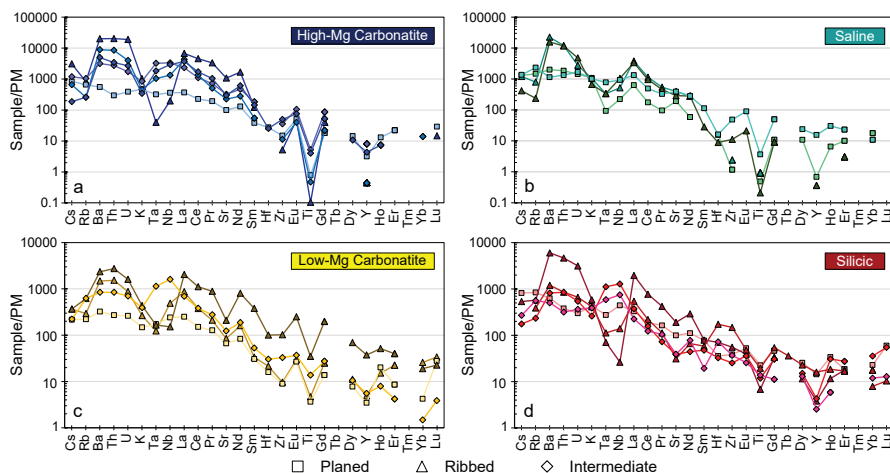
Figure 9. Primitive-mantle (PM)-normalized trace-element patterns of representative saline, silicic, low-Mg carbonatitic and high-Mg carbonatitic HDFs. Two repeating patterns of enrichment in the most incompatible elements are observed in all HDF compositional types: 'Ribbed' with LILE and LREE enrichments and HFSE and alkali depletions similar to calcalkaline magmas and continental crustal rocks, and 'Planed' which has lower LILE and LREE abundances and 'smoother' overall patterns similar to oceanic basalts. Intermediate patterns with a positive Ta–Nb anomaly are also observed in all HDF types. See sections '*Trace element compositions*' for additional details and '*Trace element analysis*' for the conversion of concentration in the diamond to concentration in the HDF. Primitive-mantle (PM) values are from McDonough and Sun (1995).

Major element composition

The compositional space spanned by HDFs in fibrous diamonds is huge, from highly silicic melts to carbonatitic and saline compositions. The high water and carbonate content distinguishes them from any of the melts we know at the surface such as basalts or granites and even from erupted kimberlites, lamproites, or carbonatites. Yet, fibrous diamonds from mines all over the world carry the same four types of HDFs (see '*Geographical distribution of HDFs'* below). The major element composition of all diamonds is presented in Figs. 7 and 8, and in the Supplementary compilation of HDF data Excel file that accompanies this paper (Weiss et al. 2022). Tables 1–4 present the composition of the four HDF types. These compositions (shown in Figs. 7 and 8) were compiled by averaging 11–37 diamonds for the various HDF types, ignoring isolated extreme analyses.

The tables present the compositions in four ways. Table 1 provides the major elements that were measured by EPMA normalized to 100 wt% and allowing for excess oxygen due to chlorine ($Cl*15.999/2/35.45$). This is the standard way to present the composition, avoiding the uncertainty associated with the IR determination of water and CO_2. The **silicic** HDFs are highly siliceous ($SiO_2 = 57$ wt%, with some HDFs reaching up to 65 wt%), and rich in K_2O (12.4 wt%, with more scatter and values up to 22 wt%) and Al_2O_3 (10 wt%). Many diamonds form a continuous array between this component and **low-Mg carbonatitic** HDFs that are richer in CaO, FeO and MgO (up to 15 wt% MgO). **High-Mg carbonatitic** HDFs form a distinct group, especially through their very high MgO (>15 wt%). CaO (~20 wt%) and FeO (~14 wt%) are also high, while SiO_2 and Al_2O_3 are low (9 and 3 wt% respectively). The K_2O content varies between localities (see '*Geographical distribution of HDFs*' below; Fig. 8d) with some carrying more than 20 wt%, while many others only contain 5–12 wt% K_2O. The **saline** HDFs are mostly (K,Na)Cl with a few percent of Fe-, Ca-, Ba- and Mg-carbonates and little SiO_2, Al_2O_3, TiO_2 and P_2O_5. The BaO concentration in Table 1 averages two distinct

groups, saline HDFs with high BaO (~13 wt%) in Canadian and Russian diamonds and those with low BaO content (~1 wt%) in South-African diamonds.

In Table 2 we added the calculated CO_2 (based on the EPMA analysis, see section '*H_2O and CO_2 in the HDFs: Connecting EPMA and FTIR*' above) and the H_2O components (based on the IR data) and renormalized to 100 wt% (again accounting for excess oxygen due to chlorine). These two values are less accurate but are useful for understanding the nature of the HDFs. CO_2 makes up 25 and 32 wt% of the low- and high-MgO carbonatitic HDFs, respectively, but only 11 wt% of the saline HDFs and <5 wt% of the silicic ones. The water content of the HDFs varies between 8 wt% in the high-Mg carbonatitic HDFs to 21 wt% in the saline ones. We note that the water content we calculate depends on the choice of the absorption coefficient, which is not well constrained. The results presented here were calculated using the high value of $\varepsilon_{water} = 109$ (AU/cm)/(mole/liter). If the lower value is used the water content increases by a few percent, and up to ~26 wt% in the saline endmember.

Table 3 presents the data in atomic proportions. The water content was normalized to 55.5 moles or 1 kg of water, so all elements are in molal concentration (moles/1 kg water). With 1.6 to ~4.6 ions per water molecule, it is clear that the HDFs are not hydrous solutions, but rather melts or supercritical fluids with a high content of carbonate and water. To get a feeling for the nature of these melts, Table 4 groups the various components by their anions: silicates, carbonates (including both metal and carbonate ions), phosphates, halides and water. Together, the HDFs show a wide range of miscibility among the various components. Carbonate and water are always present. Phosphate is always a minor constituent. Silicates and halides are variable but also appear in all HDFs. During analysis, the best way to distinguish an HDF from a micromineral inclusion is that the HDF analysis carries all the major elements.

The sole indication for the presence of sulfide HDFs in diamonds is provided by three fibrous diamonds from Yubileinaya, Siberia (Klein-BenDavid et al. 2003). The diamonds contain carbonatitic HDF with $CO_2/(CO_2+H_2O)$ ratio between 0.26–0.65, but also carry other microinclusions rich in S, Ni and Fe with Ni/(Ni+Fe) that ranges between 0.3–0.7. The S/(S+Ni+Fe) ratio of individual inclusions varies between 0.35–0.64, suggesting that this is a melt rather than a mineral composition. The presence of small amounts of alkali elements and Mg are indicative of a melt as well. The sulfide melts coexist with carbonatitic HDFs, but the data is insufficient for defining the relation between the two fluids. TEM studies of microinclusions in other diamonds (e.g., Logvinova et al. 2019a) showed that sulfides, if present, make up only a trivial fraction of most inclusions.

Trace element composition

Trace element abundance patterns of HDFs (Fig. 9) reveal very high concentrations of incompatible elements relative to primitive mantle (PM) values. The REE are fractionated and variable, mostly negative anomalies exist for the alkali elements (K, Rb, and Cs), high field strength elements (HFSE: Ti, Zr, Nb, Hf, Ta), Sr and Y relative to elements of similar compatibility (e.g., Schrauder et al. 1996; Zedgenizov et al. 2007, 2009, 2011; Tomlinson et al. 2009; Weiss et al. 2009, 2013b; Skuzovatov et al. 2012 ; Smith et al. 2012; Klein-BenDavid et al. 2014; Gubanov et al. 2019; Timmerman et al. 2019). A closer look reveals two main patterns (see below), which are present in all the four HDF types.

Correlations between the trace element composition and HDF types were only identified within a few studies, and mainly within diamonds of the same locality. Namely, the concentrations of Rb, Cs, Ba, Th, U, LREE and Sr decrease linearly from silicic to low-Mg carbonatitic HDFs in diamonds from Jwaneng, Botswana (Schrauder et al. 1996). Similarly, La/Dy ratios decreasing from silicic to low-Mg carbonatitic compositions were observed in HDFs in diamonds from Yakutia, Siberia, (Zedgenizov et al. 2007, 2009, 2011). These observations suggest that carbonate-rich HDFs are more enriched in incompatible elements than silicic ones.

Conversely, Ba, U and Th concentrations and La/Dy ratios all increase from silicic to low-Mg carbonatitic HDFs in diamonds from Kankan, Guinea (Weiss et al. 2009). Compared with the silicic to low-Mg carbonatitic array, the high-Mg carbonatitic compositions exhibit the highest (Nb,Ta,Ba,Th,U)/alkalis, LREE/MREE and LREE/HREE ratios, both in Yakutia and in Kankan (e.g., Zedgenizov et al. 2007; Weiss et al. 2009, 2011; Skuzovatov et al. 2012; Gubanov et al. 2019). In general, high-Mg carbonatitic HDFs in Siberian diamonds are characterized by high levels of Nb and Ta compared to Ba, Th, U, alkalis and LREE contents (i.e., PM normalized $(La,Th,Ba,U)/Nb_{PM}$ ratios <1; Figs. 10 and 11). But lower Nb and Ta levels were recorded in some other Siberian diamonds (Zedgenizov et al. 2009, 2011), in diamonds from Kankan and Diavik (Weiss et al. 2011, 2015), and are even lower in high-Mg carbonatitic HDFs from Finsch (i.e., $(La,Th,Ba,U)/Nb_{PM} \gg 1$; Fig. 9; Weiss and Goldstein 2018).

The saline HDFs are distinct from the other types. This is seen in their elevated La/Pr and La/Dy ratios compared to all other HDFs (Fig. 11); Th/U and Ba/U ratios are also higher in the saline HDFs. Moreover, a few studies pointed out that the Sr* $(Sr/\sqrt{(Pr \times Nd)})_{PM}$ anomaly is positive for most saline HDFs and negative for all other types (Fig. 11d; Klein-BenDavid et al. 2014; Weiss et al. 2015). Similarly, the Eu* anomaly (expressed here as Eu/Sm_{PM}, because of the lack of sufficient Gd data) in the saline HDFs is > 1, compared to the majority of all other HDFs, which have either negative anomalies ($Eu/Sm_{PM} < 1$) or no anomaly (Fig. 11c; Smith et al. 2012; Weiss et al. 2013b, 2015; Klein-BenDavid et al. 2014).

When all the available HDF trace element data are examined (Supplementary compilation of HDF data, Weiss et al. 2022), the observed relationship between Ba, Th, U and LREE enrichment and Nb, Ta and alkalis depletion is the most persistent. This is expressed as positive correlations between ratios such as La/Nb, Th/Nb, Ba/Rb and U/K, regardless of the HDF major-element compositions or their host diamond provenance (Fig. 10a,b).

Based on these characteristics, Weiss at al. (2008b, 2013b) identified two main trace element patterns in all four HDF types (Fig. 9). One with large ion lithophile element (LILE) and LREE enrichment, and HFSE and alkali depletion, similar to calcalkaline magmas and continental crustal rocks. The other has lower LILE and LREE abundances and 'smoother' overall trace-element patterns similar to oceanic basalts. These patterns were designated first as 'Tables' and 'Benches' (Weiss et al. 2008b), and later as 'fibrous-low' and 'fibrous-high' (Rege et al. 2010) or 'Ribbed' and 'Planed' patterns (Weiss et al. 2013b), respectively. The two are best distinguished using co-variation diagrams of (Th,U)/(Nb,Rb) vs. (La,Ce)/(Nb,Rb) (Fig. 10), where $(La,Th)/Nb_{PM} \approx 100$, $La/Rb_{PM} \approx 25$ and $Th/Rb_{PM} \approx 50$ for the fractionated 'Ribbed' pattern and $(La,Th)/Nb_{PM} \approx 0.5$, $La/Rb_{PM} \approx 0.2$ and $Th/Rb_{PM} \approx 0.5$ for the unfractionated 'Planed' pattern (excluding a few extreme compositions). The two trace element patterns are observed in all four major element HDF types (Fig. 9). Intermediate patterns that vary through the complete range between the two also exist. The consistency of the two patterns in HDFs of differing compositions, from different mantle localities, well separated in space and time, overcomes the small trace element variations between HDF types observed in single localities. This emphasizes the main feature of major-trace element systematics—the trace elements are decoupled from the major element composition of the HDF (Weiss et al. 2013b).

Sr, Nd and Pb isotopic compositions

The pioneering work of Akagi and Masuda (1988) provided the first Sr isotope data of HDFs in five diamonds from DRC. The $^{87}Sr/^{86}Sr$ ratios ranged between 0.7038 to 0.7052 and showed no correlation with $^{87}Rb/^{86}Sr$ values indicative of an isochronous relationship. Similarly, all later studies of HDFs from Botswana, Canada, Siberia, DRC, and Guinea (42 diamonds in total), yielded no Rb–Sr isochron systematics (Klein-BenDavid et al. 2010, 2014; Smith et al. 2012; Weiss et al. 2015).
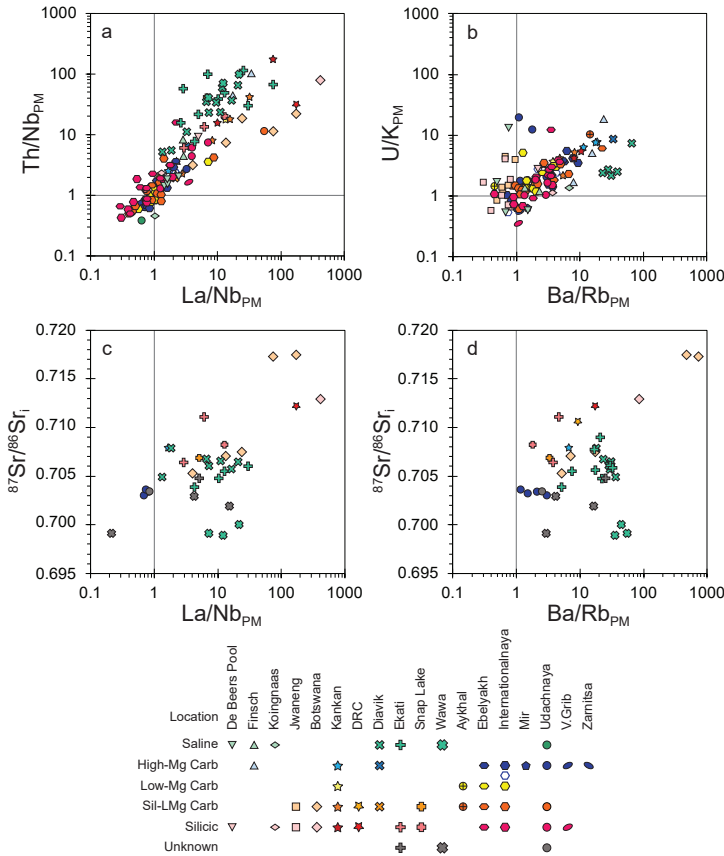
Figure 10. Trace element and Sr isotope ratios of HDFs in fibrous diamonds. The observed relationships between La/Nb, Th/Nb, Ba/Rb and U/K (**a, b**) reflect the variation between the two incompatible element patterns, 'Ribbed' and 'Planed' (Fig. 9), that characterize HDFs, regardless of their major-element compositional type or their host diamond provenance. It emphasizes the decoupling of trace elements from the major element composition of the HDF. Despite the relatively small number of available radiogenic isotope analyses of HDFs, silicic to low-Mg carbonatitic HDFs (as well as high-Mg carbonatite compositions) show a broad correspondence between initial $^{87}Sr/^{86}Sr_i$ isotope values and incompatible element ratios (**c, d**), which suggests a relationship between metasomatic enrichment of the source rocks and the elevated $^{87}Sr/^{86}Sr$ signature. PM - primitive mantle values of McDonough and Sun (1995).

Saline HDFs in diamonds from the ~2.7 Ga Wawa deposit (Smith et al. 2012) show very low initial $^{87}Sr/^{86}Sr$ ratios ($^{87}Sr/^{86}Sr_i$ = 0.699–0.703, Fig. 10c). In contrast, all four types of HDFs from Phanerozoic kimberlites span a wide range of $^{87}Sr/^{86}Sr_i$ ratios, from MORB-like depleted values (i.e., 0.703–0.704) to more radiogenic compositions. Highly radiogenic compositions of $^{87}Sr/^{86}Sr_i$ >0.710 and up to 0.723 are observed solely in silicic to low-Mg carbonatitic HDFs (Fig. 10c,d; Klein-BenDavid et al. 2010, 2014). These HDFs, mainly in DRC and Botswanan diamonds, also exhibit positive correlations between Sr isotopic composition and trace element concentrations. Klein-BenDavid et al. (2010, 2014) suggested that the correlation indicates a relationship between metasomatic enrichment of the source rocks and the elevated $^{87}Sr/^{86}Sr$ signature of HDFs derived from these sources. For silicic to low-Mg carbonatitic HDFs, a general and robust relationship is apparent between higher $^{87}Sr/^{86}Sr$ isotopic values and elevated La/Nb, Th/Nb and Ba/Rb ratios (Fig. 10c,d). Similar systematics exist for high-Mg carbonatitic compositions. These relationships suggest that a
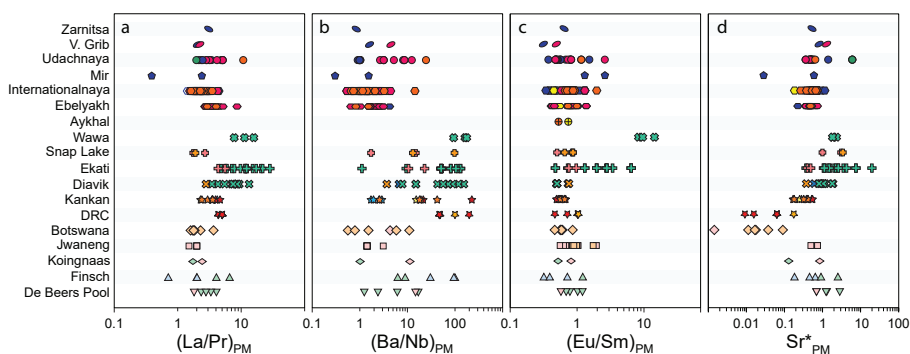
Figure 11. Comparison of La/Pr, Ba/Nb, Eu* (expressed here as Eu/Sm) and Sr* (Sr/√(Pr×Nd)) anomalies of HDFs from different mines and lithosphere provinces. Symbol color relates to HDF composition: saline HDFs are shown in **green** and high-Mg carbonatitic HDFs in **blue**. Low-Mg carbonatitic HDFs are shown in **yellow**, silicic HDFs in **red** and intermediate compositions between them in **orange**. For additional information refer to the legend of Fig. 8. PM – concentrations are normalized to the primitive mantle values of McDonough and Sun (1995).

radiogenic Sr isotopic signature is related to a more strongly fractionated ('Ribbed') trace element pattern within HDFs of the same type. Saline HDFs from the Northwest Territories (Ekati and Diavik) do not show these relationships; rather they exhibit positive correlations between $^{87}Sr/^{86}Sr_i$ and Th/U, La/Pr, and La/Sm, as well as Sr* and Eu* anomalies (see Fig. 3 of Weiss et al. 2015).

Radiogenic isotopic data for Nd and Pb from HDFs are very scarce, only five diamonds (all silicic to low-Mg carbonatitic) were analyzed for their Nd and only three for their Pb isotopic composition (Klein-BenDavid et al. 2010, 2014). The $^{143}Nd/^{144}Nd$ ratios range between 0.5118 to 0.5105 and correlate negatively with the Sr isotopic composition. The few diamonds analyzed for Pb isotopic compositions display high $^{207}Pb/^{204}Pb$ ratios (15.62–15.67) compared to depleted MORB mantle (DMM) or kimberlites and modest $^{206}Pb/^{204}Pb$ ratios (17.87–18.12), placing them at a slightly more radiogenic position than calculated primitive mantle sources (Kamber and Collerson 1999; Murphy et al. 2003; Klein-BenDavid et al. 2010, 2014).

Noble gas compositions

Fibrous diamonds are highly enriched in noble gases. Crushing yields ^4He concentrations of 10^{-6}–10^{-5} cm^3 STP/g and ^{40}Ar between 10^{-7}–10^{-6} cm^3 STP/g (Burgess et al. 1998; Broadley et al. 2018; Timmerman et al. 2018b, 2019; Weiss et al. 2021). In most cases, similar concentrations were measured by fibrous diamond graphitization (Ozima and Zashu 1991; Wada and Matsuda 1998; Burgess et al. 2009), which suggests that most of the gas is trapped in the microinclusions and released by crushing alone. Equivalent high He concentrations were only found in "popping rock" mid-ocean ridge basalts (Moreira et al. 1998). Burgess et al. (1998) combined these data with $^{40}Ar/K$ and $^4He/^{40}Ar*$ (*corrected for atmospheric ^{40}Ar) and determined that He and Ar are present in the trapped HDFs (rather than HDF+diamond) at concentrations of 10^{-3} cm^3 STP/g, corresponding to enrichment by 3 orders of magnitude over present-day upper mantle values.

The $^3He/^4He$ isotopic ratios of HDFs in most analyzed diamonds from Africa, Siberia, and Canada vary between 2–8 Ra (the atmospheric ratio of 1.39×10^{-6}; Burgess et al. 1998, 2009; Weiss et al. 2017, 2021; Timmerman et al. 2018b), similar to the range of MORB ($^3He/^4He$ = 8 ± 1 Ra; Graham 2002), recycled subducted surface material (Kurz et al. 1982) and subcontinental lithospheric mantle (SCLM, 6.1 ± 2.1 Ra; Day et al. 2015). Only a few HDFs have higher ratios (10–11.2 Ra) or lower, radiogenic values of <1 Ra (Burgess et al. 1998;

Broadley et al. 2018; Timmerman et al. 2019; Weiss et al. 2021). Broadley et al. (2018) suggested that the variation between SCLM and the upper range of ^{3}He/^{4}He ratios of the HDFs reflects a mixture between lithospheric and deep volatile noble gas components originating from a mantle plume, whereas ^{3}He/^{4}He<1 was postulated to result from the accumulation of radiogenic ^{4}He atoms produced by α-decay of U and Th (Burgess et al. 1998). Weiss et al. (2017) showed that ^{3}He/^{4}He ratios of HDFs correlate negatively with the amount of K_2O and positively with the carbonate component in fibrous diamonds from Africa, which reflects increasing ^{3}He/^{4}He from saline to low-Mg carbonatitic to high-Mg carbonatitic HDFs. Exceptional are the South African silicic and carbonatitic HDFs which have much lower ^{3}He/^{4}He compared to silicic and carbonatitic compositions from Botswana and Guinea, to the degree that their ^{3}He/^{4}He ratios are lower (more radiogenic) compared to diamonds with saline HDFs from the same locations. This could suggest a complex evolution of the source of the fluids or represent different metasomatic events at different times over the history of the local continental mantle. The latter alternative is consistent with the observed negative correlation between ^{4}He contents and Ra values and positive correlation with increasing U–Th concentrations in HDFs from South Africa and DRC (Timmerman et al. 2018b, 2019).

It was suggested that by combining He isotope analyses with U–Th-He abundance measurements, the geochronology of HDF-bearing diamonds and C–O–H metasomatism can be constrained (Weiss et al. 2017; Timmerman et al. 2019). Indeed, the slope of ^{4}He vs. U–Th variation of HDFs in the few DRC diamonds deviates from the ~70 Ma eruption age of their possibly related kimberlite, indicating that these diamonds formed 10 to several hundred Myr before their host kimberlites (Timmerman et al. 2019). However, that study did not take into account the possibility of diffusive loss of He, which is critical for a meaningful interpretation of (U–Th)/He data and for constraining ages (Farley 2002). The issue was recently addressed by Weiss et al. (2021), who showed that the budget of He in a diamond is affected by diffusion over geological time scales. Taking into account the impact of possible He diffusion on the ^{3}He/^{4}He ratios of South African diamonds and considering the thermal and tectonic history of the Kaapvaal craton, they suggested an upper limit of ~$1.8 \pm 0.2 \times 10^{-19}$ cm^2/s for the diffusivity of He in fibrous diamonds. This diffusion limit provides a means to directly place an upper and lower limit on the timing of diamond crystallization and C–O–H metasomatism of the SCLM. For the analyzed diamonds from South Africa, it constrained the timing of diamond formation during three metasomatic events in the late-Mesozoic, Paleozoic and Proterozoic, each by a different HDF type (saline, silicic and carbonatitic, respectively; Weiss et al. 2021).

The ^{40}Ar/^{36}Ar values of fibrous diamonds are high, typically >3000, and reach values above 40,000 (Turner et al. 1990). Wada and Matsuda (1998) showed that in fibrous diamonds from DRC, such isotopic variation form a trend with ^{36}Ar concentrations, between air-like Ar (^{36}Ar > 10^{-9} cm^3 STP/g and ^{40}Ar/^{36}Ar ≈ 3 00; Lee et al. 2006) and a mantle component similar to MORB 'popping rock' source (^{36}Ar < 10^{-10} and ^{40}Ar/^{36}Ar >30,000; Moreira et al. 1998). However not all fibrous diamonds fall on such a trend, as evident by those from Canada which exhibit high ^{36}Ar and high ^{40}Ar/^{36}Ar (Johnson et al. 2000; Burgess et al. 2009). These isotopic values indicate that the high content of ^{36}Ar in the HDF microinclusions is derived from their mantle source. ^{20}Ne/^{22}Ne and ^{21}Ne/^{22}Ne ratios reach values up to ~11 and ~0.06, respectively (Wada and Matsuda 1998; Broadley et al. 2018). Within the ^{20}Ne/^{22}Ne–^{21}Ne/^{22}Ne space, the HDFs Ne isotopic compositions are distinct from those of air and fall between the air–MORB mixing line and the air–solar mixing line. For Xe, the ^{129}Xe/^{130}Xe vs. ^{136}Xe/^{130}Xe isotopic ratios of a few fibrous diamonds from DRC correlate and lie on a mixing line defined by air and MORB (Wada and Matsuda 1998). Timmerman et al. (2018b, 2019) are the only available studies thus far that provide information about noble gases heavier than He for fibrous diamonds with known HDF compositions. Using the crushing technique, these authors measured ^{40}Ar/^{36}Ar

ratios between 480–3600 for fibrous diamonds containing silicic to low-Mg carbonatitic HDFs, $^{40}Ar/^{36}Ar$ ratios between 390–1940 for high-Mg carbonatitic HDFs, and values in the range of 380–30,000 for saline compositions. The $^{40}Ar/^{36}Ar$ ratios obtained by step-heating diamond graphitization of a few of the silicic to low-Mg carbonatitic HDFs yielded values that varied between 670 and 15,400 (Timmerman et al. 2019). $^{129}Xe/^{130}Xe$ vs. $^{136}Xe/^{130}Xe$ isotopic compositions of all HDF types in 7 diamonds that they analyzed lay on mixing lines between air and MORB or air and crust (Staudacher and Allègre 1982). Timmerman et al. (2018b) noted that the $^{36}Ar/^{130}Xe$ and $^{84}Kr/^{130}Xe$ ratios for the analyzed saline, silicic to low-Mg carbonatitic, and high-Mg carbonatitic HDFs all fall in the compositional field for sea-water, sediments, and crustal endmembers and are distinct from atmospheric Ar/Xe and Kr/Xe compositions.

Halogen compositions

Unfortunately, only four diamonds were measured for both their major element and halogen compositions (Jwaneng diamonds analyzed by Schrauder and Navon 1994 and Johnson et al. 2000). However, K is commonly analyzed together with the halogens and its concentration in the HDFs is overall uniform, allowing for the use of K/Cl to identify the type of the HDF and normalize the results. The average K/Cl of diamonds from the Ekati mine, Canada (Johnson et al. 2000; Burgess et al. 2009) is close to one, which is suggestive of saline HDFs, similar to most major element analyses of diamonds from that mine (Fig. 12).

Cl concentrations in the Ekati HDFs vary between 20–35 wt%, the Br content of most samples is 1000–2000 ppm, with Br/Cl ratios of 0.001–0.003. Some diamonds reach Br levels of up to 3 wt% and extreme molar Br/Cl ratios (up to 0.063, Johnson et al. 2000). Iodine is also enriched: 10–30 ppm and I/Cl of 1–3×10^{-5} in most samples, and up to 1200 ppm and I/Cl = 1.7×10^{-3} in the most fractionated sample. The ratios of most samples fall close to the MORB field and extend towards values typical of altered oceanic crust. However, Br concentrations are highly enriched in comparison to PM (~$10^4 \times$ PM) and even more in
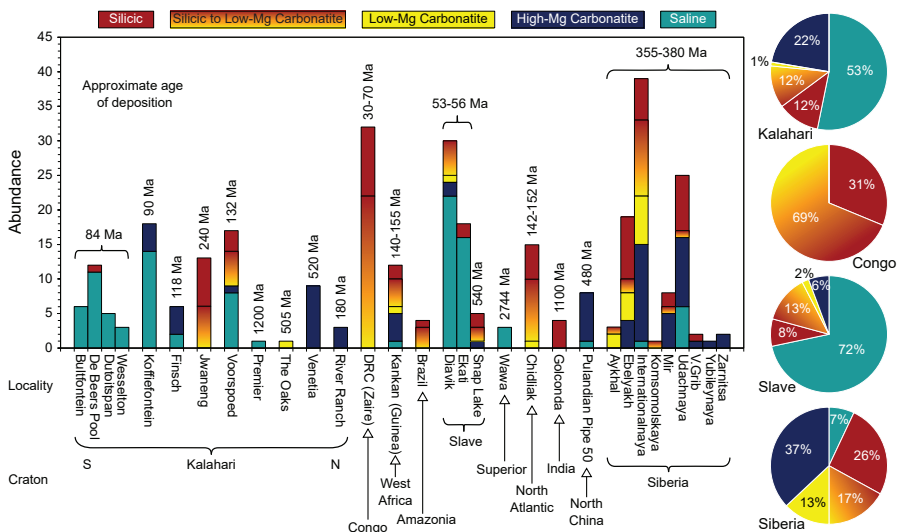

Figure 12. Worldwide abundance and distribution of HDF compositions, separated by locations and cratons. Relative abundances are presented for selected cratons. The database for this figure includes available published sources (Weiss et al. 2022) and data for Bultfontein, Dutoitspan, Wesselton, Premier, The Oaks, River Ranch (Weiss, unpublished data); Venetia (Kempe et al. 2021b); Chidliak (Elazar and Weiss 2021); Golconda (Schrauder 1997) and Pulandian (Mershon et al. 2021). The Kalahari Craton includes the Kaapvaal and Zimbabwe Cratons with the Limpopo Belt between them.

comparison to the depleted MORB reservoir. Iodine is enriched to levels of $1500–2500 \times$ PM. Separation of a saline fluid from a silicate melt was proposed as a possible reason for the extreme values (Burgess et al. 2009). Fractionation of halides, which was observed experimentally (Förster et al. 2019) may also play a role in removing Cl, K and Na and enrich the residual fluid in Br and I (Johnson et al. 2000).

Diamonds from DRC, Jwaneng (Botswana) and Aikhal (Siberia) have K/Cl of 2–10 and are silicic to low-Mg carbonatitic. Assuming K_2O content of 13 wt%, (Table 2), we obtain Cl concentration of 1–3 wt%, similar to the EPMA measurements, 30–60 ppm Br, and 1–3 ppm I (with some diamonds reaching up to 17 ppm). Br/Cl ratios vary between $1–2 \times 10^{-3}$, close to the seawater value, somewhat higher than MORB and similar to altered oceanic crust (Burgess et al. 2009; Broadley et al. 2018). I/Cl ratios of $0.5–3 \times 10^{-5}$ are higher than seawater and span a broad area with MORB values at the center (see Fig. 5 of Burgess et al. 2009). These ratios represent enrichment of 300–800 over the PM value for Cl, $250–700 \times$ PM for Br and 80–300 for I, similar to levels of other incompatible elements. Halogen concentrations are extremely high in saline HDFs, though they are highly enriched in the other types as well. Such enrichment in halogen concentrations and elevated Br/Cl and I/Cl ratios further strengthen the argument for the involvement of a subducted component in the generation of HDFs.

High-density fluid microinclusions in non-fibrous diamonds

The formation mechanism for fibrous diamonds from the HDFs they trapped is broadly accepted, whereas the mode of formation of NFMC diamonds is less clear. The differences in texture, nitrogen aggregation and age, as well as the tight carbon isotopic composition of fibrous diamonds relative to the wide range of NFMC and polycrystalline diamonds, left the door open for other mechanisms of growth. Thus, it is interesting to examine whether HDFs, their fingerprints, or other fluids are found in non-fibrous diamonds.

Bulanova et al. (1988) and Novgorodov et al. (1990) reported 10–30 μm inclusions of potassium aluminosilicate glasses associated with inclusions of K-feldspar and other eclogitic minerals in colorless NFMC diamonds from Mir. Shatsky et al. (2019) reported two melt+clinopyroxene inclusions, with a SiO_2- and Al_2O_3-rich bulk composition, in two alluvial NFMC diamonds from Ebelyakh, Siberia. A single microinclusion composed of Fe, Si, P, Mg, K, Ca, Al and carbonate was identified by Jacob et al. (2011) in a FIB foil cut from a polycrystalline framesite from Orapa, but no additional information was provided. Using TEM on foils cut from Juina (Brazil) NFMC diamonds, Kaminsky et al. (2009, 2013) described a suite of HDF-related multiphase inclusions, mostly smaller than 1 μm in size. The suite included carbonates (magnesite, $Na_2Mg(CO_3)_2$ and Ba- and Sr-carbonates), phosphates, phlogopite, chlorides, fluorides, sulfides and pores (that probably included residual low-density fluids), and was designated: carbonate-halide association.

Weiss et al. (2014) were the first to identify HDFs, similar to those found in fibrous diamonds, within NFMC diamonds. They found and analyzed two microinclusion-rich layers near the edge of an NFMC Finsch diamond and used X-ray topography to show that the diamond is monocrystalline throughout. The inner layer carried carbonatitic HDFs, while the outer layer was saline. They also characterized six saline inclusions in the NFMC core of a coated diamond from Kankan. Recently, Kempe et al. (2021a) identified 3 silicic microinclusions in the NFMC core of a coated diamond from Voorspoed. A systematic search for inclusions in NFMC diamonds was conducted by Jablon and Navon (2016), who examined twinning planes of 30 twinned diamonds (macles) from Venetia and Voorspoed, as well as the diamond adjacent to the planes. Inclusions were absent in the majority of diamonds however, 32 shallow, subsurface microinclusions were identified in 8 of the macles. All were found where the twinning plane formed corners. Twelve inclusions in two diamonds carried

submicrometer orthopyroxene and a K–Mg carbonate. The other 20 carried HDFs. Twelve inclusions in four Venetia diamonds carried high-Mg carbonatitic HDF and a silicic inclusion was found in another. In Voorspoed, three saline microinclusions were found in one diamond, and four silicic to carbonatitic ones in another. The level of nitrogen aggregation of the inclusion-bearing diamonds is the same as that of other 40 macles and 23 octahedral diamonds from the same batch. This is true for both localities (Jablon and Navon 2016).

Larger carbonate inclusions were found in a few Siberian diamonds. Sobolev et al. (1997) reported phlogopite associated with calcite (and dolomite, see Sobolev et al. 2009) in three NFMC diamonds from the Sputnik kimberlite. They did not provide the proportions of the two phases, but the combined composition of $CaCO_3$ and phlogopite brings the analysis close to that of silicic–carbonatitic HDFs. On a TiO_2 vs. Mg# diagram, the phlogopites fall in the eclogitic field that is associated with the silicic–carbonatitic HDFs (Sobolev et al. 2009). Raman spectroscopy of a particularly large ($43 \times 30 \times 23$ µm) carbonate inclusion in a NFMC diamond (Logvinova et al. 2019b) revealed that it consists of three distinct carbonates, which according to TEM-EDS analyses have a combined bulk composition of $0.1(Na_{0.5}K_{1.5})CO_3 \cdot 0.9(Ca_{0.57}Mg_{0.43})CO_3$. This is very close to the composition of high-Mg carbonatitic HDFs, but with slightly elevated CaO content and no measurable SiO_2, Al_2O_3, TiO_2, BaO or Cl, which are normally present at the few wt% level in such HDFs.

Aiming their micro-Raman at the interface between mineral inclusions and the host NFMC diamond, Nimis et al. (2016) characterized bands of $Si_2O(OH)_6$ and $Si(OH)_4$ at 650 and 800 cm^{-1} as well as water bands at 1650 and >3300 cm^{-1}. These bands are caused by a thin film of a hydrous residual fluid with dissolved silicates. The presence of the thin layer (<1.5 µm) of low-density material at the diamond-inclusion interface was confirmed by X-ray tomography. CO_2 could not be identified as its Raman bands are too close to the intense diamond line. Neither CH_4 nor N_2 were detected.

Another line of evidence for the presence of HDFs in NFMC diamonds derives from trace element analysis. Early efforts were reviewed in section '*Trace elements analyses*' above. A major improvement came with the introduction of the off-line laser ablation method (McNeill et al. 2009; Klein BenDavid et al. 2010). McNeill et al. (2009) studied gem-quality NFMC diamonds from South Africa, Siberia and Venezuela, distinguished between a group enriched in Ba, U and La over Nb and another with smoother, less fractionated patterns, and concluded that the two groups bear resemblance to HDFs in fibrous diamonds (Weiss et al. 2008a,b). Melton et al. (2012) examined fragments of 10 clear NFMC diamonds that carried garnet inclusions. The trace element abundance pattern of the diamond richest in trace elements was similar to that of HDFs in fibrous diamonds. Krebs et al. (2019) conducted a more comprehensive study of gem and near-gem NFMC diamonds from Finsch and Newlands mines, South Africa. They reported that they "see the same spectrum of fluids in both high-purity gem and near-gem diamonds that was previously documented in fibrous diamonds. 'Planed' and 'Ribbed' trace element patterns characterize not only the HDF inclusions in fibrous diamonds but also in gem diamonds". Another significant result of this study was the identification of similar patterns in silicate-bearing and sulfide-bearing NFMC diamonds from the Victor mine, Canada. Timmerman et al. (2019b) reached a similar conclusion for silicate- and sulfide-bearing NFMC diamonds from the Koffiefontein, Letlhakane and Orapa mines, South Africa; their trace element signatures are similar to those of fibrous diamonds and they record both 'Planed' (unfractionated) and 'Ribbed' (significant inter-element fractionation) patterns.

There is little evidence for other fluids trapped in NFMC diamonds. Chepurov et al. (1994), Tomilenko et al. (1997) and Smith et al. (2014, 2015) reported the presence of CO_2, N_2 and hydrocarbons in secondary fluid inclusions, larger than 1 µm, along healed cracks in diamonds from North-East Siberia and Africa. Nanoinclusions carrying solid molecular nitrogen were

described in sublithospheric diamonds from Juina, the Urals and South Africa (Kagi et al. 2016, Rudloff-Grund et al. 2016, Navon et al. 2017, Sobolev et al. 2019). Navon et al. (2017) suggested that they formed by exsolution of nitrogen from the diamond matrix and not by direct trapping of nitrogen-rich fluid. Solid CO_2 was reported in diamonds from Colorado (Chinn et al. 1995a,b) and an unknown source (Schrauder and Navon 1993). Mixed-habit diamonds from Zimbabwe contain measurable CH_4 (Smit et al. 2016) and Smith et al. (2016) found thin films of CH_4+H_2 around metallic inclusions in clear sublithospheric diamonds.

In summary, the present dataset of direct measurements of fluids and trace elements in NFMC diamonds clearly shows the presence of HDFs similar to those found in fibrous diamonds. Evidence for other fluids are sporadic and their source is less clear.

TEMPORAL AND GEOGRAPHICAL DISTRIBUTION OF HIGH-DENSITY FLUIDS

Temporal distribution of high-density fluids

A decade ago, the prevailing concept on the formation of fibrous diamonds and their HDFs asserted that they formed episodically in the mantle, close in time to the eruption of their host kimberlite over the last ~500 Ma. This assumption, that fibrous diamonds are young, was based on the short mantle residence time of fibrous diamonds at mantle temperatures, as evident by their low nitrogen aggregation (~100% A-centers, no B-centers and no platelets; Fig. 2), and the Phanerozoic emplacement ages of most kimberlites that carried these diamonds to the surface (e.g., Boyd et al. 1987; Navon 1999; Faure 2010; Gurney et al. 2010). However, in recent years, new data changed this idea: a) even diamonds with only A-centers may survive for many millions of years at 900–1000 °C (Fig. 2); b) HDFs were discovered in fibrous diamonds from Proterozoic and Archean deposits; c) fibrous diamonds with both A- and B-centers and platelets were identified at various mines d) in a few mines, nitrogen aggregation indicates several events of fibrous diamond formation, each with its own characteristic HDF type and e) U–Th/He dating of fibrous diamonds yielded ages older than 750 Myr.

The 2.7 Ga metaconglomerates near Wawa (Smith et al. 2012), as well as the 1.2 Ga Premier kimberlite (Weiss unpublished data), host fibrous diamonds that contain HDFs (Fig. 12). This is direct evidence for the antiquity of HDFs and their presence in the mantle at least since late Archean times. The fibrous diamonds, in both localities, have nitrogen in A-centers only, indicative of a short mantle residence time. The HDFs in both cases are solely saline, and more specifically, of the "high-Ba" group (Fig. 8f).

Reports of fibrous diamonds that carry nitrogen in both A- and B-centers came first from the Siberian craton. Nitrogen aggregation ratios varying between 10–70 %B (where %B = $100N_B/(N_A+N_B)$, and N is the nitrogen content in A- and B-centers) were found in fibrous diamonds from the Aikhal, Internationalnaya, Mir, Nyurbinskaya and Udachnaya kimberlites (Zedgenizov et al. 2006, 2009, 2020; Skuzovatov et al. 2011). These diamonds carried silicic to low-Mg carbonatitic and high-Mg carbonatitic HDFs. Later, fibrous diamonds with B-centers were documented at Finsch, De Beers Pool and Voorspoed on the Kaapvaal craton (Weiss et al. 2018; Weiss and Goldstein 2018; Kempe et al. 2021a). The aggregation ratios varied between 10–35 %B, and the diamonds carried all four HDF types (saline, silicic, low- and high-Mg carbonatitic compositions). In these localities, a few generations of fibrous diamonds were identified, each with its distinct HDF composition. Lastly, ratios of 10–40 %B were recently detected in fibrous diamonds from Pulandian, North China craton (a dozen of those carried high-Mg carbonatitic HDFs and one contained saline compositions; Mershon et al. 2021). HDFs were also found in a NFMC diamond from Finsch with 17 %B (low-Mg carbonatitic HDFs; Weiss et al. 2014), and in clear NFMC diamonds from Voorspoed and Venetia with 40–65 %B (saline, silicic to low-Mg carbonatitic and high-Mg carbonatitic HDFs; Jablon and Navon 2016).

Together, all these diamonds indicate much longer mantle residence times compared with the majority of fibrous diamonds that carry only A-centers at similar nitrogen concentrations. They show that fibrous diamond and the HDF they carry are not necessarily connected to kimberlite eruptions and formed episodically over extended geological periods. This is true in various lithospheric provinces and for all four HDF types. The above ideas are supported by the recent U–Th/He geochronology of HDF-bearing fibrous diamonds from the Congo and Kaapvaal cratons, indicating penetration of HDFs and formation and survival of fibrous diamonds in the SCLM over a time span of >1 billion years (Timmerman et al. 2019b; Weiss et al. 2021).

Geographical distribution of high-density fluids

Fibrous diamonds are documented in many localities from all Archean cratons (Fig. 12). This indicates the global distribution, the long history, and the ubiquity of the four HDF types in the deep continental lithosphere. However, some differences exist when comparing the compositions of similar HDF types from various localities.

Silicic to low-Mg carbonatitic HDFs. Silicic to low-Mg carbonatitic compositions were reported from the Kaapvaal craton (Schrauder and Navon 1994; Weiss et al. 2018; Kempe et al. 2021a; Weiss unpublished data), the Congo craton (Navon et al. 1988; Kopylova et al. 2010; Kosman et al. 2016; Timmerman et al. 2019), the West African craton (Weiss et al. 2009), the Amazonian craton (Shiryaev et al. 2005), the Slave craton (Klein-BenDavid et al. 2007; Logvinova et al. 2008b; Weiss et al. 2015), the North Atlantic craton (Elazar and Weiss 2021), India (Schrauder et al. 1994), and the Siberian craton (Klein-BenDavid et al. 2009; Zedgenizov et al. 2009, 2011; Skuzovatov et al. 2016; Gubanov et al. 2019). The Siberian HDFs have the most extreme compositions on both ends of the silicic to low-Mg carbonatitic array, with SiO_2 both >65 and <15 wt% (on a carbonate- and water-free basis; Figs. 7a and 8a). As noted by Elazar et al. (2021) the HDFs from Siberia also form a distinct high-Al trend compared to similar HDF compositions from all other localities/cratons (Fig. 8c). CaO enrichment, while more restricted, is observed for HDFs in Ebelyakh fibrous diamonds (Fig. 8b) and elevated FeO values were recorded for Internationalnaya (not shown). These enrichments are compensated by lower K_2O contents (typically <10 wt%, Fig. 8d), as well as lower P_2O_5 (not shown) and Cl values (Fig. 7b). Another distinction of the Siberian silicic to low-Mg carbonatitic HDFs is their lower (Th,La,Ba)/Nb ratios (Figs. 10a and 11).

High-Mg carbonatitic HDFs. The high-Mg carbonatitic HDFs in Siberian fibrous diamonds (e.g., Klein-BenDavid et al. 2009; Zedgenizov et al. 2009, 2011; Skuzovatov et al. 2016; Gubanov et al. 2019) also show some unique compositional characteristics compared with those from the Slave craton (Klein-BenDavid et al. 2007; Logvinova et al. 2008b), the Kalahari craton (Timmerman et al. 2018a; Weiss and Goldstein 2018; Kempe et al. 2021a,b; Weiss unpublished data), the West African craton (Weiss et al. 2009) and the North China craton (Mershon et al. 2021). At Internationalnaya, Al_2O_3 and FeO contents are higher than at any other locality worldwide (Fig. 8c). All Siberian high-Mg carbonatitic HDFs have lower BaO contents resulting in lower Ba/Rb and Ba/K ratios compared to high-Mg carbonatitic HDFs from other localities/cratons (Figs. 10b and 11). In addition, the general enrichment of incompatible elements in such HDFs from Siberia is moderate, characterized by $La/Sm_{PM} < 20$, compared with values between 20–80 in other localities; (La,Th)/(Nb,Rb) and Sr/Rb show similar behavior, i.e., lower ratios in Siberia compared to other provinces.

Saline HDFs. Saline HDFs were identified in fibrous diamonds from the Kaapvaal craton (Izraeli et al. 2001; Timmerman et al. 2018a,b; Weiss and Goldstein 2018; Weiss et al. 2018; Kempe et al. 2021a; Weiss unpublished data), the West African craton (Weiss et al. 2009), the Slave craton (Klein-BenDavid et al. 2007; Tomlinson et al. 2006; Weiss et al. 2015), the Superior craton (Smith et al. 2012), the North China craton (Mershon et al. 2021), and the Siberian craton (Zedgenizov et al. 2018). No diamonds with saline HDFs were found in the

Congo craton. Saline HDFs from Udachnaya have higher TiO_2 concentrations (~5 wt%), the ones from Koffiefontein are higher in FeO (10–20 wt%), and those from De Beers Pool have elevated Na_2O (mostly >15 wt%), compared to all other localities (Fig. 8e).

A striking dichotomy is observed for BaO (Fig. 8f), which is very high in saline HDFs from the Slave craton (10–18 wt%) and Udachnaya (13–15 wt%), but much lower in those from the Kaapvaal craton (BaO < 8 wt%). HDFs from the 1.2 Ga Premier kimberlite, on the Kaapvaal craton, have the highest BaO concentration (8 wt%, Weiss unpublished data) and those from the > 2.7 Ga Wawa deposit (14–17 wt%) are as enriched as other Canadian HDFs, indicating that high Ba levels in saline HDFs existed for billions of years. The Ba enrichment in the Slave craton HDFs is reflected in higher Ba/Rb and Ba/Nb ratios, which coincide with well-developed fractionated 'Ribbed' trace element patterns of the Slave saline HDFs (i.e., high (La,Th)/(Nb,Rb) and LREE/(MREE,HREE) ratios; Figs. 10a,b and 11).

High-density fluids and lithospheric lithology

The petrology of the source rocks of the HDFs, as well as the wall-rocks they interact with during migration, must be important in determining their major and trace element composition (e.g., Tomlinson et al. 2009; Zedgenizov et al. 2009; Weiss et al. 2011, 2013b; Gubanov et al. 2019). Figure 12 presents the abundances of the various HDF types globally and emphasizes that it varies between localities and cratons. For example, only silicic to low-Mg carbonatitic HDFs were reported in fibrous diamonds from Jwaneng, Botswana (Schrauder and Navon 1994), DRC (mostly from the Mbuji-Mayi area, Navon et al. 1988; Kopylova et al. 2010) and the CH-7 kimberlite at Chidliak (Baffin Island, Canada, Elazar and Weiss 2021). In Jwaneng and Chidliak, an eclogite-dominated source for diamonds is indicated by mineral inclusions in diamonds and kimberlite indicator minerals (Gurney et al. 1995; Pell et al. 2013; Gress et al. 2018; Xia 2018). Similarly, eclogitic minerals dominate the assemblage in Mbuji Mayi diamond inclusions (Mvuemba-Ntanda et al. 1982) and ~90% of the xenoliths are eclogitic (El-Fadili et al. 1999). The association between HDF type and the dominant diamond-host lithology in these three deposits agrees with the strong connection that has been established between silicic to low-Mg carbonatitic HDF compositions and hydrous/carbonated eclogites (see '*Formation of silicic to low-Mg carbonatitic HDFs*' below for details). Similar relations can be identified at other localities, although the correlations are not as defined as in the examples above.

In Siberia, most of the 100 analyzed fibrous diamonds are from the Udachnaya and Internationalnaya kimberlites (25 and 39 diamonds, respectively). In both kimberlites, fibrous diamonds carry all the HDF types (Figs. 7 and 12), but the representation of the various types is not uniform. The proportions of {saline}:{silicic to low-Mg carbonatitic}:{high-Mg carbonatitic} HDFs is 25:36:39 in Udachnaya, and 3:62:35 in Internationalnaya. Peridotite is the predominant diamond host lithology in Yakutian kimberlites, as evident by diamond inclusions and xenoliths (Sobolev 1977; Kharkiv et al. 1997, as cited by Ionov et al. 2010; Sobolev et al. 2004). This explains the predominance of high-Mg carbonatitic HDFs in the two localities, as this HDF type has been linked to a carbonated peridotite source (see '*Formation of high-Mg carbonatitic HDFs*' below for details). However, it cannot account for the significant abundance of silicic to low-Mg carbonatitic HDFs. We also note that saline HDFs are more abundant in fibrous diamonds from the Udachnaya kimberlite, where Cl was detected in melt inclusions in groundmass olivine (Kamenetsky et al. 2009). In comparison, at the Ebelyakh placers the majority of the 19 analyzed fibrous diamonds carry silicic to low-Mg carbonatitic HDFs (90%), with a minor representation of high-Mg carbonatitic (10%) and no saline compositions, quite distinct from the observed proportions in Udachnaya and Internationalnaya (Fig. 12). Within the framework of the apparent relationship between HDF type and diamond-host lithology, these differences follow the known distribution of mineral inclusions in diamonds from the Siberian placers, which are dominated by an eclogitic suite (>70%; Shatsky et al. 2015), compared to largely peridotitic inclusions in diamond at Udachnaya and Internationalnaya (Sobolev et al. 2004).

High-density fluid types in the southwestern Kaapvaal and the central Slave craton are dominated by saline compositions (>80%; Fig. 12). Many of the fibrous diamonds with saline HDFs carry micro-mineral inclusions or mixed mineral-HDF microinclusions and can therefore be assigned to either an eclogitic or a peridotitic paragenesis. Most of those samples are associated with peridotitic hosts (Izraeli et al. 2001; Tomlinson et al. 2006; Klein-BenDavid et al. 2007; Weiss et al. 2015, 2018). This is consistent with the predominance of peridotite in both lithosphere provinces based on mineral inclusions in diamonds and xenoliths abundances (e.g., Gurney et al. 1979; Lawless et al. 1979; Skinner 1989; Stachel et al. 2003; Menzies et al. 2004; Tappert et al. 2005). In the southwestern Kaapvaal, the minority (25%) of saline HDFs associated with micro-mineral inclusions are of eclogitic affinity (most of which are from Koffiefontein; Izraeli et al. 2001; Timmerman et al. 2018a,b; Weiss and Goldstein 2018; Weiss et al. 2018; Weiss unpublished data), while the remaining 75% are associated with peridotitic inclusions. In contrast, in the central Slave eclogitic minerals are only associated with silicic HDFs and only peridotitic minerals are found in diamonds with saline HDFs (Tomlinson et al. 2006; Weiss et al. 2015). High-Mg carbonatitic HDFs are solely linked to peridotitic micro-mineral inclusions in both cratons (including the Witwatersrand East Block of the Kaapvaal; Klein-BenDavid et al. 2004; Weiss et al. 2018; Kempe et al. 2021a; Weiss unpublished data).

In addition, a temporal gap was identified between saline HDFs and other compositional types in the Kaapvaal (Weiss and Goldstein 2018; Weiss et al. 2018, 2021; Kempe et al. 2021a). Such a gap, based on nitrogen aggregation of the host diamonds, was not observed in the central Slave (Tomlinson et al. 2006; Klein-BenDavid et al. 2007; Weiss et al. 2015). In both cases, saline HDFs invaded the lithosphere and interacted with different lithologies, as evident by major and trace elements and isotopic variations of the HDFs, and the HDF-associated micro-mineral inclusions (Izraeli et al. 2001, 2004; Tomlinson et al. 2009; Weiss et al. 2015, Weiss and Goldstein 2018). However, while in the Kaapvaal this fluid-rock interaction did not lead to melting of silicates and formation of non-saline HDFs (Weiss et al. 2018), in the Slave both silicic and carbonatitic HDFs formed by *in situ* melting as the saline HDFs traversed mixed peridotite-eclogite lithosphere (Weiss et al. 2015). This difference in the impact of saline HDF percolation through both lithospheres is attributed to the extremely refractory nature of diamond-bearing harzburgite/dunite in the Kaapvaal, compared to the significantly less depleted Slave lithosphere (as well as the Siberian one; Stachel et al. 2003; Stachel and Harris 2008).

THE FORMATION OF HIGH-DENSITY FLUIDS

Pressure and temperature of fibrous diamond formation

The lithospheric origin of fibrous diamonds is manifested in a few independent lines of evidence:

a) The majority of fibrous diamonds carry high nitrogen concentrations that reside only in A-centers, and most of those with both A- and B-centers have low B/(B+A) ratios (see '*Temporal distribution of HDFs*' above). At the top of the asthenosphere, at ~1400 °C, B-centers would develop in a very short time, a few thousand years or less (Fig. 2, Taylor et al. 1996; Leahy and Taylor 1997), indicating that the fibrous diamonds grew in the lithosphere at cooler temperatures.

b) Based on the shift of the IR peaks of secondary quartz in silicic HDF-bearing diamonds, Navon (1991) estimated that fibrous diamond originated at lithospheric pressures of 4–7 GPa.

c) Geothermobarometry on micro-mineral inclusions that are found together with the HDF microinclusions yielded low temperatures of 1000–1185 ± 200 °C for Koffiefontein fibrous diamonds (Izraeli et al. 2001) and 1000 ± 100 °C for De Beers Pool ones (Weiss et al. 2018). Tomlinson et al. (2006) obtained a range of 930–1010 °C from larger mineral inclusions they

found in fibrous diamonds from Panda. These are all lithospheric temperatures that correspond to pressures of 4–6 GPa along cratonic geotherms (e.g., Hasterok and Chapman 2011), and fall in the lower part of the temperature range obtained from mineral inclusions in NFMC lithospheric diamonds (e.g., Stachel and Harris 2008; Nimis et al. 2020; Nimis 2022).

High-density fluids as low-volume melts

The major and trace element chemistry of the HDFs indicates that they are low-volume melts, e.g., low-degree partial melts, percolating melts that interacted with a large volume of rock, or the very last residue following crystallization of a volumetrically more abundant parental melt. The high levels of enrichment in many incompatible elements can only be reached if the HDFs represent small fractions. Water comprises ~8–21 wt% of the HDFs (Table 2) compared with 100–500 ppm in the primitive mantle (McDonough and Sun 1995), corresponding to enrichment by a factor of 300–1500. Carbon, K and Cl yield similar factors of ~450, 500 and 1,000–10,000, respectively. Even if the source was enriched relative to primitive mantle, the melt/rock ratio must be small. Trace elements reveal similar enrichment in incompatible elements (Fig. 9) as do estimates based on the enrichment in He and Ar (~10^3–10^4, Turner et al. 1990, Burgess et al. 1998). Also, experimental studies of melting of peridotite or eclogite in the presence of CO_2 and/or H_2O have shown that melts of similar major element composition only form close to the solidus (see below).

Trace element abundance patterns of HDFs are best explained by equilibration with mantle peridotite without accessory phases for the 'Planed', and with the presence of mica and titanates for 'Ribbed' patterns (Weiss et al. 2013b). Such equilibration may happen during melting, but also during percolation or crystallization. The higher abundances of Ba, Th, U and LREE in the 'Ribbed' patterns, suggest an even lower fraction of partial melting for such HDFs. This allows for the survival of mica, titanates, and zircon in the source (or their growth during percolation) and leads to the formation of the typical negative anomalies in alkalies, Ti, Nb, Ta, Zr and Hf.

The positive correlation of Sr isotopic ratios with La/Nb ratios (low in 'Planed' and high in 'Ribbed' HDFs, Klein-BenDavid et al. 2014) suggests that the different patterns originate at the source or during percolation, as it is difficult to explain the isotope-trace-element correlation by fractionation. The origin of the 'Planed' patterns with low $^{87}Sr/^{86}Sr$ ratios can be linked to a source in the convective asthenosphere (similar to that of Group I kimberlites and ocean-island basalts, OIBs, e.g., Hofmann 1997; Paton et al. 2007), while the high $^{87}Sr/^{86}Sr$ ratios and the 'Ribbed' patterns reflect old enrichment of the source region that lies, most probably, in the lithosphere (e.g., Smith 1983; Giuliani et al. 2015).

Immiscible separation between the various high-density fluids

Schrauder and Navon (1994) considered three processes for the formation of the silicic to low-Mg carbonatitic HDFs: melting, crystallization, and immiscibility. The immiscibility scenario gained popularity with the discovery of the saline HDFs (Izraeli et al. 2001; Klein-BenDavid et al. 2004, 2007). Klein-BenDavid et al. (2007) pointed out the absence of intermediate compositions between the silicic and the saline endmembers (Fig. 7) and suggested that crystallization of carbonates drives carbonatitic melts into an immiscibility gap where silicic and saline melts segregate. Safonov et al. (2007, 2009) conducted experiments in the $CaMgSi_2O_6$–($CaCO_3$, Na_2CO_3)–KCl system and found such an immiscibility gap. However, in their water-free system, the evolution was from the immiscible saline and silicic melts at high temperatures towards one carbonatitic composition at lower temperatures. Contrasting fluid evolution recorded in zoned diamonds (Shiryaev et al. 2005; Weiss et al. 2009) and the variability of $^{87}Sr/^{86}Sr$ led to the rejection of the immiscibility model (Weiss et al. 2009).

Formation of high-Mg carbonatitic high-density fluids

Zedgenizov et al. (2007, 2009, 2011) reviewed a few possible models for the formation of high- and low-Mg carbonatitic HDFs. They recognized the similarity of the high-Mg compositions to kimberlites, but also pointed out differences between these HDFs and kimberlitic magmas. Following the distinction between low-Mg and high-Mg carbonatitic HDFs (Klein-BenDavid et al. 2009), Weiss et al. (2009, 2011) established a strong connection between high-Mg carbonatitic HDFs and a carbonated peridotite source, based on the results of near-solidus melting experiments (Dalton and Presnall 1998; Dasgupta and Hirschmann 2007; Brey et al. 2008). This is supported by the association of high-Mg carbonatitic HDFs solely with peridotitic micro-mineral inclusions (e.g., Klein-Ben David et al. 2004; Weiss et al. 2018; Gubanov et al. 2019).

In view of the possible connection between high-Mg carbonatitic and saline HDFs (Klein-BenDavid et al. 2004), Weiss et al. (2009) examined potential options for the formation of such an array. Their preferred scenario was the penetration of saline HDF into a carbonated peridotite. The saline component provides a source for K, Cl and Ba, and may provide many of the trace elements of the carbonatitic HDF. Later, Weiss et al. (2011) distinguished between Udachnaya HDFs with high-K_2O and 'Planed' patterns and those from Kankan with low-K_2O and more 'Ribbed' pattern. They emphasized the close similarity of the trace element abundance patterns to those of Group I and Group II kimberlites and suggested that both high-Mg carbonatitic HDFs and kimberlites form by melting of carbonated peridotite, with or without phlogopite. The HDFs represent a lower degree of melting (~0.5% for Udachnaya and ~0.2% for Kankan) compared with Group I and II kimberlites (2% and 0.8%, respectively; see Fig. 6 and 7 of Weiss et al. 2011). Klein-BenDavid et al. (2014) reported the Sr isotope compositions of Udachnaya and Kankan HDFs. The values measured for Udachnaya (0.7043–0.7053) fall in the range of Group I kimberlites, and those measured in a Kankan diamond (0.7079) overlap with Group II kimberlites.

More evidence for the similarities between kimberlites and high-Mg carbonatitic HDFs comes from melting experiments of carbonated peridotite, where the first melt at the solidus is similar in composition to the HDFs (e.g., Dasgupta and Hirschmann 2007) and approaches that of kimberlite at higher melt fractions (e.g., Dalton and Presnall 1998; Brey et al. 2009). In summary, melting of a carbonated peridotite, either due to heating or due to penetration of saline fluids is the preferred scenario for the formation of high-Mg carbonatitic HDFs.

Formation of silicic to low-Mg carbonatitic high-density fluids

The high silica content of the silicic HDFs is not at equilibrium with peridotite and calls for another source rock. Experiments in the eclogite-H_2O system at 4–6 GPa produce highly silicic, water-rich fluids that resemble HDFs (Kessel et al. 2005). Kiseeva et al. (2012) demonstrated that even in the eclogite–CO_2 system, the first melt is silicic, rich in SiO_2, Al_2O_3 and K_2O, which is joined by an immiscible carbonatitic melt at higher temperatures. The carbonatitic melt they produced is low in MgO and its composition resembles that of the low-Mg carbonatitic HDFs, but with low K_2O, reflecting the high CO_2/K_2O ratio of 11 of the starting material (much higher than the mantle value of ~1.5; McDonough and Sun 1995). Other experimental melts in the eclogite–CO_2 system are also close to the low-Mg carbonatitic HDFs (e.g., Hammouda 2003; Yaxley and Brey 2004). The connection between silicic to low-Mg carbonatitic HDFs and eclogites is also supported by the association of such compositions with omphacite and eclogitic garnet micromineral inclusions (e.g., Klein-Ben David et al. 2009; Weiss et al. 2009, 2015; Gubanov et al. 2019). Subducted sediments are another possible source for producing some silicic to low-Mg carbonatitic HDFs (e.g., Bulatov et al. 2014).

Weiss et al. (2009) suggested that the continuous array from the hydrous-silicic to low-Mg carbonatitic HDFs is the result of dissolution of carbonates in H_2O- and K_2O-rich silicic melts with increasing temperature. Litasov et al. (2010) favored evolution in the opposite direction and argue that in an eclogite–CO_2–Cl system, more silicates are dissolved into an initial carbonatitic melt with increasing temperature and degree of melting.

Recently Elazar et al. (2019) have shown that for eclogites containing both water and CO_2 the initial melt is not silicic or carbonatitic, but rather of intermediate composition. They suggested that it is the CO_2/H_2O ratio of the source rather than temperature that controls the position of the near-solidus melt along the silicic to low-Mg carbonatitic array. Dvir et al. (2017) provided evidence that near solidus fluids and melts in the lherzolite–H_2O–CO_2 system also fall close to the central part of the silicic to low-Mg carbonatitic array. In their experiments with CO_2/H_2O ratios of ~0.1 and 0.5 (by weight), the melt of the CO_2-rich composition has higher MgO and lower SiO_2 content compared with the melt of the H_2O-rich one, supporting the role of the source CO_2/H_2O ratio in controlling the silicic–carbonatitic character of the HDF. Further evidence for the control exerted by the source CO_2/H_2O ratio rather than by temperature and the degree of melting is provided by the composition of the HDFs. Silicic and low-Mg carbonatitic compositions have similar levels of K_2O, TiO_2 and Cl (Table 2). Temperature control should lead to increasing melt fraction and dilution of these incompatible elements, but such a trend is not observed in the analytical data. The similar (U,Th,La)/K of the silicic and low-Mg carbonatitic HDF types (Fig. 10b) further strengthens this suggestion.

In summary, the array represents the melting of eclogites that contain water and carbonates in variable amounts. Figures 7 and 8 show that most of the silicic to low-Mg carbonatitic HDFs fall in the middle of the array, indicating that the majority originate from rocks that carry both water and carbonates. Sediments are less probable, but possible sources of some of the HDFs.

Formation of saline high-density fluids

The saline HDFs are the most intriguing as they do not resemble any mantle melts that erupt on Earth's surface. Melting of peridotite or eclogite source-rocks is unlikely to form K-rich saline HDFs. K and Cl have similar incompatibility, but while the average molar K/Cl ratio of the HDFs is 0.68 ± 0.14 1σ (Supplementary compilation of HDF data, Weiss et al. 2022), the mantle ratio, as defined by MORB and OIB glasses, falls in the range of 6–45 (e.g., Kendrick et al. 2013, 2017). Fractionation of mantle melts is also unlikely. Most carry low concentrations of both K and Cl and require extensive fractionation that is not expected to produce a uniform residual K- and Cl-rich saline HDF.

Klein-BenDavid et al. (2007) noted a consistent negative correlation of MgO and CaO with Cl content in saline HDFs. They examined fractionation of Mg-rich carbonates from a carbonatitic HDF, concluded that extreme fractionation is needed, and noted the difficulty to remove potassium (relative to Cl). Carbonates, phlogopite and high-Si mica micro-mineral inclusions were found in association with saline HDFs (Izraeli et al. 2004, Weiss et al. 2018), but mica removal is limited by the low abundance of silica and alumina, and crystallization of K-bearing carbonates is required. This is not impossible (e.g., Shatskiy et al. 2016, Arefiev et al. 2019), but such phases are rare (Logvinova et al. 2019a). Last, HDFs of intermediate compositions between carbonatitic and saline compositions are not common in fibrous diamonds (Figs. 7 and 8, but see Klein-BenDavid et al. 2004). Similar difficulties exist for a possible fractionation from a silicic composition to form saline HDFs.

The high Cl content of the saline HDFs and the association with water and carbonates strongly suggests a subducted source (Izraeli et al. 2001; Tomlinson et al. 2006; Weiss et al. 2015, 2018; Timmerman et al. 2018a). Indeed, the K/Cl ratio of the saline HDFs is within the range of altered oceanic crust (K/Cl = 0.3–2; Ito et al. 1983; Sano et al. 2008).

This alternative is also supported by the pronounced positive Eu and Sr anomalies of saline HDFs in fibrous diamonds from the Slave craton (Weiss et al. 2015), which reflect the involvement of plagioclase during low-pressure crustal processes of protolith formation. Low ^{3}He/^{4}He isotopic ratios of South African saline HDF (2.7–4.4 Ra), further strengthen a connection with recycled subducted surface material (Weiss et al. 2017, 2021a; Timmerman et al. 2018b).

The chemical evolution of saline HDFs is not yet clear. Weiss et al. (2015) suggested that they originated as pore fluids trapped in the crust during low-pressure hydrothermal alteration. The high K/Na ratios evolved through the consumption of H_2O and Na during spilitization (hydration of basalt) and/or due to preferential incorporation of sodium into eclogitic minerals (principally omphacite) at high pressure (Izraeli et al. 2001). Dehydration at 150–200 km depth can generate highly saline fluids. Marine sediments are another possible source for the saline HDFs, based on high-pressure–temperature reaction experiments with peridotite (Förster et al. 2019). The equilibrium fluid in these experiments was not analyzed, but the crystallization of euhedral alkali chloride with K/Na = 0.3–6 and Cl/(Na+K) = 1.03 ± 0.44 molar ratios suggest growth from a fluid that is comparable to the saline HDFs.

Once formed, saline HDFs flow through different mantle lithologies. This is indicated by their association with micro-mineral inclusions. The most common are olivine, pyroxene and garnet with compositions typical for 'normal' mantle peridotites, websterites or eclogites (Izraeli et al. 2001, 2004; Klein-BenDavid et al. 2004; Tomlinson et al. 2006; Weiss et al. 2015, 2018; Timmerman et al. 2018a,b). These compositions and the association of similar HDFs with different mantle lithologies suggest that the minerals represent a preexisting mantle through which the saline HDF percolates rather than the lithology of their source. Fluid–rock interaction is also reflected in the trace element and isotopic composition of the saline HDFs.

Weiss et al. (2009, 2015) further suggested that the introduction of saline HDFs may induce *in situ* melting of carbonated-peridotite or eclogite, leading to the formation of high-Mg carbonatitic or silicic to low-Mg carbonatitic HDFs, respectively. This model connects all the HDF types to a common parental saline composition.

HIGH-DENSITY FLUIDS AND DIAMOND FORMATION

High-density fluids are excellent media for the nucleation and growth of diamonds. The lowest conditions for diamond synthesis, 1150 °C, 5.7 GPa, were achieved in the system $(K,Na)_2CO_3 + C_2H_2O_4$ (oxalic acid) + C (graphite) (Pal'yanov et al. 1999), which is a simple analog of carbonatitic HDFs. Similar temperatures were calculated for minerals included in fibrous diamonds (Izraeli et al. 2001; Weiss et al. 2018). Still, while the growth of fibrous diamonds from the HDFs they trap is widely accepted, the formation mode of NFMC diamonds is debated (e.g., Cartigny et al. 2014; Stachel et al. 2017).

It is agreed that mantle diamonds are metasomatic minerals and that their carbon is generally supplied by the metasomatic fluids (Haggerty 1986; Stachel and Luth 2015). However, two issues are still debated: a) the state of the fluids—subsolidus low-density fluids such as water or methane, or high-density fluids such as the diamond HDFs, kimberlites and similar melts. b) the oxidation state of the fluid—evidence was collected supporting the full wide range of carbon redox states, from carbonates and CO_2 (with C^{+4}) to CH_4 (C^{-4}).

Stachel and Luth (2015) used a solidus curve sketched by Wyllie (1987) to argue that the solidus of harzburgites+H_2O+CO_2 lies at ~1270 °C (at P >6 GPa), some 170 °C above that for lherzolite. However, Brey et al. (2011) have shown that at 1100 °C and 6 GPa K-rich carbonatitic melts coexist with harzburgites. The solidus of lherzolite + K_2O + CO_2 overlaps that of the harzburgite system. Adding water may lower the solidi to even lower temperatures.

Low-density hydrous fluids with 60–80 wt% water also exist with peridotite under such conditions (5–6 GPa, 1000 °C, Kessel et al. 2015). But if carbonate is also present, the water fraction decreases to 35–45 wt% (Dvir et al. 2017), not much higher than in the HDFs. At 1100 °C, above the solidus it falls to 28 wt%. It may be even lower if the K_2O/H_2O in the experiment (0.03–0.08) would be closer to the mantle ratio of ~1 (Kessel et al. 2015). We conclude that hydrous fluids at 5–6 GPa and 1100 °C would dissolve incompatible components such as carbonates, K_2O, Cl and incompatible trace elements and would resemble the HDFs documented in diamonds. Presumably, the water fraction in equilibrium with harzburgites is somewhat higher, but we expect that the difference between such assumed hydrous fluid and HDFs is rather small.

The carbonate-bearing HDFs present the best choice for the oxidation state of carbon in diamond-forming fluids, not only for fibrous diamonds, but for most NFMC diamonds as well. HDFs were identified in NFMC diamonds (Weiss et al. 2014; Jablon and Navon 2016; Kempe et al. 2021) and their trace element signature was also found in gem and semi-gem diamonds (Krebs et al. 2019). We note that they may also carry a small proportion of reduced carbon compounds (Kopylova et al. 2010).

A common argument against an extensive role for HDFs as the source of most NFMC diamonds is the oxidation state of the lithosphere that is below the EMOD buffer ($MgSiO_3 + MgCO_3 = Mg_2SiO_4 + C + O_2$). However, as shown by Stagno et al. (2013), pure carbonate melt is stable at more reducing conditions than EMOD, and if the carbonate fraction is diluted, its stability in the melt extends to cover even more reducing conditions (by up to ~2 log units). As pointed out by Stachel and Luth (2015) the buffering capacity of the lithosphere is small, and an oxidized melt can migrate through a reduced lithosphere, react with it and deposit diamonds over a long distance.

Can HDFs carry other species of carbon besides carbonates? This interesting possibility was presented by Stachel et al. (2017) for a C–O–H low-density fluid. Based on thermodynamic modeling, they argued that CO_2 (or carbonates) and CH_4 can coexist and react with each other to form diamonds. The idea is also supported by thermodynamic modeling of water-peridotite and water-eclogite systems that predict the coexistence of diverse oxidized and reduced carbon species (Sverjensky and Huang 2015; Huang and Sverjensky 2020). Can this be applied to HDFs? Kopylova et al. (2010) reported absorption at 2800–3000 cm^{-1} in IR spectra of fibrous diamonds from DRC and related it to CH_3 and CH_2 groups. We note that this region is prone to contamination on the diamond surface, but future studies should examine carefully the IR spectra of fibrous diamonds and look for the existence of organic reduced and oxidized species predicted by the thermodynamic models. If found, this will increase the diamond forming capacity of HDFs.

The collection of observations to date identifies HDFs as the best candidates for the formation of most lithospheric diamonds, however they are not the only ones. Observations of CH_4 in diamonds are rare (Smit et al. 2016) and growth from CH_4, or CH_4-H_2O low-density fluids was suggested based on modeling of isotopic fractionation (e.g., Thomassot et al. 2007; Smit et al. 2019). Experimental studies found that "in oxidized fluids (CO_2; CO_2–H_2O; H_2O), the intensity of spontaneous nucleation, the rate of diamond growth on seed crystals, and the degree of graphite-diamond transformation are considerably higher than those in reduced fluids (H_2O–CH_4; CH_4–H_2)" (Palyanov et al. 2015), but a recent study does suggest nucleation and growth of diamond in the harzburgite+CH_4 system (Matjuschkin et al. 2020). Smith et al. (2016) reported the finding of iron–nickel–carbon–sulfur inclusion in lower mantle diamonds, but metallic iron inclusions are known from shallower diamonds as well (Bulanova et al. 1998), and this mode of growth may be important and efficient where metallic melts exist (e.g., below 250 km, Frost and McCammon 2008).

HIGH-DENSITY FLUIDS, DIAMONDS, AND METASOMATISM

Experimental studies showed that hydrous, saline, carbonate and carbonate–silicate melts with compositions that are similar to all HDF types can efficiently crystallize diamonds (e.g., Akaishi et al. 1990; Pal'yanov et al. 1999, 2002; Litvin 2009; Bureau et al. 2016). Carbon isotopes confirm the growth of diamonds from carbon supplied by the HDFs (Klein-BenDavid et al. 2004: Shiryaev et al. 2005). Growth from a fluid is also consistent with the morphology and symmetric growth patterns of diamonds (Sunagawa 1984; Bulanova 1995; Tappert and Tappert 2005). Their close association with veins and alteration zones in xenoliths (e.g., Schulze et al. 1996; Howarth et al. 2014; Logvinova et al. 2015), and metasomatic minerals (e.g., Meyer 1987; Leost et al. 2003; Bulanova et al. 2004; Zedgenizov et al. 2018), indicate that diamond formation is a by-product of HDF-rock metasomatic interaction.

Elevated concentrations of incompatible elements in garnet and clinopyroxene, which would otherwise be refractory and depleted in composition, are evidence for metasomatism (Shimizu 1975; Hoal et al. 1994; Shimizu and Richardson 1987). Among these, sub-calcic garnets globally exhibit sinusoidal chondrite-normalized (CN) REE pattern, which is, perhaps, the most identified geochemical feature attributed to the formation of diamonds (Stachel et al. 1998, 2004; Grütter et al. 2004). The varying REE enrichment patterns in metasomatized garnets, both in xenoliths and as mineral inclusions in diamonds, are commonly explained as the result of a two-stage evolution of the continental lithospheric mantle, i.e., intensive chemical depletion by melting, followed by re-fertilization via enriched fluids or melts (e.g., Stachel and Harris 2008; Klein-BenDavid and Pearson 2009; Lazarov et al. 2012; Aulbach et al. 2013; Shu and Brey 2015; Shchukina et al. 2019). Stachel et al. (2004) attributed the sinusoidal REE patterns to the interaction of a C–O–H fluid highly enriched in incompatible elements with a depleted 'pre-metasomatic' garnet. Alternatively, Pearson et al. (1995) and Malkovets et al. (2007) suggested that the sinusoidal pattern is a primary feature and was formed upon direct garnet crystallization during a reaction between a silica-bearing CH_4-rich fluid and chromite-bearing harzburgite, which represent a pre-metasomatized Archean lithospheric mantle (Griffin et al. 2008). In either case, the fluids responsible for the sinusoidal REE pattern in mantle garnets are also associated with diamond formation.

Methane-rich fluid inclusions were identified in olivine phenocrysts from orogenic harzburgite (Song et al. 2009) and ophiolitic dunite (Liu and Fei 2006), but trace element data of such fluids are not available. Thus, the formation of sinusoidal patterns in lherzolite and harzburgite garnets and garnet inclusions in diamonds by interaction with methane-rich fluids cannot be assessed.

Ziberna et al. (2013) and Shu and Brey (2015) modeled the sinusoidal patterns in peridotitic garnets and showed that they can result through interaction between a representative kimberlite or a hypothetical enriched carbonatitic melt with a depleted garnet. The choice of kimberlites (or any other highly alkaline melt) as a metasomatic agent is reasonable, as they satisfy the need for an LREE/HREE enriched fluid to interact with the 'pre-metasomatic' garnet (Stachel et al. 2004). However, their composition at depth is still debatable. HDFs have equal, and some even higher, LREE/HREE ratios and are well characterized, pristine samples of deep fluids capable of metasomatizing the continental lithosphere.

Weiss et al. (2009, 2014) used a simple mass balance expression, $\phi C_{m,i} + (1-\phi)C_{g,i} = \phi C_{m,f} + (1-\phi)C_{g,f}$, to model the evolution of REE patterns in a garnet during interaction with a HDF. Where ϕ is the melt mass fraction, which in an open system metasomatic process may be larger than the actual porosity, and C_i and C_f are the initial and final concentrations of an element in the melt (m) or the garnet (g). This simplified expression ignores the other phases in the system, but provides a good approximation for harzburgite where garnet is the main depository of many trace elements. Using $C_{m,i}$ = HDF, $C_{g,i}$ = 'pre-metasomatic' garnet of Stachel et al.

(2004), and assuming equilibrium at the final stage, $C_{m,f} = C_{g,f}/D_{(garnet/HDF)}$, Weiss et al. (2009, 2014) showed that the reacted garnet ($C_{g,f}$) can develop sinusoidal and 'normal' REE patterns that are close to those of harzburgite and lherzolite garnets (Fig. 13). Similarly, 'U' or 'V' shaped REE patterns in ultradepleted harzburgite garnets can be formed due to interaction with a very small amount of HDFs ($\phi \ll 1\%$; Gibson et al. 2013). The important terms controlling the amplitude and shape of the garnet pattern are the REE pattern of the initial HDF and ϕ. For example, a more pronounced sinusoidal pattern is developed in garnet interacting with HDFs that have La/Dy$_{CN} \approx 100$ compared to those having La/Dy$_{CN} \approx 10$ (Fig. 13a), and the 'Dip' around Dy gets shallower (Lu/Dy decreases) with increasing ϕ (Fig. 13b). Based on this, Weiss et al. (2014) suggested that the progression of peridotite garnets from strongly sinusoidal (mostly in harzburgite) to normal REE patterns (common in lherzolite) can be explained by interaction with increasing amounts of the same HDF, rather than attributing the harzburgite patterns to interaction with low-density fluids and the lherzolite patterns to interaction with melts (Griffin et al. 1999; Stachel and Harris 2008; Banas et al. 2009). Here, we demonstrate that introducing HDFs to an eclogitic 'depleted' garnet produces an REE pattern with flat and elevated HREE–MREE and decreasing LREE values, which closely resemble the characteristic 'normal' REE pattern of eclogite garnets in mantle xenoliths and diamond inclusions (Fig. 13c; e.g., Stachel et al. 2004; Satchel and Harris 2008; Jacob 2004). Thus, HDFs can account for metasomatism in both peridotite and eclogite, two lithologies that are in close association with them, as evident from the micro-mineral inclusions recorded in fibrous diamonds (e.g., Tomlinson et al. 2006; Weiss et al. 2018).

High-density fluids provide a unique record of the compositions and nature of deep mantle fluids. Their high volatile content (Table 2) and the strong enrichment in incompatible elements of all HDF types (Fig. 9), make them effective metasomatic agents. The presence of HDFs in eclogitic garnets (Elazar et al. 2021) demonstrates their ability to migrate and react with lithospheric rocks over a range of depths (McKenzie 1989). Indeed, the mineralogy and chemical composition of xenoliths/xenocrysts and some alkaline magmas suggest a prevalent involvement of HDFs, in addition to other melts, in mantle metasomatism through time (e.g., Richardson et al. 1984; Erlank et al. 1987; Menzies 1990; O'Reilly and Griffin 2013).

HIGH-DENSITY FLUIDS, KIMBERLITES, AND ALKALI MANTLE MELTS

Diamonds are xenocrysts in kimberlites, as indicated by their occurrence in mantle xenoliths (Sobolev and Kuznetsova 1966; Viljoen et al. 1992; Smart et al. 2009; Aulbach et al. 2011), by the high pressures of inclusions in diamond (e.g., Meyer 1987; Liu et al. 1990; Izraeli et al. 2001; Stachel and Harris 2008; Nimis 2020), and by the old ages of most diamonds, much older than that of their host kimberlite (e.g., Richardson et al. 1984; Gurney et al. 2010; Koornneef et al. 2017, and references therein). Still, Akagi and Masuda (1988) and Schrauder et al. (1996) proposed a genetic relation between diamond-forming HDFs and kimberlites at depth, based on their similar trace element patterns. This similarity has been broadly confirmed for HDFs and kimberlites from different lithospheric provinces (e.g., Tomlinson et al. 2009; Zedgenizov et al. 2007, 2017; Rege et al. 2010; Weiss et al. 2011; Skuzovatov et al. 2012). Among the HDFs, the closest resemblance to kimberlites is demonstrated by the high-Mg carbonatitic type. This is based on their common high Nb,Ta/La ratio and their depletion in K, Rb and Cs compared with other highly incompatible elements like Ba, U, Th and La (Fig. 14a; Weiss et al. 2011). Notably, this trace element pattern characterizes the unique HIMU alkali ocean island basalts (OIB; having a high U/Pb ratio, μ) from the Cook-Austral islands (Chauvel et al. 1997; Willbold and Stracke 2006), St. Helena (Kawabata et al. 2011), and Bermuda (Mazza et al. 2019), as well as lavas from the Grande Comore island (Class et al. 1998) and oceanic and continental basanites (e.g., Weinstein et al. 2006; Pilet et al. 2008, 2011).
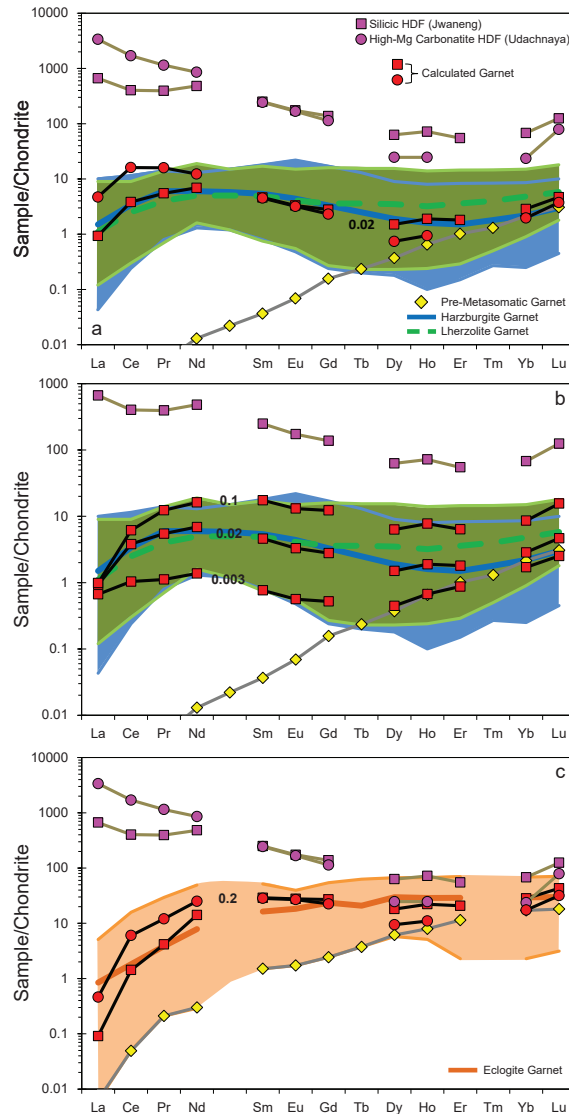
Figure 13. Rare earth element (REE) patterns of HDFs and of garnet inclusions in diamonds. (**a**) Calculated equilibrium patterns for garnet (**black line with red symbols**), formed by the interaction of HDFs (**gray line with pink symbol**) with a pre-metasomatic garnet (**gray line with yellow diamond symbols**; Stachel et al. 2004). The sinusoidal pattern amplitude is controlled by the HDF LREE/HREE enrichment. The average patterns of harzburgitic and lherzolitic garnets (**thick blue solid and green dashed lines**) and the corresponding ranges (**shaded blue and green areas**, Stachel et al. 2004) are shown for comparison. (**b**) The effect of the melt mass fraction (**black numbers**) on the amplitude and shape of the calculated sinusoidal patterns of the garnet. (**c**) Introducing HDFs into a 'depleted' eclogitic garnet produces REE patterns that closely resemble the characteristic 'normal' REE pattern of eclogitic garnets in mantle xenoliths and diamond inclusions (**thick orange solid line and shaded area**; Stachel et al. 2004). The calculations for peridotitic garnet (a and b) use the partition coefficients of Brey et al. (2008), though other sets of partition coefficients lead to similar results (e.g., Green 1994; Salters and Stracke 2004; Dasgupta et al. 2009), except for D_{La}, which varies significantly between different studies and is set here to 0.0015. For eclogitic garnet (c), the partition coefficients of Green et al. (2000) are used. Chondrite REE values are from McDonough and Sun (1995). See section '*HDFs, diamonds and metasomatism*' and Weiss et al. (2014) for additional details, and section '*Trace element analysis*' for the conversion of concentration in the diamond to concentration in the HDF.

The trace element patterns of HDFs, kimberlites and HIMU-basalts are subparallel (Fig. 14a), with their main difference being the abundances of highly incompatible elements and varying depletion in Ti, Zr and Hf (and Sr in the case of some basanites) compared to rare earth elements of similar incompatibility. These differences may reflect source heterogeneity, the degree of partial melting, the retention of accessory phases during melting, or different element partitioning in carbonatitic versus silicate melts. An important issue is the close link between the trace-element composition of HDFs trapped at depth and surface kimberlites and basalts, which indicates that the incompatible element content of the latter does not change much on their way to the surface. Moreover, it suggests similar enrichment and depletion processes experienced by their mantle source over geologic time, because batch melting of either a depleted source or a primitive mantle composition cannot reproduce the characteristic negative anomalies of the alkalis together with high Nb and Ta levels of these enriched melts.

Both carbonates (as minerals or melts) and peridotite are required for the generation of high-Mg carbonatitic HDFs and kimberlites (see section '*Formation of high-Mg carbonatitic HDFs*' above). The same constituents were suggested for the source of HIMU OIBs, based on their high CaO and Ca/Al ratios (Dasgupta et al. 2007; Jackson and Dasgupta 2008; Castillo 2015) and the high Mn/Fe and Ca/Al ratios of their olivine phenocrysts compared to other oceanic basalts (Weiss et al. 2016; Mazza et al. 2019). Similarly, a metasomatized peridotite source was proposed for basanites based on experimentally produced key major- and trace-element features (Pilet et al. 2008, 2011). Within this framework, carbonate can be introduced into peridotite through metasomatic interaction with HDFs and/or kimberlite melts, which form almost identical trace elements enriched sources at different mixing ratios (Weiss et al. 2011). Such interaction, for example, the addition of 0.5% of high-Mg carbonatitic HDF or 2.5% of kimberlitic melt into a depleted peridotite, mimics the trace-element patterns of some Archean metasomatized mantle xenoliths (e.g., Schmidberger and Francis 2001; Grégoire et al. 2003; Simon et al. 2007; Wittig et al. 2008) and the average post-Archean SCLM (McDonough 1990). These mantle-derived samples are a natural manifestation that illustrates the impact of carbonatite/kimberlite on depleted peridotite within the lithosphere. A source with similar trace element compositions is expected to form in the mantle transition-zone and deep upper mantle, as a result of similar interaction between carbonatitic melts which originate from subducting carbonated oceanic crust and the ambient mantle (Walter et al. 2008; Litasov et al. 2013; Regier et al. 2020).

To test the possible petrogenetic link between high-Mg carbonatitic HDFs and kimberlites, Weiss et al. (2011) used the trace element composition of available Archean xenoliths and the average post-Archean SCLM as natural representatives for a metasomatized carbonated peridotite and examined the products of melting. Figure 14b shows that simple batch melting of such a source closely reproduces the pattern of kimberlites. The same source can account for the pattern of HIMU basalts and basanites at higher melt fraction; however, the more compatible elements are too low in the produced melt. Weiss et al. (2016) found that batch melting of a mixture of 'normal' (trace-element-depleted) and metasomatized peridotite closely reproduces the complete trace element pattern of such basalts (Fig. 14c). They assumed a simple mixing of 80:20, respectively, between the two lithologies to produce a mixed peridotite source. The more enriched Bermuda lavas lie above the calculated melt, but with parallel pattern (Fig. 14c, Mazza et al. 2019). Such a pattern is reproduced at a lower melt fraction of a source with higher proportions of metasomatized peridotite.

The unique trace element patterns of kimberlites and HIMU-flavored alkali basalts require a distinctive enriched source that carries the signature of carbonatitic metasomatism (Hauri et al. 1993; Dalton and Presnall 1998; Saal et al. 1998; Greenwood et al. 1999; Le Roex et al. 2003; Dasgupta et al. 2007; Brey et al. 2008; Jackson and Dasgupta 2008). The impact of high-Mg carbonatitic HDFs on mantle peridotite can produce such a source. Other HDF types have different compositions and trace element patterns, but similar metasomatic
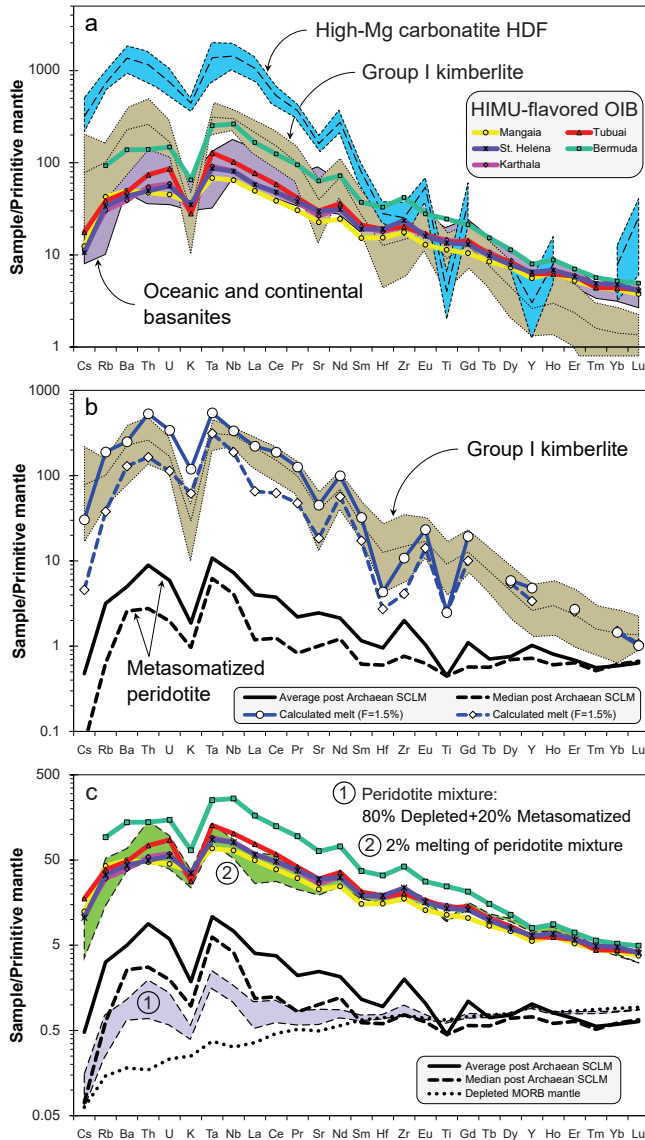
Figure 14. HDFs, kimberlites and alkali mantle melts. (**a**) Normalized trace element patterns comparing high-Mg carbonatitic HDFs from Udachnaya, global Group I kimberlites, HIMU-flavored alkali OIB, and oceanic and continental basanites. (**b**) Batch melting of a metasomatized peridotite (represented by average and median post Archean SCLM; McDonough 1990), with mantle mineralogy of Ol =66%, Opx =26%, Cpx = 3%, Grt = 5% and Carb <1%. Using partition coefficients for mineral/carbonatitic-melt (Dasgupta et al. 2009) closely reproduces the pattern of kimberlites at partial melt fraction (*F*) of 1.5–2%. (**c**) Batch melting of a mixture of 80% 'normal' depleted MORB mantle (Salters and Stracke 2004) and 20% of the metasomatized peridotite of (b) result in a trace element pattern comparable to many HIMU-flavored alkali OIBs and oceanic and continental basanites. The calculations assume equilibrium with a residual modal mineralogy of Ol = 72%, Opx = 20%, Cpx = 2%, Gr = 5% and Carb = 1%; partition coefficients for silicate/basaltic melt from alphaMELTS (Smith and Asimow 2005), and F = 2%. The pattern of the metasomatized SCLM can be formed by interaction with HDFs. See section '*HDFs, kimberlites and alkali mantle melts*' and Weiss et al. (2011, 2016) for additional details.

potential upon interaction with mantle lithologies. The passage of such HDFs through and the interaction with different mantle lithologies impart chemical 'stains' that result in enriched mantle sources. In turn, the melting of such sources conveys these unique chemical and isotope compositional signatures to mantle-derived magmas that erupt at the Earth's surface. However, this is not a "chicken & egg" situation. HDFs with 'Planed' pattern (Fig. 9) may be derived directly from melting of depleted or primitive mantle and evolve into the other patterns as they percolate through the mantle (Weiss et al. 2013b).

SUMMARY AND CONCLUSIONS

Lithospheric diamonds form at depths >140 km beneath the Earth's surface from circulating carbon- and water-rich (C–O–H) fluids. High-density fluids (HDFs) encapsulated in microinclusions in fibrous diamonds are the best-preserved and most common samples of such fluids. Fibrous diamonds and the HDFs they carry are documented in localities of diverse ages and geographical provenance, mostly from Africa, Canada and Siberia, but also from Brazil, India and China, indicating their global distribution and long history in the subcontinental lithospheric mantle.

About 300 fibrous diamonds have been analyzed to date for their HDF major element compositions, roughly 200 of those have also been analyzed for trace element content, and some for their radiogenic isotope composition (mostly Sr isotope ratios). Four types of major element compositions, i.e., saline, silicic to low-Mg carbonatitic and high-Mg carbonatitic HDFs, are ubiquitous worldwide. Trace element compositions of HDFs also have consistent patterns globally, regardless of their host diamond provenance. Two repeating patterns are revealed: a highly fractionated one and a smoother one. The first is characterized by LILE and LREE enrichment, and HFSE and alkali depletion, similar to calcalkaline magmas and continental crustal rocks. The second has lower LILE and LREE abundances and 'smoother' overall trace-element pattern similar to oceanic basalts. These two patterns, as well as intermediate compositions, have been identified in all four types of HDFs, indicating the decoupling between major and trace elements of HDFs. The available Sr isotopic signatures suggest a relationship to the characteristics of their mantle sources, as also reflected in the trace element patterns.

A strong connection has been established between silicic to low-Mg carbonatitic HDF compositions and hydrous/carbonated eclogites, based on the association of these HDFs with eclogitic mineral inclusions, as well as their similarity to experimental near-solidus melts in the H_2O-CO_2-eclogite system. Similar arguments have been used to establish a connection between high-Mg carbonatitic HDFs and a carbonated peridotite source. Saline HDFs are more enigmatic and their chemical evolution and source rock are not as clear. At present, the most robust hypothesis is that saline HDFs originate from a subducted source, which is supported by their high Cl content, low K/Cl ratio, positive Eu and Sr anomalies and low $^3He/^4He$ isotopic ratios. Once formed, saline HDFs can percolate through different mantle lithologies, and induce *in situ* melting of carbonated-peridotite or eclogite, leading to compositional transition and the formation of silicic and carbonatitic HDF types.

The varying abundance of HDF types in different cratons is fascinating, and likely related to the petrological and physical characteristics of the local lithospheres. For example, the abundance of silicic to low-Mg carbonatitic HDFs in DRC and Jwaneng, two lithospheres with dominance of eclogitic diamonds, is prominent. Other observations, like the high abundance of saline HDFs in the Slave and southwestern Kaapvaal, are clear, but not yet reconciled. In addition, the distinct high-Al trend of silicic to low-Mg carbonatitic HDFs in Siberia compared to other lithosphere provinces, or the striking dichotomy between high-Ba saline HDFs from the Slave and low-Ba ones in the Kaapvaal, are unresolved. Integrated studies on HDF compositions and the local host lithosphere, as well as additional HDF isotopic analyses which are still scarce, are likely to shed light on such issues.

High-density fluids are excellent media for the nucleation and growth of diamonds. Here we summarized recent observations that indicate the involvement of HDFs in the formation of most (but not all) diamonds, fibrous and non-fibrous alike. The most widely recognized geochemical feature attributed to the formation of lithospheric diamonds are metasomatized garnets, which globally exhibit enriched REE patterns. Such patterns can form by the interaction of any HDF type with a depleted garnet in both peridotite and eclogite lithologies, thus strengthening the connection between diamond formation and HDFs. The prevalence of similar metasomatized garnets in mantle-derived xenoliths, together with the similarity in trace elements between HDFs (in particular high-Mg carbonatitic ones), kimberlites, HIMU-flavored alkali OIB and oceanic and continental basanites, reflect the impact of HDFs on the deep lithospheric mantle and their role in deep Earth processes.

High-density fluids provide a unique record of the compositions and nature of deep mantle C–O–H-bearing fluids. Their high volatile content, strong enrichment in incompatible elements and possible relation to subduction processes, make HDFs a key player in the global circulation of volatiles. However, to date, there are no robust age constraints for HDFs, nor for their host fibrous diamonds. Future progress in analytical techniques and/or sampling methods for analyzing HDFs, especially for determining their radiogenic isotope composition, are likely to offer a remedy and provide comprehensive chemical characteristics and meaningful geological ages of HDFs in diamonds. It will potentially elucidate the origin of all HDF types, the relationship between them, and the ages of their host diamonds and the metasomatic processes that led to their formation. Such new data will provide the opportunity to understand the complex history of alteration events in different lithospheric provinces, the type of fluids involved, and relate these deep mantle events to regional tectonics and magmatic history. Since HDFs trapped in diamonds are the most pristine samples of an abundant C–O–H-bearing fluids in Earth's mantle, they are likely to provide important contributions to our understanding of the deep carbon and water cycle throughout Earth's history.

ACKNOWLEDGMENTS

REFERENCES

Akagi T (1999) Relationship of strontium isotope ratio and chemical composition of micro inclusions in fibrous diamonds: Implication for isotopically different components of the upper mantle. Geochem J 33:101–107

Akagi T, Masuda A (1988) Isotopic and elemental evidence for a relationship between kimberlite and Zaire cubic diamonds. Nature 336:665–667

Akaishi M, Kanda H, Yamaoka S (1990) Synthesis of diamond from graphite-carbonate system under very high temperature and pressure. J Cryst Growth 104:578–581

Anand M, Taylor LA, Misra KC, Carlson WD, Sobolev NV (2004) Nature of diamonds in Yakutian eclogites: Views from eclogite tomography and mineral inclusions in diamonds. Lithos 77:333–348

Angress JF, Smith, SD (1965) The observation of defect-activated one-phonon infra-red absorption in diamond coat. Philos Mag 12:415–417

Araújo DP, Griffin WL, O'Reilly SY, Grant KJ, Ireland T, Holden P, van Achterbergh E (2009) Microinclusions in monocrystalline octahedral diamonds and coated diamonds from Diavik, Slave Craton: Clues to diamond genesis. Lithos 112:724–735

Arefiev AV, Shatskiy A, Podborodnikov IV, Litasov KD (2019) The K_2CO_3–$CaCO_3$–$MgCO_3$ system at 6 GPa: Implications for diamond forming carbonatitic melts. Minerals 9:558

Aulbach S, Stachel T, Heaman LM, Carlson JA (2011) Microxenoliths from the Slave craton: Archives of diamond formation along fluid conduits. Lithos 126:419–434

Aulbach S, Griffin WL, Pearson NJ, O'Reilly SY (2013) Nature and timing of metasomatism in the stratified mantle lithosphere beneath the central Slave craton (Canada). Chem Geol 352:153–169

Banas A, Stachel T, Phillips D, Shimizu N, Viljoen KS, Harris JW (2009) Ancient metasomatism recorded by ultra-depleted garnet inclusions in diamonds from DeBeers Pool, South Africa. Lithos 12:736–746

Basu S, Jones AP, Verchovsky AB, Kelley SP, Stuart FM (2013) An overview of noble gas (He, Ne, Ar, Xe) contents and isotope signals in terrestrial diamond. Earth Sci Rev 126:235–249

Bauer MH (1896) Edelsteinkunde (English translation, 1904, by LJ Spencer) Reprinted 1968. Dover Publications, New York

Bibby DM (1979) Zonal distribution of impurities in diamond. Geochim Cosmochim Acta 43:415–423

Bibby DM (1982) Impurities in natural diamond. *In:* Chemistry and Physics of Carbon. Vol 18. Thrower PA (ed) Marcel Dekker CRC Press, New York, p 1–91

Bodnar RJ (2003) Introduction to fluid inclusions. *In:* Fluid inclusions: Analysis and interpretation. Vol 32. Samson I, Anderson A, Marshall D (eds) Mineralogical Association of Canada, Short Course, p 1–8

Boyd SR, Mattey DP, Pillinger CT, Milledge HJ, Mendelssohn M, Seal M (1987) Multiple growth events during diamond genesis: an integrated study of carbon and nitrogen isotopes and nitrogen aggregation state in coated stones. Earth Planet Sci Lett 86:341–353

Brey GP, Bulatov VK, Girnis AV, Lahaye Y (2008) Experimental melting of carbonated peridotite at 6–10 GPa. J Petrol 49:797–821

Brey GP, Bulatov VK, Girnis AV (2009) Influence of water and fluorine on melting of carbonated peridotite at 6 and 10 GPa. Lithos 112:249–259

Brey GP, Bulatov VK, Girnis AV (2011) Melting of K-rich carbonated peridotite at 6–10 GPa and the stability of K-phases in the upper mantle. Chem Geol 281:333–342

Broadley MB, Kagi H, Burgess R, Zedgenizov D, Mikhail S, Almayrac M, Ragozin A, Pomazansky B, Sumino H (2018) Plume-lithosphere interaction, and the formation of fibrous diamonds. Geochem Perspect Lett 8:26–30

Bulanova GP (1995) The formation of diamond. J Geochem Explor 53:1–23

Bulanova GP, Novgorodov PG, Pavlova LA (1988) The first find of a melt inclusion in diamond from the Mir pipe. Geokhimiya 5:756–765

Bulanova GP, Griffin WL, Ryan CG (1998) Nucleation environment of diamonds from Yakutian kimberlites. Mineral Mag 62:409–419

Bulanova GP, Muchemwa E, Pearson DG, Griffin BJ, Kelley SP, Klemme S, Smith CB (2004) Syngenetic inclusions of yimengite in diamond from Sese kimberlite (Zimbabwe)—evidence for metasomatic conditions of growth. Lithos 77:181–192

Bulatov VK, Brey GP, Girnis AV, Gerdes A, Höfer HE (2014) Carbonated sediment–peridotite interaction and melting at 7.5–12 GPa. Lithos 200:368–385

Bureau H, Frost DJ, Bolfan-Casanova N, Leroy C, Esteve I, Cordier P (2016) Diamond growth in mantle fluids. Lithos 265:4–15

Burgess R, Johnson LH, Mattey DP, Harris JW, Turner G (1998) He, Ar and C isotopes in coated and polycrystalline diamonds. Chem Geol 146:205–217

Burgess R, Layzelle E, Turner G, Harris JW (2002) Constraints on the age and halogen composition of mantle fluids in Siberian coated diamonds. Earth Planet Sci Lett 197:193–203

Burgess R, Kiviets GB, Harris JW (2004) Ar–Ar age determinations of eclogitic clinopyroxene and garnet inclusions in diamonds from the Venetia and Orapa kimberlites. Lithos 77:113–124

Burgess R, Cartigny P, Harrison D, Hobson E, Harris J (2009) Volatile composition of microinclusions in diamonds from the Panda kimberlite, Canada: Implications for chemical and isotopic heterogeneity in the mantle. Geochim Cosmochim Acta 73:1779–1794

Cartigny P, Harris JW, Javoy M (2001) Diamond genesis, mantle fractionations and mantle nitrogen content: a study of δ^{13}C–N concentrations in diamonds. Earth Planet Sci Lett 185:85–98

Cartigny P, Palot M, Thomassot E, Harris JW (2014) Diamond formation: a stable isotope perspective. Annu Rev Earth Planet Sci 42:699–732

Castillo PR (2015) The recycling of marine carbonates and sources of HIMU and FOZO ocean island basalts. Lithos 216:254–263

Chauvel C, McDonough W, Guille G, Maury R, Duncan R (1997) Contrasting old and young volcanism in Rurutu Island, Austral chain. Chem Geol 139:125–143

Chepurov AI, Tomilenko AA, Shebanin AP, Sobolev NV (1994) Fluid inclusions in natural diamonds from placers of Yakutia. Dokl Akad Nauk 336:662–665

Chinn IL, Gurney JJ, Milledge JH, Taylor WR, Woods PA (1995a) Cathodoluminescence properties of CO_2-bearing and CO_2-free diamonds from the George Creek K1 kimberlite dike. Int Geol Rev 37:254–258

Chinn IL, Gurney JJ, Milledge HJ, Taylor WR, McCallum ME (1995b) CO_2-bearing diamonds from the George Creek K1 kimberlite dyke of the Colorado-Wyoming State Line District. International Kimberlite Conference: Extended Abstracts 6:113–115

Chrenko RM, McDonald RS, Darrow KA (1967) Infra-red spectra of diamond coat. Nature 213:474–476

Clark CD, Davey ST (1984) One-phonon infrared absorption in diamond. J Phys C: Solid State 17:1127–1140

Class C, Goldstein SL, Altherr R, Bachèlery P (1998) The process of plume–lithosphere interactions in the ocean basins—the case of Grande Comore. J Petrol 39:881–903

Dalpé C, Hudon P, Ballantyne DJ, Williams D, Marcotte D (2010) Trace element analysis of rough diamond by LA-ICP-MS: A case of source discrimination? J Forensic Sci 55:1443–1456

Dalton JA, Presnall DC (1998) The continuum of primary carbonatitic–kimberlitic melt compositions in equilibrium with lherzolite: data from the system CaO–MgO–Al$_2$O$_3$–SiO$_2$–CO$_2$ at 6 GPa. J Petrol 39:1953–1964

Dasgupta R, Hirschmann MM (2007) A modified iterative sandwich method for determination of near-solidus partial melt compositions. II. Application to determination of near-solidus melt compositions of carbonated peridotite. Contrib Mineral Petrol 154:647–661

Dasgupta R, Hirschmann MM, Smith ND (2007) Partial melting experiments of peridotite + CO$_2$ at 3 GPa and genesis of alkalic ocean island basalts. J Petrol 48:2093–2124

Dasgupta R, Hirschmann MM, McDonough WF, Spiegelman M, Withers AC (2009) Trace element partitioning between garnet lherzolite and carbonatite at 6.6 and 8.6 GPa with applications to the geochemistry of the mantle and of mantle-derived melts. Chem Geol 262:57–77

Day JM, Barry PH, Hilton DR, Burgess R, Pearson DG, Taylor LA (2015) The helium flux from the continents and ubiquity of low-^{3}He/^{4}He recycled crust and lithosphere. Geochim Cosmochim Acta 153:116–133

Dvir O, Pettke T, Fumagalli P, Kessel R (2011) Fluids in the peridotite–water system up to 6 GPa and 800 C: new experimental constrains on dehydration reactions. Contrib Mineral Petrol 161:829–844

Elazar O, Weiss Y (2021) Extension tectonics and mantle metasomatism in the North Atlantic Craton mirrored in diamond microinclusions. Israel Geological Society Annual meeting, Yeruham 2021, Abstract Book, p 33–34, https://en.igs.org.il/annual-conference

Elazar O, Frost D, Navon O, Kessel R (2019) Melting of H$_2$O and CO$_2$-bearing eclogite at 4–6 GPa and 900–1200 °C: Implications for the generation of diamond-forming fluids. Geochim Cosmochim Acta 255:69–87

Elazar O, Kessel R, Huang J-X, Marquardt K, Navon O (2021) Silicic microinclusions in a metasomatized eclogite from Roberts Victor mine, South Africa. Lithos 388:106057

El Fadili S, Demaiffe D, Gurney JJ (1999) Petrology of eclogite and granulite nodules from the Mbuji Mayi kimberlites (Kasai, Congo): the significance of kyanite–omphacite intergrowths. *In:* Proceedings of the 7th International Kimberlite Conference. Vol 1. Gurney JJ, Gurney JL, Pascoe MF, Richardson SH (eds) Red Roof Designs, Cape Town, p 205–213

Erlank AJ, Waters FG, Hawkesworth CJ, Haggerty SE, Allsopp HL, Rickard RS, Menzies MA (1987) Evidence for mantle metasomatism in peridotite nodules from the Kimberley pipes, South Africa. *In:* Mantle Metasomatism. Menzies MA, Hawkesworth J (eds) Academic, London, p 221–311

Evans T, Qi Z (1982) Aggregation of nitrogen in diamond. *In:* The properties of natural and synthetic diamond. Field JE (ed) Academic, London, p 259–290

Evans T, Qi Z, Maguire J (1981) The stages of nitrogen aggregation in diamond. J Phys C: Solid State 14:L379

Farley KA (2002) (U–Th)/He dating: Techniques, calibrations and applications. Rev Mineral Geochem 47:819–844

Faure S (2010) World Kimberlites CONSOREM Database (Version 3)

Fesq HW, Bibby DM, Erasmus CS, Kable EJD, Sellschop JPF (1975) A comparative trace element study of diamonds from Premier, Finsch and Jagersfontein mines, South Africa. Phys Chem Earth 817–836

Förster MW, Foley SF, Marschall HR, Alard O, Buhre S (2019) Melting of sediments in the deep mantle produces saline fluid inclusions in diamonds. Sci Adv 5:eaau2620

Frost DJ, McCammon CA (2008) The redox state of Earth's mantle. Annu Rev Earth Planet Sci 36: 389–420

Galimov EM (1984) Variations in isotopic composition of diamonds and inferences for diamond genesis conditions. Geokhimiya 8:1091–1118

Gibson SA, McMahon SC, Day JA, Dawson JB (2013) Highly refractory lithospheric mantle beneath the Tanzanian craton: evidence from Lashaine pre-metasomatic garnet-bearing peridotites. J Petrol 54:1503–1546

Giuliani A, Phillips D, Woodhead JD, Kamenetsky VS, Fiorentini ML, Maas R, Soltys A, Armstrong RA (2015) Did diamond-bearing orangeites originate from MARID-veined peridotites in the lithospheric mantle? Nat Commun 6:6837

Glazunov MP, Kobochnikov PN, Orlov YL (1967) Determination of impurities and investigation of their distribution in the natural diamonds from various places of origin with the neutron activation technique. Isotopenpraxis 3:231–235

Graham DW (2002) Noble gas isotope geochemistry of mid-ocean ridge and ocean island basalts: Characterization of mantle source reservoirs. Rev Mineral Geochem 47:247–317

Green TH (1994) Experimental studies of trace-element partitioning applicable to igneous petrogenesis—Sedona 16 years later. Chem Geol 117:1–36

Green TH, Blundy J D, Adam J, Yaxley GM (2000) SIMS determination of trace element partition coefficients between garnet, clinopyroxene and hydrous basaltic liquids at 2–7.5 GPa and 1080–1200 C. Lithos 53:165–187

Green BL, Collins AT, Breeding CM (2022) Diamond spectroscopy, defect centers, color, and treatments. Rev Mineral Geochem 88:637–688

Greenwood JC, Gibson SA, Thompson RN, Weska RK, Dickin AP (1999) Cretaceous kimberlites from the Paranatinga-Batovi region, central Brazil: geochemical evidence for subcratonic lithospheric mantle heterogeneity. *In:* Proceedings of the 7th International Kimberlite Conference. Vol 1. Gurney JJ, Gurney JL, Pascoe MF, Richardson SH (eds) Red Roof Designs, Cape Town, p 291–298

Grégoire M, Bell DR, Le Roex AP (2003) Garnet lherzolites from the Kaapvaal Craton (South Africa): trace element evidence for a metasomatic history. J Petrol 44:629–657

Gress MU, Howell D, Chinn IL, Speich L, Kohn SC, van den Heuvel Q, Schulten E, Pals ASM, Davies GR (2018) Episodic diamond growth beneath the Kaapvaal craton at Jwaneng mine, Botswana. Mineral Petrol 112:219–229

Griffin WL, Ryan CG and Win TT (1993) Trace elements in diamond: a proton microprobe study. CSIRO Restricted Report, 363R

Griffin WL, Shee SR, Ryan CG, Win TT, Wyatt BA (1999) Harzburgite to lherzolite and back again: metasomatic processes in ultramafic xenoliths from the Wesselton kimberlite, Kimberley, South Africa. Contrib Mineral Petrol 134:232–250

Griffin WL, O'Reilly SY, Afonso JC, Begg G (2008) The composition and evolution of lithospheric mantle: a re-evaluation and its tectonic implications. J Petrol 50:1185–1204

Grütter HS, Gurney JJ, Menzies AH, Winter F (2004) An updated classification scheme for mantle-derived garnet, for use by diamond explorers. Lithos 77 841–857

Gubanov N, Zedgenizov D, Sharygin I, Ragozin A (2019) Origin and evolution of high-Mg carbonatitic and low-Mg carbonatitic to silicic high-density fluids in coated diamonds from Udachnaya kimberlite pipe. Minerals 9:734

Gurney JJ, Zweistra P (1995) The interpretation of the major element compositions of mantle minerals in diamond exploration. J Geochem Explor 53:293–309

Gurney JJ, Jacob WRO, Dawson JB (1979) Megacrysts from the Monastery kimberlite pipe, South Africa. *In:* The Mantle Sample: Inclusions in Kimberlites and Other Volcanics. Boyd FR, Meyer HOA (eds), AGU, Washington DC, p 227–243

Gurney JJ, Helmstaedt HH, Richardson SH, Shirey SB (2010) Diamonds through time. Econ Geol 105:689–712

Guthrie Jr GD, Veblen DR, Navon O, Rossman GR (1991) Submicrometer fluid inclusions in turbid-diamond coats. Earth Planet Sci Lett 105:1–12

Haggerty SE (1986) Diamond genesis in a multiply-constrained model. Nature 320:34–38

Hammouda T (2003) High-pressure melting of carbonated eclogite and experimental constraints on carbon recycling and storage in the mantle. Earth Planet Sci Lett 214:357–368

Harris JW (1968) Recognition of diamond inclusions. Part 1. Syngenetic mineral inclusions. Part 2. Epigenetic Mineral Inclusions. Ind Diamond Rev 28:402–410:458–461

Harte B, Gurney JJ, Harris JW (1980) The formation of peridotitic suite inclusions in diamonds. Contrib Mineral Petrol 72:181–190

Hasterok D, Chapman DS (2011) Heat production and geotherms for the continental lithosphere. Earth Planet Sci Lett 307:59–70

Hauri EH, Hart SR (1993) Re–Os isotope systematics of HIMU and EMII oceanic island basalts from the south Pacific Ocean. Earth Planet Sci Lett 114353–371

Hoal KEO, Hoal BG, Erlank AJ, Shimizu N (1994) Metasomatism of the mantle lithosphere recorded by rare earth elements in garnets. Earth Planet Sci Lett 126:303–313

Hofmann AW (1997) Mantle geochemistry: the message from oceanic volcanism. Nature 385:219–229

Howarth GH, Sobolev NV, Pernet-Fisher JF, Barry PH, Penumadu D, Puplampu S, Ketcham RA, Maisano JA, Taylor D, Taylor LA (2014) The secondary origin of diamonds: multi-modal radiation tomography of diamondiferous mantle eclogites. Int Geol Rev 56:1172–1180

Howell D, O'Neill CJ, Grant KJ, Griffin WL, Pearson NJ, O'Reilly SY (2012) μ-FTIR mapping: Distribution of impurities in different types of diamond growth. Diamond Relat Mater 29:29–36

Huang F, Sverjensky DA (2020) Mixing of carbonatitic into saline fluid during panda diamond formation. Geochim Cosmochim Acta 284:1–20

Ionov DA, Doucet LS, Ashchepkov IV (2010) Composition of the lithospheric mantle in the Siberian craton: new constraints from fresh peridotites in the Udachnaya-East kimberlite. J Petrol 51:2177–2210

Ito E, Harris DM, Anderson Jr AT (1983) Alteration of oceanic crust and geologic cycling of chlorine and water. Geochim Cosmochim Acta 47:1613–1624

Izraeli ES, Harris JW, Navon O (2001) Brine inclusions in diamonds: a new upper mantle fluid. Earth Planet Sci Lett 187:323–332

Izraeli ES, Harris JW, Navon O (2004) Fluid and mineral inclusions in cloudy diamonds from Koffiefontein, South Africa. Geochim Cosmochim Acta 68:2561–2575

Jablon BM, Navon O (2016) Most diamonds were created equal. Earth Planet Sci Lett 443:41–47

Jackson MG, Dasgupta R (2008) Compositions of HIMU, EM1, and EM2 from global trends between radiogenic isotopes and major elements in ocean island basalts. Earth Planet Sci Lett 276:175–186

Jacob DE (2004) Nature and origin of eclogite xenoliths from kimberlites. Lithos 77:295–316

Jacob DE, Wirth R, Enzmann F, Kronz A, Schreiber A (2011) Nano-inclusion suite and high resolution micro-computed-tomography of polycrystalline diamond (framesite) from Orapa, Botswana. Earth Planet Sci Lett 308:307–316

Jacob DE, Dobrzhinetskaya L, Wirth R (2014) New insight into polycrystalline diamond genesis from modern nanoanalytical techniques. Earth Sci Rev 136:21–35

Javoy M, Pineau F, Demaiffe D (1984) Nitrogen and carbon isotopic composition in the diamonds of Mbuji Mayi (Zaire). Earth Planet Sci Lett 68:399–412

Johnson LH, Burgess R, Turner G, Milledge HJ, Harris JW (2000) Noble gas and halogen geochemistry of mantle fluids: comparison of African and Canadian diamonds. Geochim Cosmochim Acta 64:717–732

Kagi H, Lu R, Davidson P, Goncharov AF, Mao HK, Hemley RJ (2000) Evidence for ice VI as an inclusion in cuboid diamonds from high *PT* near infrared spectroscopy. Mineral Mag 64:1089–1097

Kagi H, Zedgenizov DA, Ohfuji H, Ishibashi H (2016) Micro-and nano-inclusions in a superdeep diamond from São Luiz, Brazil. Geochem Int 54:834–838

Kaiser W, Bond WL (1959) Nitrogen, a major impurity in common type I diamond. Phys Rev 115:857

Kamber BS, Collerson KD (1999) Origin of ocean island basalts: a new model based on lead and helium isotope systematics. J Geophys Res: Solid Earth 104:25479–25491

Kamenetsky VS, Maas R, Kamenetsky MB, Paton C, Phillips D, Golovin AV, Gornova MA (2009) Chlorine from the mantle: magmatic halides in the Udachnaya-East kimberlite, Siberia. Earth Planet Sci Lett 285:96–104

Kaminsky F, Wirth R, Matsyuk S, Schreiber A, Thomas R (2009) Nyerereite and nahcolite inclusions in diamond: evidence for lower-mantle carbonatitic magmas. Mineral Mag 73:797–816

Kaminsky FV, Wirth R, Schreiber A (2013) Carbonatitic inclusions in deep mantle diamond from Juina, Brazil: new minerals in the carbonate-halide association. Can Mineral 51:669–688

Kamiya Y, Lang AR (1965) On the structure of coated diamonds. Philos Mag 11:347–356

Kawabata H, Hanyu T, Chang Q, Kimura JI, Nichols AR, Tatsumi Y (2011) The petrology and geochemistry of St. Helena alkali basalts: evaluation of the oceanic crust-recycling model for HIMU OIB. J Petrol 52:791–838

Kempe Y, Navon O, Chinn I, Weiss Y (2021a) Multiple metasomatic diamond-forming events in a cooling lithosphere beneath Voorspoed, South Africa. Lithos 106285

Kempe Y, Weiss Y, Navon O (2021b) Time-temperature relations and formation history of diamonds from the Venetia and Voorspoed Mines, South Africa. Israel Geological Society Annual meeting, Yeruham 2021, Abstract Book, p 66–67, https://en.igs.org.il/annual-conference

Kendrick MA, Arculus R, Burnard P, Honda M (2013) Quantifying brine assimilation by submarine magmas: Examples from the Galápagos Spreading Centre and Lau Basin. Geochim Cosmochim Acta 123:150–165

Kendrick MA, Hémond C, Kamenetsky VS, Danyushevsky L, Devey CW, Rodemann T, Jackson MG, Perfit MR (2017) Seawater cycled throughout Earth's mantle in partially serpentinized lithosphere. Nat Geosci 10:222–228

Kennedy GC, Nordlie BE (1968) The genesis of diamond deposits. Econ Geol 63:495–503

Kessel R, Ulmer P, Pettke T, Schmidt MW, Thompson AB (2005) The water–basalt system at 4 to 6 GPa: Phase relations and second critical endpoint in a K-free eclogite at 700 to 1400 °C. Earth Planet Sci Lett 237:873–892

Kessel R, Pettke T, Fumagalli P (2015) Melting of metasomatized peridotite at 4–6 GPa and up to 1200 °C: an experimental approach. Contrib Mineral Petrol 169:37

Kharkiv AD, Zinchuk NN, Zuev VM (1997) History of Diamond. Nedra, Moscow

Kiseeva ES, Yaxley GM, Hermann J, Litasov KD, Rosenthal A, Kamenetsky VS (2012) An experimental study of carbonated eclogite at 3.5–5.5 GPa—implications for silicate and carbonate metasomatism in the cratonic mantle. J Petrol 53:727–759

Klein-BenDavid O, Pearson DG (2009) Origins of subcalcic garnets and their relation to diamond forming fluids—case studies from Ekati (NWT-Canada) and Murowa (Zimbabwe). Geochim Cosmochim Acta 73:837–855

Klein-BenDavid O, Logvinova AM, Izraeli ES, Sobolev NV, Navon O (2003) Sulfide melt inclusions in Yubileinaya (Yakutia) diamonds. International Kimberlite Conference: Extended Abstracts 8

Klein-BenDavid O, Izraeli ES, Hauri E, Navon O (2004) Mantle fluid evolution—a tale of one diamond. Lithos 77:243–253

Klein-BenDavid O, Wirth R, Navon O (2006) TEM imaging and analysis of microinclusions in diamonds: A close look at diamond-growing fluids. Am Mineral 91:353–365

Klein-BenDavid O, Izraeli ES, Hauri E, Navon O (2007) Fluid inclusions in diamonds from the Diavik mine, Canada and the evolution of diamond-forming fluids. Geochim Cosmochim Acta 71:723–744

Klein-BenDavid O, Logvinova AM, Schrauder M, Spetius ZV, Weiss Y, Hauri EH, Kaminsky FV, Sobolev NV, Navon O (2009) High-Mg carbonatitic microinclusions in some Yakutian diamonds—a new type of diamond-forming fluid. Lithos 112:648–659

Klein-BenDavid O, Pearson DG, Nowell GM, Ottley C, McNeill JC, Cartigny P (2010) Mixed fluid sources involved in diamond growth constrained by Sr–Nd–Pb–C–N isotopes and trace elements. Earth Planet Sci Lett 289:123–133

Klein-BenDavid O, Pearson DG, Nowell GM, Ottley C, McNeill JC, Logvinova A, Sobolev NV (2014) The sources and time-integrated evolution of diamond-forming fluids–Trace elements and isotopic evidence. Geochim Cosmochim Acta 125:146–169

Koornneef JM, Gress MU, Chinn IL, Jelsma HA, Harris JW, Davies GR (2017) Archaean and Proterozoic diamond growth from contrasting styles of large-scale magmatism. Nat Commun 8:648

Kopylova M, Navon O, Dubrovinsky L, Khachatryan G (2010) Carbonatitic mineralogy of natural diamond-forming fluids. Earth Planet Sci Lett 291:126–137

Kosman CW, Kopylova MG, Stern RA, Hagadorn JW, Hurlbut JF (2016) Cretaceous mantle of the Congo craton: Evidence from mineral and fluid inclusions in Kasai alluvial diamonds. Lithos 265:42–56

Krebs MY, Pearson DG, Stachel T, Laiginhas F, Woodland S, Chinn I, Kong J (2019) A common parentage-low abundance trace element data of gem diamonds reveals similar fluids to fibrous diamonds. Lithos 324:356–370

Kurz MD, Jenkins WJ, Hart SR (1982) Helium isotopic systematics of oceanic islands and mantle heterogeneity. Nature 297:43–47

Kvasnytsya VM, Wirth R (2009) Nanoinclusions in microdiamonds from Neogenic sands of the Ukraine (Samotkan'placer): A TEM study. Lithos 113:454–464

Landau LD, Lifshitz EM (1987) Fluid Mechanics: Course of Theoretical Physics. Vol. 6 Pergamon

Lang AR (1974a) Glimpses into the growth history of natural diamonds. J Cryst Growth 24:108–115

Lang AR (1974b) Space-filling by branching columnar single-crystal growth: An example from crystallisation of diamond. J Cryst Growth 23:151–153

Lang AR, Walmsley JC (1983) Apatite inclusions in natural diamond coat. Phys Chem Mineral 9:6–8

Lawless PJ, Gurney JJ, Dawson JB (1979) Polymict peridotites from the Bultfontein and De Beers mines, Kimberley, South Africa. *In:* The Mantle Sample: Inclusions in Kimberlites and Other Volcanics. Boyd FR, Meyer HOA (eds), AGU, Washington DC, p 145–155

Lazarov M, Brey GP, Weyer S (2012) Evolution of the South African mantle—a case study of garnet peridotites from the Finsch diamond mine (Kaapvaal craton); Part 2: Multiple depletion and re-enrichment processes. Lithos 154:210–223

Le Roex AP, Bell DR, Davis P (2003) Petrogenesis of Group I Kimberlites from Kimberley, South Africa: Evidence from Bulk-rock Geochemistry. J Petrol 44:2261–2286

Leahy K, Taylor WR (1997) The influence of the Glennie domain deep structure on the diamonds in Saskatchewan kimberlites. Russ Geol Geophys 38:481–490

Lee J-Y, Marti K, Severinghaus JP, Kawamura K, Yoo H-S, Lee JB, Kim JS (2006) A redetermination of the isotopic abundances of atmospheric Ar. Geochim Cosmochim Acta 70:4507–4512

Leost I, Stachel T, Brey GP, Harris JW, Ryabchikov ID (2003) Diamond formation and source carbonation: mineral associations in diamonds from Namibia. Contrib Mineral Petrol 145:15–24

Litasov KD, Safonov OG, Ohtani E (2010) Origin of Cl-bearing silica-rich melt inclusions in diamonds: Experimental evidence for an eclogite connection. Geology 38:1131–1134

Litasov KD, Shatskiy A, Ohtani E, Yaxley GM (2013) Solidus of alkaline carbonatite in the deep mantle. Geology 41:79–82

Litvin YA (2009) The physicochemical conditions of diamond formation in the mantle matter: experimental studies. Russ Geol Geophys 50:1188–1200

Liu W, Fei PX (2006) Methane-rich fluid inclusions from ophiolitic dunite and post-collisional mafic–ultramafic intrusion: the mantle dynamics underneath the Palaeo-Asian Ocean through to the post-collisional period. Earth Planet Sci Lett 242:286–301

Liu LG, Mernagh T, Jaques A (1990) A mineralogical Raman spectroscopy study on eclogitic garnet inclusions in diamonds from Argyle. Contrib Mineral Petrol 105:156–161

Logvinova AM, Wirth R, Fedorova EN, Sobolev NV (2008a) Nanometre-sized mineral and fluid inclusions in cloudy Siberian diamonds: new insights on diamond formation. Eur J Mineral 20:317–331

Logvinova AM, Klein-BenDavid O, Wirth R, Pearson DG, Navon O, Weiss Y, Pokhilenko NP (2008b) Diamond forming fluids from Snap Lake–a comprehensive study. International Kimberlite Conference: Extended Abstracts 9

Logvinova AM, Wirth R, Tomilenko AA, Afanas'ev VP, & Sobolev NV (2011) The phase composition of crystal-fluid nanoinclusions in alluvial diamonds in the northeastern Siberian Platform. Russ Geol Geophys 52:1286–1297

Logvinova AM, Taylor LA, Fedorova EN, Yelisseyev AP, Wirth R, Howarth G, Reutsky VN, Sobolev NV (2015) A unique diamondiferous peridotite xenolith from the Udachnaya kimberlite pipe, Yakutia: role of subduction in diamond formation. Russ Geol Geophys 56:306–320

Logvinova AM, Wirth R, Zedgenizov DA, Taylor LA (2018) Carbonate–silicate–sulfide polyphase inclusion in diamond from the Komsomolskaya Kimberlite Pipe, Yakutia. Geochem Int 56:283–291

Logvinova A, Zedgenizov D, Wirth R (2019a) Specific multiphase assemblages of carbonatitic and Al-rich silicic diamond-forming fluids/melts: TEM observation of microinclusions in cuboid diamonds from the placers of Northeastern Siberian Craton. Minerals 9:50

Logvinova AM, Shatskiy A, Wirth R, Tomilenko AA, Ugap'eva SS, Sobolev NV (2019b) Carbonatite melt in type Ia gem diamond. Lithos 342:463–467

Lonsdale K, Milledge HJ (1965) X-ray diffraction studies on diamond and some related materials. *In:* Physical Properties of Diamond. Berman R (ed) Clarendon Press, Oxford, p 12–68

Malkovets VG, Griffin WL, O'Reilly SY, Wood BJ (2007) Diamond, subcalcic garnet, and mantle metasomatism: Kimberlite sampling patterns define the link. Geology 35:339–342

Matjuschkin V, Woodland AB, Frost DJ, Yaxley GM (2020). Reduced methane-bearing fluids as a source for diamond. Sci Rep 10:6961

Mazza SE, Gazel E, Bizimis M, Moucha R, Béguelin P, Johnson EA, McAleer RJ, Sobolev AV (2019) Sampling the volatile-rich transition zone beneath Bermuda. Nature 569:398–403

McDonough WF (1990) Constraints on the composition of the continental lithospheric mantle. Earth Planet Sci Lett 101:1–18

McDonough WF, Sun SS (1995) The composition of the Earth. Chem Geol 120:223–253

McKenzie D (1989) Some remarks on the movement of small melt fractions in the mantle. Earth Planet Sci Lett 95:53–72

McNeill J, Pearson DG, Klein-BenDavid O, Nowell GM, Ottley CJ, Chinn I (2009) Quantitative analysis of trace element concentrations in some gem-quality diamonds. J Phys: Condens Matter 21:364207

Melton CE, Giardini AA (1974) The composition and significance of gas released from natural diamonds from Africa and Brazil. Am Mineral 59:775–782

Melton, CE, Giardini AA (1975) Experimental results and a theoretical interpretation of gaseous inclusions found in Arkansas natural diamonds. Am Mineral 60:413–417

Melton CE, Giardini AA (1976) Experimental evidence that oxygen is the principal impurity in natural diamonds. Nature 263:309–310

Melton CE, Salotti CA, Giardini AA (1972) The observation of nitrogen, water, carbon dioxide, methane and argon as impurities in natural diamonds. Am Mineral 57:1518–1523

Melton GL, McNeill J, Stachel T, Pearson DG, Harris JW (2012) Trace elements in gem diamond from Akwatia, Ghana and DeBeers Pool, South Africa. Chem Geol 314:1–8

Menzies A, Westerlund K, Grütter H, Gurney J, Carlson J, Fung A, Nowicki T (2004) Peridotitic mantle xenoliths from kimberlites on the Ekati Diamond Mine property, NWT, Canada: Major element compositions and implications for the lithosphere beneath the central Slave craton. Lithos 77:395–412

Menzies MA (1990) Continental mantle. Oxford University Press, New York

Mershon RB, Navon O, Weiss Y (2021) Microinclusions and Nitrogen Aggregation in Diamonds from Pulandian, China. Israel Geological Society Annual meeting, Yeruham 2021, Abstract Book, p 83–84, https://en.igs.org.il/annual-conference

Meyer HOA (1987) Inclusions in diamond. *In:* Mantle xenoliths. Nixon P (ed) John Wiley & Sons Ltd, Chichester, p 501–522

Meyer HOA, Boyd FR (1972) Composition and origin of crystalline inclusions in natural diamonds. Geochim Cosmochim Acta 36:1255–1273

Moore M, Lang AR (1972) On the internal structure of natural diamonds of cubic habit. Philos Mag 26:1313–1325

Moreira M, Kunz J, Allègre C (1998) Rare gas systematics in popping rock: Isotopic and elemental compositions in the upper mantle. Science 279:1178–1181

Murphy DT, Kamber BS, Collerson KD (2003) A refined solution to the first terrestrial Pb-isotope paradox. J Petrol 44:39–53

Mvuemba-Ntanda FM, Moreau J, Meyer HOA (1982) Particularites des inclusions cristallines primaires des diamants du Kasai, Zaire. Can Mineral 20:217–230

Navon O (1989) Chemical and mineralogical characterization of micro-inclusions in diamonds. PhD Dissertation, California Institute of Technology, Pasadena, California

Navon O (1991) High internal pressures in diamond fluid inclusions determined by infrared absorption. Nature 353:746–748

Navon O (1999) Formation of diamonds in the Earth's mantle. *In:* Proceedings of the 7th International Kimberlite Conference. Vol 2. Gurney JJ, Gurney JL, Pascoe MF, Richardson SH (eds), Red Roof Designs, Cape Town, p 584–604

Navon O, Hutcheon ID, Rossman GR, Wasserburg GJ (1988) Mantle-derived fluids in diamond micro-inclusions. Nature 335:784–789

Navon O, Wirth R, Schmidt C, Jablon BM, Schreiber A, Emmanuel S (2017) Solid molecular nitrogen (δ-N2) inclusions in Juina diamonds: Exsolution at the base of the transition zone. Earth Planetary Sci Lett 464:237–247

Nimis P (2022) Pressure and temperature data for diamonds. Rev Mineral Geochem 88:533–566

Nimis P, Alvaro M, Nestola F, Angel RJ, Marquardt K, Rustioni G, Harris JW, Marone F (2016) First evidence of hydrous silicic fluid films around solid inclusions in gem-quality diamonds. Lithos 260:384–389

Nimis P, Preston R, Perritt SH, Chinn IL (2020) Diamond's depth distribution systematics. Lithos 376:105729

Novgorodov PG, Bulanova GP, Pavlova LA, Mikhailov VN, Ugarov VV, Shebanin AP, Argunov KP (1990) Inclusions of potassic phases, coesite and omphacite in the coated diamond crystal from the "Mir" pipe. Dokl Akad Nauk 310:439–443

O'Reilly SY, Griffin WL (2013) Mantle Metasomatism. *In:* Metasomatism and the Chemical Transformation of Rock: The Role of Fluids in Terrestrial and Extraterrestrial Processes. Harlov DE, Austrheim H (eds) Springer Berlin, Heidelberg, p 471–533

Orlov IL (1977) The Mineralogy of the Diamond. John Wiley & Sons, New York

Orlov YL, Bulienkov NA, Martovitsky VP (1980) The spherocrystals of diamond-new type of natural single crystals having a fibrous structure. Dokl Akad Nauk 252:703–707

Orlov YL, Bulienkov NA, Martovitsky VP (1982) A study of the internal structure of variety III diamonds by X-ray section topography. Phys Chem Mineral 8:105–111

Ozima M, Zashu S (1991) Noble gas state of the ancient mantle as deduced from noble gases in coated diamonds. Earth Planet Sci Lett 105:13–27

Pal'yanov YN, Sokol AG, Borzdov YM, Khokhryakov AF, Sobolev NV (1999) Diamond formation from mantle carbonate fluids. Nature 400:417–418

Pal'yanov N, Sokol AG, Borzdov M, Khokhryakov AF (2002) Fluid-bearing alkaline carbonate melts as the medium for the formation of diamonds in the Earth's mantle: an experimental study. Lithos 60:145–159

Palyanov YN, Kupriyanov IN, Khokhryakov AF, Ralchenko VG (2015) Crystal growth of diamond. *In*: Handbook of Crystal Growth. Vol 2. Rudolph P (ed) Elsevier, Amsterdam, p 671–713

Paton C, Hergt JM, Phillips D, Woodhead JD, Shee SR (2007) New insights into the genesis of Indian kimberlites from the Dharwar Craton via in situ Sr isotope analysis of groundmass perovskite. Geology 35:1011–1014

Pearson DG, Shirey SB, Carlson RW, Boyd FR, Pokhilenko NP, Shimizu N (1995) Re-Os, Sm-Nd, and Rb-Sr isotope evidence for thick Archaean lithospheric mantle beneath the Siberian craton modified by multistage metasomatism. Geochim Cosmochim Acta 59:959–977

Pell J, Grütter H, Neilson S, Lockhart G, Dempsey S, Grenon H (2013). Exploration and discovery of the Chidliak kimberlite province, Baffin Island, Nunavut: Canada's newest diamond district. *In:* Proceedings of 10th International Kimberlite Conference. Vol 2. Pearson DG, Grütter HS, Harris JW, Kjarsgaard BA, O'Brien H, Rao NVC, Sparks S (eds) Springer, New Delhi, p 209–227

Pilet S, Baker MB, Stolper EM (2008) Metasomatized lithosphere and the origin of alkaline lavas. Science 320:916–919

Pilet S, Baker MB, Müntener O, Stolper EM (2011) Monte Carlo simulations of metasomatic enrichment in the lithosphere and implications for the source of alkaline basalts. J Petrol 52:1415–1442

Prinz M, Mansoni DV, Hlava PF, Keil K (1975) Inclusions in diamonds: Garnet lherzolite and eclogite assemblages. Phys Chem Earth 797–815

Rege S, Jackson S, Griffin WL, Davies RM, Pearson NJ, O'Reilly SY (2005) Quantitative trace-element analysis of diamond by laser ablation inductively coupled plasma mass spectrometry. J Anal At Spectrom 20:601–611

Rege S, Griffin WL, Pearson NJ, Araújo D, Zedgenizov D, O'Reilly SY (2010) Trace-element patterns of fibrous and monocrystalline diamonds: Insights into mantle fluids. Lithos 118:313–337

Regier ME, Pearson DG, Stachel T, Luth RW, Stern RA, Harris JW (2020) The lithospheric-to-lower-mantle carbon cycle recorded in superdeep diamonds. Nature 585:234–238

Resano M, Vanhaecke F, Hutsebaut D, De Corte K, Moens L (2003) Possibilities of laser ablation-inductively coupled plasma-mass spectrometry for diamond fingerprinting. J Anal At Spectrom 18:1238–1242

Richardson SH, Gurney JJ, Erlank AJ, Harris J (1984) Origin of diamonds in old enriched mantle. Nature 310:198–202

Roedder E (1984) Fluid inclusions. Reviews in Mineralogy. Vol 12. Mineralogical Society of America, Washington DC

Rondeau B, Fritsch E, Moore M, Thomassot E, Sirakian JF (2007) On the growth of natural octahedral diamond upon a fibrous core. J Cryst Growth 304:287–293

Rudloff-Grund J, Brenker FE, Marquardt K, Howell D, Schreiber A, O'Reilly SY, Griffin WL, Kaminsky FV (2016) Nitrogen nanoinclusions in milky diamonds from Juina area, Mato Grosso State, Brazil. Lithos 265:57–67

Ryan CG, Cousens DR, Sie SH, Griffin WL, Suter GF, Clayton E (1990) Quantitative PIXE microanalysis of geological material using the CSIRO proton microprobe. Nucl Instrum Methods Phys Res, Sect B 47:55–71

Saal AE, Hart SR, Shimizu N, Hauri EH, Layne GD (1998) Pb isotopic variability in melt inclusions from oceanic island basalts, Polynesia. Science 282:1481–1484

Safonov OG, Perchuk LL, Litvin YA (2007) Melting relations in the chloride–carbonate–silicate systems at high-pressure and the model for formation of alkalic diamond–forming liquids in the upper mantle. Earth Planet Sci Lett 253:112–128

Safonov OG, Chertkova NV, Perchuk LL, Litvin YA (2009) Experimental model for alkalic chloride-rich liquids in the upper mantle. Lithos 112:260–273

Salters VJ, Stracke A (2004) Composition of the depleted mantle. Geochem Geophys Geosyst 5:Q05B07

Sano T, Miyoshi M, Ingle S, Banerjee NR, Ishimoto M, Fukuoka T (2008) Boron and chlorine contents of upper oceanic crust: basement samples from IODP Hole 1256D. Geochem Geophys Geosyst 9:Q12O15

Schmidberger SS, Francis D (2001) Constraints on the trace element composition of the Archean mantle root beneath Somerset Island, Arctic Canada. J Petrol 42:1095–1117

Schrauder M (1997) Fluids in Diamonds from Africa, Russia and India. PhD Dissertation. University of Vienna, Vienna, Austria

Schrauder M, Navon O (1993) Solid carbon dioxide in a natural diamond. Nature 365:42–44

Schrauder M, Navon O (1994) Hydrous and carbonatitic mantle fluids in fibrous diamonds from Jwaneng, Botswana. Geochim Cosmochim Acta 58:761–771

Schrauder M, Navon O, Szafranek D, Kaminsky FV, Galimov EM (1994) Fluids in Yakutian and Indian diamonds. Goldschmidt Conference Edinburgh, Mineral Mag A 58:813–814

Schrauder M, Koeberl C, Navon O (1996) Trace element analyses of fluid-bearing diamonds from Jwaneng, Botswana. Geochim Cosmochim Acta 60:4711–4724

Schulze DJ, Wiese D, Steude J (1996) Abundance and distribution of diamonds in eclogite revealed by volume visualization of CT X-ray scans. J Geol 104:109–114

Seal M (1966) Nature of diamond coat. Philos Mag 13:645–648

Seal M (1970) Some observations on inclusions and localized type II structures in diamond. *In:* Proceedings of Diamond Conference, Oxford, Chapter 16

Shah CJ, Lang AR (1963) An unusual distribution of precipitates in a diamond. Mineral Mag J M Soc 33:594–599

Shatskiy A, Litasov KD, Palyanov YN, Ohtani E (2016) Phase relations on the K_2CO_3–$CaCO_3$–$MgCO_3$ join at 6 GPa and 900–1400 °C: Implications for incipient melting in carbonated mantle domains. Am Mineral 101:437–447

Shatsky VS, Zedgenizov DA, Ragozin AL, Kalinina VV (2015) Diamondiferous subcontinental lithospheric mantle of the northeastern Siberian Craton: Evidence from mineral inclusions in alluvial diamonds. Gondwana Res 28:106–120

Shchukina EV, Agashev AM, Pokhilenko NP (2017) Metasomatic origin of garnet xenocrysts from the V. Grib kimberlite pipe, Arkhangelsk region, NW Russia. Geosci Front 8:641–651

Shimizu N (1975) Rare earth elements in garnets and clinopyroxenes from garnet lherzolite nodules in kimberlites. Earth and Planet Sc Lett 25:26–32

Shimizu N, Richardson SH (1987) Trace element abundance patterns of garnet inclusions in peridotite-suite diamonds. Geochim Cosmochim Acta 51:755–758

Shiryaev, AA, Izraeli ES, Hauri EH, Zakharchenko OD, Navon O (2005) Chemical, optical and isotopic investigation of fibrous diamonds from Brazil. Russ Geol Geophys 46:1185–1201

Shu Q, Brey GP (2015) Ancient mantle metasomatism recorded in subcalcic garnet xenocrysts: Temporal links between mantle metasomatism, diamond growth and crustal tectonomagmatism. Earth Planet Sci Lett 418:27–39

Simon NSC, Carlson RW, Pearson DG, Davies GR (2007) The origin and evolution of the Kaapvaal cratonic lithospheric mantle. J Petrol 48:589–625

Skinner CP (1989) The petrology of peridotite xenoliths from the Finsch kimberlite, South Africa. S Afr J Geol 92:197–206

Skuzovatov SY, Zedgenizov DA, Shatsky VS, Ragozin AL, Kuper KE (2011) Composition of cloudy microinclusions in octahedral diamonds from the Internatsional'naya kimberlite pipe (Yakutia). Russ Geol Geophys 52:85–96

Skuzovatov SY, Zedgenizov DA, Ragozin AL, Shatsky VS (2012) Growth medium composition of coated diamonds from the Sytykanskaya kimberlite pipe (Yakutia). Russ Geol Geophys 53:1197–1208

Skuzovatov S, Zedgenizov D, Howell D, Griffin WL (2016) Various growth environments of cloudy diamonds from the Malobotuobia kimberlite field (Siberian craton). Lithos 265:96–107

Smart KA, Heaman LM, Chacko T, Simonetti A, Kopylova M, Mah D, Daniels D (2009) The origin of high-MgO diamond eclogites from the Jericho Kimberlite, Canada. Earth Planet Sci Lett 284:527–537

Smit KV, Shirey SB, Stern RA, Steele A, Wang W (2016) Diamond growth from C–H–N–O recycled fluids in the lithosphere: Evidence from CH4 micro-inclusions and $\delta^{13}C$–$\delta^{15}N$–N content in Marange mixed-habit diamonds. Lithos 265:68–81

Smit KV, Stachel T, Luth RW, Stern RA (2019) Evaluating mechanisms for eclogitic diamond growth: An example from Zimmi Neoproterozoic diamonds (West African craton). Chem Geol 520:21–32

Smith CB (1983) Pb, Sr and Nd isotopic evidence for sources of southern African Cretaceous kimberlites. Nature 304:51–54

Smith PM, Asimow PD (2005) Adiabat_1ph: A new public front-end to the MELTS, pMELTS, and pHMELTS models. Geochem Geophys Geosyst 6:Q02004

Smith EM, Kopylova MG, Dubrovinsky L, Navon O, Ryder J, Tomlinson EL (2011) Transmission X-ray diffraction as a new tool for diamond fluid inclusion studies. Mineral Mag 75:2657–2675

Smith EM, Kopylova MG, Nowell GM, Pearson DG, Ryder J (2012) Archean mantle fluids preserved in fibrous diamonds from Wawa, Superior craton. Geology 40:1071–1074

Smith EM, Kopylova MG, Frezzotti ML, Afanasiev VP (2014) N-rich fluid inclusions in octahedrally-grown diamond. Earth Planet Sci Lett 393:39–48

Smith EM, Kopylova MG, Frezzotti ML, Afanasiev VP (2015) Fluid inclusions in Ebelyakh diamonds: Evidence of CO2 liberation in eclogite and the effect of H_2O on diamond habit. Lithos 216:106–117

Smith EM, Shirey SB, Nestola F, Bullock ES, Wang J, Richardson SH, Wang W (2016) Large gem diamonds from metallic liquid in Earth's deep mantle. Science 354:1403–1405

Sobolev VS (1960) Conditions of formation of diamond deposits. Geol Geofiz 1:3–20

Sobolev N (1977) Deep-seated inclusions in kimberlites and the problem of the composition of the upper mantle. (Translated from the Russian edition, 1974). AGU, Washington DC

Sobolev NV, Kuznetsova IK (1966) Mineralogy of diamond-bearing eclogites. Dokl Akad Nauk 167:1365

Sobolev NV, Kaminsky FV, Griffin WL, Yefimova ES, Win TT, Ryan CG, Botkunov AI (1997) Mineral inclusions in diamonds from the Sputnik kimberlite pipe, Yakutia. Lithos 39:135–157

Sobolev NV, Logvinova AM, Zedgenizov DA, Seryotkin YV, Yefimova E, Floss C, Taylor LA (2004) Mineral inclusions in microdiamonds and macrodiamonds from kimberlites of Yakutia: a comparative study. Lithos 77:225–242

Sobolev NV, Logvinova AM, Efimova ES (2009) Syngenetic phlogopite inclusions in kimberlite-hosted diamonds: implications for role of volatiles in diamond formation. Russ Geol Geophys 50:1234–1248

Sobolev NV, Logvinova AM, Tomilenko AA, Wirth R, Bul'bak TA, Luk'yanova LI, Fedorova EN, Reutsky VN, Efimova ES (2019) Mineral and fluid inclusions in diamonds from the Urals placers, Russia: Evidence for solid molecular N2 and hydrocarbons in fluid inclusions. Geochim Cosmochim Acta 266:197–219

Song S, Su L, Niu Y, Lai Y, Zhang L (2009) CH_4 inclusions in orogenic harzburgite: evidence for reduced slab fluids and implication for redox melting in mantle wedge. Geochim Cosmochim Acta 73:1737–1754

Speich L, Kohn SC (2020) QUIDDIT-QUantification of infrared active defects in diamond and inferred temperatures. Comput Geosci 144:104558

Speich L, Kohn SC, Bulanova GP, Smith CB (2018) The behaviour of platelets in natural diamonds and the development of a new mantle thermometer. Contrib Mineral Petrol 173:39

Stachel T, Harris JW (1997) Diamond precipitation and mantle metasomatism–evidence from the trace element chemistry of silicate inclusions in diamonds from Akwatia, Ghana. Contrib Mineral Petrol 129:143–154

Stachel T, Harris JW (2008) The origin of cratonic diamonds — Constraints from mineral inclusions. Ore Geol Rev 34:5–32

Stachel T, Luth RW (2015) Diamond formation—Where, when and how? Lithos 220:200–220

Stachel T, Viljoen KS, Brey G, Harris JW (1998) Metasomatic processes in lherzolitic and harzburgitic domains of diamondiferous lithospheric mantle: REE in garnets from xenoliths and inclusions in diamonds. Earth Planet Sci Lett 159:1–12

Stachel T, Harris JW, Tappert R, Brey GP (2003) Peridotitic diamonds from the Slave and the Kaapvaal cratons—similarities and differences based on a preliminary data set. Lithos 71:489–503

Stachel T, Aulbach S, Brey GP, Harris JW, Leost I, Tappert R, Viljoen KF (2004) The trace element composition of silicate inclusions in diamonds: A review. Lithos 77:1–19

Stachel T, Chacko T, Luth RW (2017) Carbon isotope fractionation during diamond growth in depleted peridotite: Counterintuitive insights from modelling water-maximum CHO fluids as multi-component systems. Earth Planet Sci Lett 473:44–51

Stagno V, Ojwang DO, McCammon CA, Frost DJ (2013) The oxidation state of the mantle and the extraction of carbon from Earth's interior. Nature 493:84–88

Staudacher T, Allègre CJ (1982) Terrestrial xenology. Earth Planet Sci Lett 60:389–406

Sumino H, Dobrzhinetskaya LF, Burgess R, Kagi H (2011) Deep-mantle-derived noble gases in metamorphic diamonds from the Kokchetav massif, Kazakhstan. Earth Planet Sci Lett 307:439–449

Sunagawa T (1984) Morphology of natural and synthetic diamond crystals. *In:* Materials Science of the Earth's Interior. Terra Scientific Publishing, Tokyo, p 303–330

Sverjensky DA, Huang F (2015) Diamond formation due to a pH drop during fluid–rock interactions. Nat Commun 6:8702

Tappert R, Tappert MC (2011) Diamonds in nature: a guide to rough diamonds. Springer Science & Business Media, Berlin, Heidelberg

Tappert R, Stachel T, Harris JW, Shimizu N (2005) Mineral inclusions in diamonds from the Panda kimberlite, Slave Province, Canada. Eur J Mineral 17:423–440

Taylor WR, Jaques AL, Ridd M (1990) Nitrogen-defect aggregation characteristics of some Australasian diamonds; time-temperature constraints on the source regions of pipe and alluvial diamonds. Am Mineral 75:1290–1310

Taylor WR, Canil D, Milledge HJ (1996) Kinetics of Ib to IaA nitrogen aggregation in diamond. Geochim Cosmochim Acta 60:4725–4733

Thomassot E, Cartigny P, Harris JW, Viljoen KF (2007) Methane-related diamond crystallization in the Earth's mantle: stable isotope evidences from a single diamond-bearing xenolith. Earth Planet Sci Lett 257:362–371

Thompson WK (1965) Infra-red spectroscopic studies of aqueous systems. Part 1. Molar extinction coefficients of water, deuterium oxide, deuterium hydrogen oxide, aqueous sodium chloride and carbon disulphide. Trans Faraday Soc 61:2635–2640

Timmerman S, Jaques AL, Weiss Y, Harris JW (2018a) N-δ13C-inclusion profiles of cloudy diamonds from Koffiefontein: Evidence for formation by continuous Rayleigh fractionation and multiple fluids. Chem Geol 483:31–46

Timmerman S, Honda M, Phillips D, Jaques AL, Harris JW (2018b) Noble gas geochemistry of fluid inclusions in South African diamonds: Implications for the origin of diamond-forming fluids. Mineral Petrol 112:181–195

Timmerman S, Yeow H, Honda M, Howell D, Jaques AL, Krebs MY, Woodland S, Pearson DG, Ávilaa JN, Ireland TR (2019) U–Th/He systematics of fluid-rich 'fibrous' diamonds–Evidence for pre-and syn-kimberlite eruption ages. Chem Geol 515:22–36

Tomilenko AA, Chepurov AI, Palyanov YN, Pokhilenko LN, Shebanin AP (1997) Volatile components in the upper mantle (from data on fluid inclusions). Geol Geofiz 38:294–303

Tomlinson EL, Müller W (2009) A snapshot of mantle metasomatism: Trace element analysis of coexisting fluid (LA-ICP-MS) and silicate (SIMS) inclusions in fibrous diamonds. Earth Planet Sci Lett 279:362–372

Tomlinson E, De Schrijver I, De Corte K, Jones AP, Moens L, Vanhaecke F (2005) Trace element compositions of submicroscopic inclusions in coated diamond: A tool for understanding diamond petrogenesis. Geochim Cosmochim Acta 69:4719–4732

Tomlinson EL, Jones AP, Harris JW (2006) Co-existing fluid and silicate inclusions in mantle diamond. Earth Planet Sci Lett 250 581–595

Turner G, Burgess R, Bannon M (1990) Volatile-rich mantle fluids inferred from inclusions in diamond and mantle xenoliths. Nature 344:653–655

Venyaminov SY, Prendergast FG (1997) Water (H_2O and D_2O) molar absorptivity in the 1000–4000 cm^{-1} range and quantitative infrared spectroscopy of aqueous solutions. Anal Biochem 248:234–245

Viljoen KS, Swash PM, Otter ML, Schulze DJ, Lawless PJ (1992) Diamondiferous garnet harzburgites from the Finsch kimberlite, Northern Cape, South Africa. Contrib Mineral Petrol 110:133–8

Wada N, Matsuda JI (1998) A noble gas study of cubic diamonds from Zaire: Constraints on their mantle source. Geochim Cosmochim Acta 62:2335–2345

Walmsley JC, Lang AR (1992a) On sub-micrometre inclusions in diamond coat: crystallography and composition of ankerites and related rhombohedral carbonates. Mineral Mag 56:533–543

Walmsley JC, Lang AR (1992b) Oriented biotite inclusions in diamond coat. Mineral Mag 56:108–111

Walter MJ, Bulanova GP, Armstrong LS, Keshav S, Blundy JD, Gudfinnsson G, Lord OT, Lennie AR, Clark SM, Smith CB, Gobbo L (2008) Primary carbonatite melt from deeply subducted oceanic crust. Nature 454:622–625

Wang W, Moses TM, Shigley JE (2003) Physical and chemical features of a large coated natural diamond crystal. Diamond Relat Mater 12:330–335

Watling, JR, Herbert HK, Barrow IS, Thomas AG (1995) Analysis of diamonds and indicator minerals for diamond exploration by laser ablation–inductively coupled plasma mass spectrometry. Analyst 120:1357–1364

Weinstein Y, Navon O, Altherr R, Stein M (2006) The role of lithospheric mantle heterogeneity in the generation of Plio-Pleistocene alkali basaltic suites from NW Harrat Ash Shaam (Israel). J Petrol 47:1017–1050

Weiss Y, Goldstein SL (2018) The involvement of diamond-forming fluids in the metasomatic 'cocktail' of kimberlite sources. Mineral Petrol 112:149–167

Weiss Y, Griffin WL, Elhlou S, Navon O (2008a) Comparison between LA-ICP-MS and EPMA analysis of trace elements in diamonds. Chem Geol 252:158–168

Weiss Y, Griffin WL, Harris JW, Navon O (2008b) Diamond-forming fluids in fibrous diamonds: The trace-element perspective. International Kimberlite Conference: Extended Abstracts 9

Weiss Y, Kessel R, Griffin WL, Kiflawi I, Klein-BenDavid O, Bell DR, Harris JW, Navon O (2009) A new model for the evolution of diamond-forming fluids: Evidence from microinclusion-bearing diamonds from Kankan, Guinea. Lithos 112:660–674

Weiss Y, Kiflawi I, Navon O (2010) IR spectroscopy: quantitative determination of the mineralogy and bulk composition of fluid microinclusions in diamonds. Chem Geol 275:26–34

Weiss Y, Griffin WL, Bell DR, Navon O (2011) High-Mg carbonatitic melts in diamonds, kimberlites and the sub-continental lithosphere. Earth Planet Sci Lett 309:337–347

Weiss Y, Kiflawi I, Navon O (2013a) The IR absorption spectrum of water in microinclusion-bearing diamonds. *In:* Proceedings of 10th International Kimberlite Conference. Vol 1. Pearson DG, Grütter HS, Harris JW, Kjarsgaard BA, O'Brien H, Rao NVC, Sparks S (eds) Springer, New Delhi, p 271–280

Weiss Y, Griffin WL, Navon O (2013b) Diamond-forming fluids in fibrous diamonds: The trace-element perspective. Earth Planet Sci Lett 376:110–125

Weiss Y, Kiflawi I, Davies N, Navon O (2014) High-density fluids and the growth of monocrystalline diamonds. Geochim Cosmochim Acta 141:145–159

Weiss Y, McNeill J, Pearson DG, Nowell, GM, Ottley CJ (2015) Highly saline fluids from a subducting slab as the source for fluid-rich diamonds. Nature 524:339–342

Weiss Y, Class C, Goldstein SL, Hanyu T (2016) Key new pieces of the HIMU puzzle from olivines and diamond inclusions. Nature 537:666–670

Weiss Y, Class C, Goldstein SL, Winckler G (2017) Ages of mantle metasomatism from U–Th–He systematics of diamond-forming COH fluids. International Kimberlite Conference: Extended Abstracts 11

Weiss Y, Navon O, Goldstein SL, Harris JW (2018) Inclusions in diamonds constrain thermo-chemical conditions during Mesozoic metasomatism of the Kaapvaal cratonic mantle. Earth Planet Sci Lett 491:134–147

Weiss Y, Kiro Y, Class C, Winckler G, Harris JW, Goldstein SL (2021) Helium in diamonds unravels over a billion years of craton metasomatism. Nat Commun 12:2667

Weiss Y, Czas J, Navon O (2022) Global published compositions of high-density fluids (HDFs) in fibrous diamonds, Version 1.0. Interdisciplinary Earth Data Alliance (IEDA)

Willbold M, Stracke A (2006) Trace element composition of mantle end-members: Implications for recycling of oceanic and upper and lower continental crust. Geochem Geophys Geosyst 7:Q04004

Wirth R (2004) Focused Ion Beam (FIB) A novel technology for advanced application of micro-and nanoanalysis in geosciences and applied mineralogy. Eur J Mineral 16:863–876

Wirth R (2009) Focused Ion Beam (FIB) combined with SEM and TEM: Advanced analytical tools for studies of chemical composition, microstructure and crystal structure in geomaterials on a nanometre scale. Chem Geol 261:217–229

Wittig N, Pearson DG, Webb M, Ottley CJ, Irvine GJ, Kopylova M, Jensen SM, Nowell GM (2008) Origin of cratonic lithospheric mantle roots: A geochemical study of peridotites from the North Atlantic Craton, West Greenland. Earth Planet Sci Lett 274:24–33

Wyllie PJ (1987) Metasomatism and fluid generation in mantle xenoliths. *In:* Mantle xenoliths. Nixon P (ed) John Wiley & Sons Ltd, Chichester, p 609–621

Wyllie PJ, Ryabchikov ID (2000) Volatile components, magmas, and critical fluids in upwelling mantle. J Petrol 41:1195–1206

Xia X (2018) Mineral inclusions in diamonds from Chidliak (Nunavut, Canada): constraining the diamond substrates. MSc Dissertation, University of Alberta, Edmonton, Alberta

Yaxley GM, Brey GP (2004) Phase relations of carbonate-bearing eclogite assemblages from 2.5 to 5.5 GPa: implications for petrogenesis of carbonatites. Contrib Mineral Petrol 146:606–619

Yelisseyev AP, Pokhilenko NP, Steeds JW, Zedgenizov DA, Afanasiev VP (2004) Features of coated diamonds from the Snap Lake/King Lake kimberlite dyke, Slave craton, Canada, as revealed by optical topography. Lithos 77:83–97

Zashu S, Ozima M, Nitoh O (1986) K–Ar isochron dating of Zaire cubic diamonds. Nature 323:710–712

Zedgenizov DA, Kagi H, Shatsky VS, Sobolev NV (2004) Carbonatitic melts in cuboid diamonds from Udachnaya kimberlite pipe (Yakutia): Evidence from vibrational spectroscopy. Mineral Mag 68:61–73

Zedgenizov DA, Harte B, Edinburgh Ion Microprobe Facility (EIMF), Shatsky VS, Politov AA, Rylov GM, Sobolev NV (2006) Directional chemical variations in diamonds showing octahedral following cuboid growth. Contrib Mineral Petrol 151:45–57

Zedgenizov DA, Rege S, Griffin WL, Kagi H, Shatsky VS (2007) Composition of trapped fluids in cuboid fibrous diamonds from the Udachnaya kimberlite: LAM-ICPMS analysis. Chem Geol 240:151–162

Zedgenizov DA, Ragozin AL, Shatsky VS, Araújo D, Griffin WL, Kagi H (2009) Mg and Fe-rich carbonate–silicate high-density fluids in cuboid diamonds from the Internationalnaya kimberlite pipe (Yakutia). Lithos 112:638–647

Zedgenizov DA, Ragozin AL, Shatsky VS, Araújo D, Griffin WL (2011) Fibrous diamonds from the placers of the northeastern Siberian Platform: Carbonate and silicate crystallization media. Russ Geol Geophys 52:1298–1309

Zedgenizov DA, Kalinina VV, Reutsky VN, Yuryeva OP, Rakhmanova MJ (2016) Regular cuboid diamonds from placers on the northeastern Siberian platform. Lithos 265:125–137

Zedgenizov DA, Malkovets VG, Griffin WL (2017a) Composition of diamond-forming media in cuboid diamonds from the V. Grib kimberlite pipe (Arkhangelsk province, Russia). Geochem J 51:205–213

Zedgenizov, D, Reutsky V, Wiedenbeck M (2017b) The Carbon and nitrogen isotope characteristics of type Ib-IaA Cuboid diamonds from alluvial placers in the northeastern Siberian platform. Minerals 7:178

Zedgenizov DA, Ragozin AL, Shatsky VS, Griffin WL (2018) Diamond formation during metasomatism of mantle eclogite by chloride-carbonate melt. Contrib Mineral Petrol 173:84

Zedgenizov DA, Skuzovatov SY, Griffin WL, Pomazansky BS, Ragozin AL, Kalinina VV (2020) Diamond-forming HDFs tracking episodic mantle metasomatism beneath Nyurbinskaya kimberlite pipe (Siberian craton). Contrib Mineral Petrol 175:106

Ziberna L, Nimis P, Zanetti A, Marzoli A, Sobolev NV (2013) Metasomatic processes in the central Siberian cratonic mantle: Evidence from garnet xenocrysts from the Zagadochnaya kimberlite. J Petrol 54:2379–2409